Compatibilization of Polyolefin Blends

A Thesis
SUBMITTED TO THE FACULTY OF
UNIVERSITY OF MINNESOTA
BY

CHRISTOPHER MURPHY THURBER

IN PARTIAL FULFILLMENT OF THE REQUIREMENTS
FOR THE DEGREE OF
DOCTOR OF PHILOSOPHY

Christopher W. Macosko, Timothy P. Lodge

August 2015

Acknowledgements

This thesis would not have been possible without my advisers, family, friends, and group members. My advisers showed amazing patience and faith in my project, my family accepted my decision to move hundreds of miles away to "the frozen north" for five years, my friends listened and supported me during difficult times, and group members provided crucial ideas, thoughts, and assistance inside and outside of lab. I cannot adequately express how important these people are to me, and how much meaning they have added to my time in grad school.

The staff at UMN have also been invaluable with their help and thoughts (Dr. David Giles, Dr. Jason Myers, and Dr. Fang Zhou especially). I have had excellent collaborators that were a pleasure to work with, from both industrial (IPRIME) and academic (Cornell and the University of Vermont) backgrounds. Countless undergraduate hours were also spent on this body of work, so I would like to offer special thanks to Adam, Romit, Jacob, Mike, Feida, and all the other dedicated undergrads in the Macosko and Lodge groups.

I would also like to express my gratitude to The Dow Chemical Company (especially Dr. Craig Silvis and Dr. Tom Peterson) and the Center for Sustainable Polymers for financial support and for the thoughtful advice, feedback, and suggestions I benefitted from over the years.

Many thanks to these people, and all the others that have helped over the years. This thesis is a testament to the team that built it.

Dedication

This thesis is dedicated to my parents, Noel and Lisa Thurber.

Abstract

Polymer blends are used to access unique combinations of properties beyond those of neat homopolymers. Blends confer flexibility in tailoring a specific material to a given application, and in some cases, they can lend improved properties compared to their constituent materials. Some examples of blend-synergistic properties in the literature include toughness enhancement, increased chemical resistance, increased modulus, and improved processability. Given the breadth of properties that can be improved by blends, they are employed extensively in commercial products, with more than a third of all polymer resins used in blends (Utracki, 2003).

Most polymer pairs are immiscible, thus their blends require compatibilization to aid dispersion in the melt state and to transfer stress across interfaces in the solid state. Block copolymers have proven to be successful compatibilizers, in both premade and reactively formed systems. This thesis focuses mainly on reactive systems. The reaction at immiscible polymer interfaces is kinetically limited and most reactions are too slow for applications, so general methods of increasing interfacial reaction rate have been investigated. This work also seeks to find new tools for measuring localization and conversion in polymer blends, with the ultimate goal of making useful, economical materials, and understanding the resulting structures.

This thesis attempts to further our knowledge of compatibilization of polyolefin blends in particulr. Chapter 2 attempts to create facile reactive compatibilization schemes for polyolefins with poly(methyl methacrylate). Chapters 3 and 4 examine the use of catalysts to increase interfacial reaction rate between functional polyethylene and polylactide. Chapter 3 demonstrates stannous octoate catalyst is localized at the interface, and blends show better compatibilization than those with a more active but non-localized tin chloride dihydrate catalyst. Chapter 4 uses cobalt octoate catalyst to increase interfacial reaction rate by ~90-fold and the extension at break of polylactide majority blends to ~200%. Structural dependence of copolymers on compatibilization efficiency in polypropylene/polyethylene blends is investigated in Chapter 5. Finally, a small scale

coextruder is created using a dual-bore capillary rheometer, with the potential to examine the effect of flow on copolymer localization, catalyst localization, and interfacial reaction rate (Chapter 6).

Table of contents

List of tables

List of figures

Chapter 1. Introduction to blend compatibilization

1.1 Introduction

Polymer blends are often employed to access unique combinations of material properties not otherwise available in neat homopolymers. Blends provide the necessary flexibility to tailor a specific material for a given application, and in some cases they provide improved properties as compared to their substituent materials. Some examples of improved properties through polymer blending include toughness enhancement, increased chemical resistance, increased modulus, and improved processability.[1–4] These properties are of great commercial importance, and as such, 36% of all polymer resins are used in blends.[5] Most polymer blends are immiscible, due to the low entropy of mixing, and consequently, blends feature internal microstructures that are dependent on processing history.

One motivational system of blends is that of polyethylene (PE) and isotactic polypropylene (iPP). Figure 1.1 shows notched impact strength (a measure of the toughness of a material) as a function of PE content.[6] While neither of the neat materials have a notched impact strength over 20 kJ/m^2, a 50/50 blend with a poly(ethylene-*co*-propylene) interfacial modifier (i.e., compatibilizer) reaches almost 100 kJ/m^2. Besides the marked improvement achieved by the blend, this result also highlights the necessity of a third, compatibilizer component to obtain the best mechanical properties, as the blends without compatibilizer did not exhibit improved notched impact strengths.

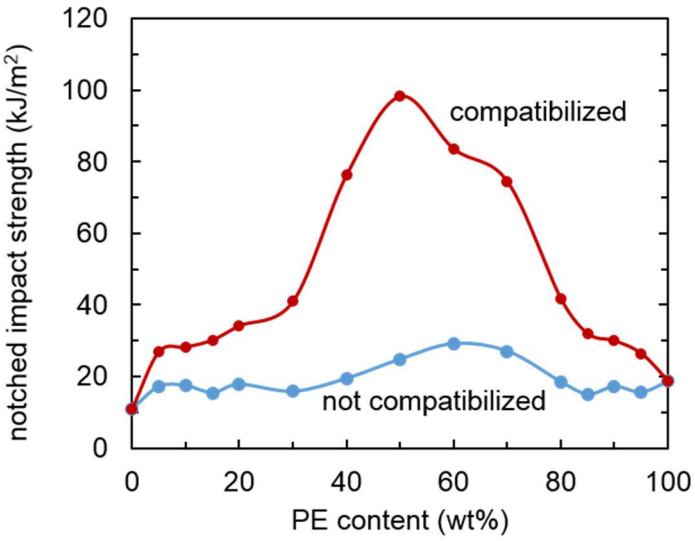

Figure 1.1. Notched impact strength for iPP/PE blends as a function of PE content and presence of poly(ethylene-*co*-propylene) compatibilizer, reproduced from Rabe et al.[6] Compatibilization has a large effect on notched impact strength.

One hurdle to overcome in immiscible polymer blending is weak interfaces between the two homopolymers. Poor stress transfer between the materials can lead to deteriorated bulk properties. The non-compatibilized iPP/PE blends show little improvement in impact strength compared to the compatibilized blends (Figure 1.1). This is because the compatibilizer facilitates stress transfer across the interface, and highlights a more general fact: the interface of immiscible polymer blends usually plays a prominent role in the bulk blend properties.

A second hurdle to overcome is morphology coarsening or phase separation during processing. Fine dispersions are necessary to achieve the best possible mechanical properties of blends.[7] In the melt state, immiscible blends will move toward their thermodynamic equilibrium: phase separated, with minimized interfacial contact. Fine morphology is created by strong shear and extension during melt processing, which is then kinetically trapped by cooling or addition of surfactants. However, if left in the melt state for an extended period of time, droplets can coalesce, leading to inconsistent and/or poor properties.

Compatibilizers, which are materials that overcome these two hurdles, will be discussed in the following sections.

1.2 Block copolymer compatibilizers

Compatibilizers are materials that reduce interfacial tension, prevent coalescence, or increase adhesion in polymer blends.[8] A major class of compatibilizers is block copolymers, with one block miscible with each homopolymer in the blend. The copolymers can assemble at the interface with one block in either material, providing a stitching across the interface (Figure 1.2). These macromolecular surfactants reduce surface tension (promoting droplet breakup) and provide steric stabilization to droplets (preventing coalescence), leading to finer dispersion (Figure 1.3).[9] Finally, block copolymer compatibilizers increase the energy of adhesion by entangling with homopolymers of both component materials.

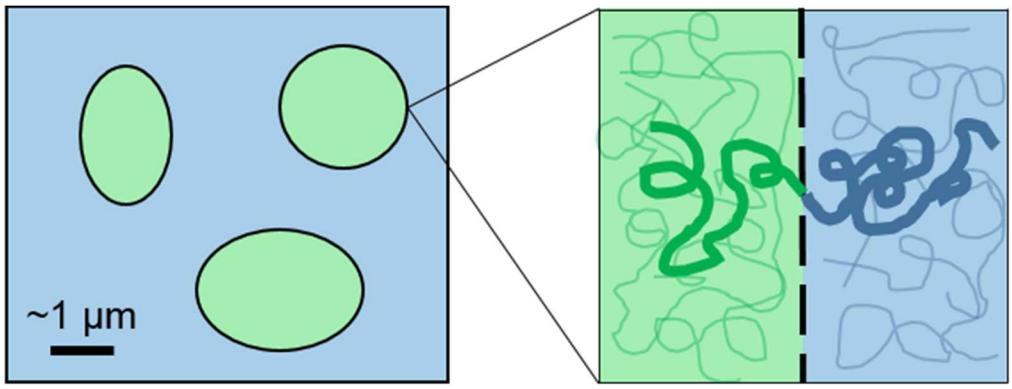

Figure 1.2. Schematic of block copolymer at the interface of an immiscible polymer blend

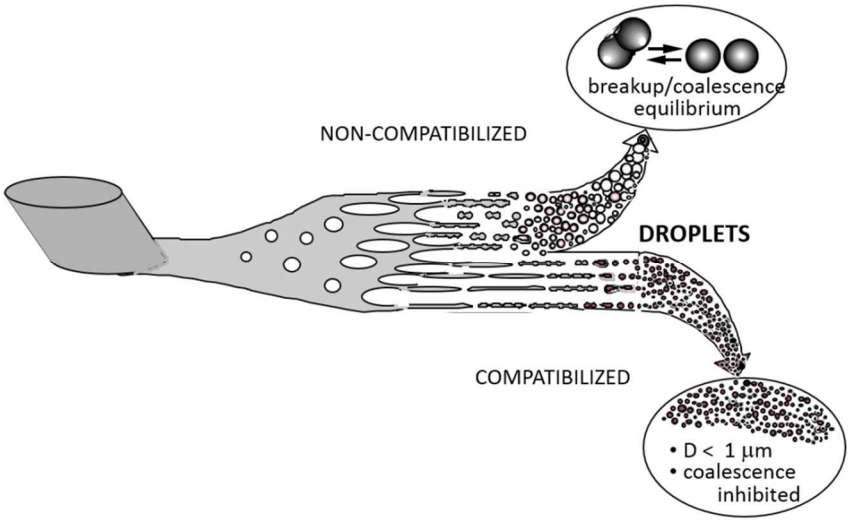

Figure 1.3. Schematic of droplet breakup and coalescence in compatibilized and non-compatibilized blends, from Macosko et al.[10]

The concentration of block copolymer at the interface strongly affects morphology. Xu et al. examined PE/poly(methyl methacrylate) (PMMA) droplet blends with PE-PMMA copolymers added at different concentrations, with the goal of improving the hardness, modulus, scratch resistance, and morphology of PE.[11,12] Figure 1.4 shows the drop size as a function of block copolymer concentration. Droplet size clearly decreases with concentration. This is partially due to a reduction in surface tension (Helfand[13] and Shull[14]), as calculated in equation (1), where γ_0 is the surface tension of the homopolymers, $\Delta\gamma$ is the change in surface tension ($\gamma - \gamma_0$), N is the degree of polymerization, Z^* is the interfacial excess of block copolymer, a is a function of interfacial excess, and R_g is the radius of gyration of a polymer chain.[15] As the interfacial excess of block copolymer increases, the surface tension decreases, leading to finer dispersion in mixing.

$$\frac{-\Delta\gamma}{\gamma_0} = \frac{a}{\sqrt{\chi N}}\left(\frac{Z^*}{R_g}\right) \tag{1}$$

Block copolymer interfacial concentration also impacts the final mechanical properties of blends. Figure 1.4 also shows modulus as a function of concentration, with

modulus increasing by almost a factor of two from 0 to 5 wt% copolymer. At higher block copolymer concentrations, its effects tend to level off as the interface becomes saturated. Similar trends have been observed in other blends for impact strength,[16,17] yield strength,[11] and elongation at break[18].

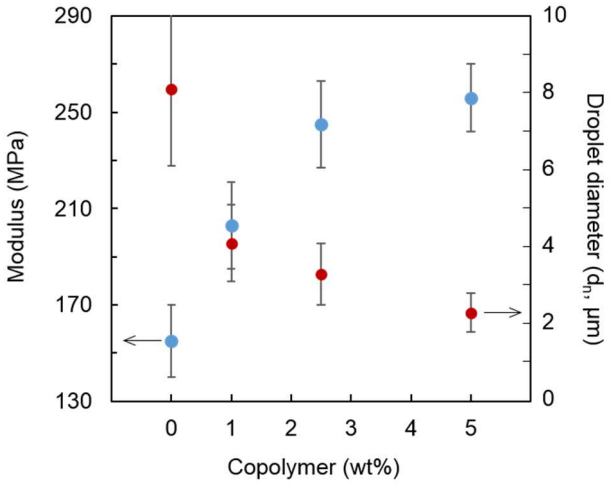

Figure 1.4. Modulus and average drop size of PE/PMMA blends as a function of copolymer compatibilizer content, data replotted from Xu et al.[11]

One of the underlying mechanisms leading to improvements in mechanical properties of compatibilized blends is interfacial adhesion, which can be directly related to the areal density of block copolymer at the interface (Σ, number/area).[19–25] At low block copolymer areal concentration, the failure mechanisms at the interface are chain scission or pullout and Σ scales linearly with the energy of adhesion (G_c). At higher Σ, plastic deformation and crazing occurs, dissipating more energy and causing $\Sigma \sim G_c^2$. Figure 1.5 shows a plot of Σ versus G_c at a flat interface between nylon and polyethylene from Song et al.[26] The predicted scaling is accurate, regardless of temperature or processing method used to create the bilayers.

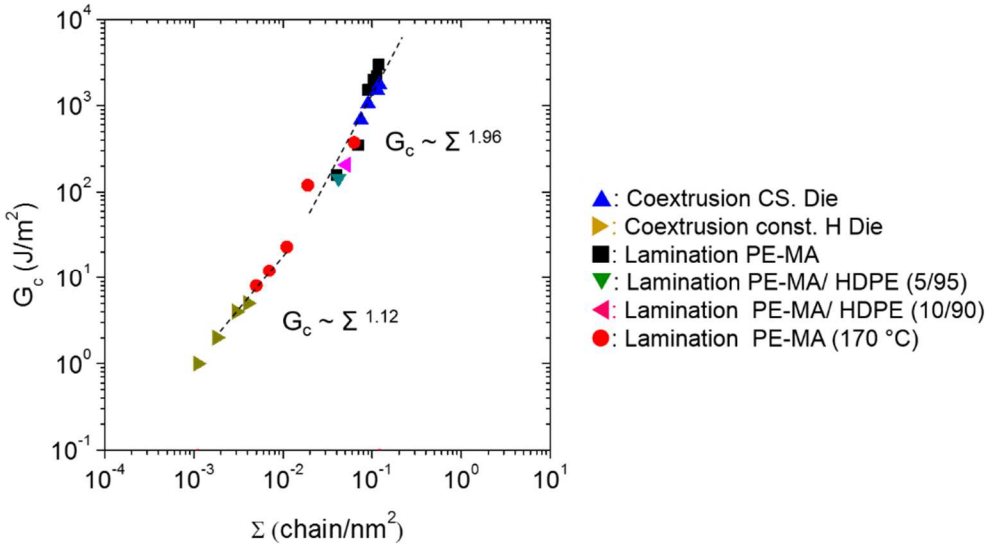

Figure 1.5. Energy of adhesion versus block copolymer areal coverage for PE/nylon bilayers made by various processing methods, at different concentrations and temperatures. Reproduced from Song et al.[26]

A well-documented issue with mixing pre-made block copolymers is the tendency for the block copolymer to become trapped in micelles instead of going to the interface.[27,28] The transmission electron microscopy (TEM) image in Figure 1.6 shows an example of block copolymer micelles composed of PS-*b*-PE in a PE/PS/PS-*b*-PE blend (87/13/0.54 vol%, reproduced from Lyu et al.).[28] For this reason, "…no blend compatibilized by premade block or grafted copolymer has been made available on the market place," according to Koning et al.[2] However, these materials are useful for model adhesion studies, and the correct balance of molecular weight, architecture, and processing may lead to interfacial localization and improved compatibility. The lack of interfacial localization has not been thoroughly tested in the literature to date.

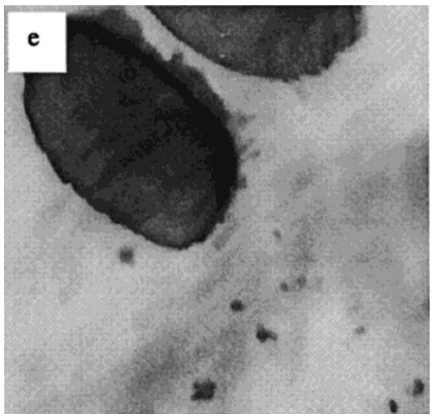

Figure 1.6 TEM of PS/PE/PS-*b*-PE blends showing micelles (87/13/0.54 vol%, reproduced from Lyu et al.[28]). PE droplets are large dark spots on top-left. Block copolymer micelles are small dark spots, predominately in the lower half of the micrograph and close to the droplet.

1.3 Reactive compatibilization overview

Reactive compatibilization is used to create block or graft copolymers at the interface of blends during melt mixing. In this method, complimentary functional groups are attached to a small number of chains for each of the homopolymers. During melt mixing, these functional groups can come to the interface and react to form block copolymers, which are thereby localized at the interface instead of residing in micelles (Figure 1.7). Interfacial localization and the relatively inexpensive process of adding functional groups (compared to making premade block copolymer) are the main advantages of this strategy.

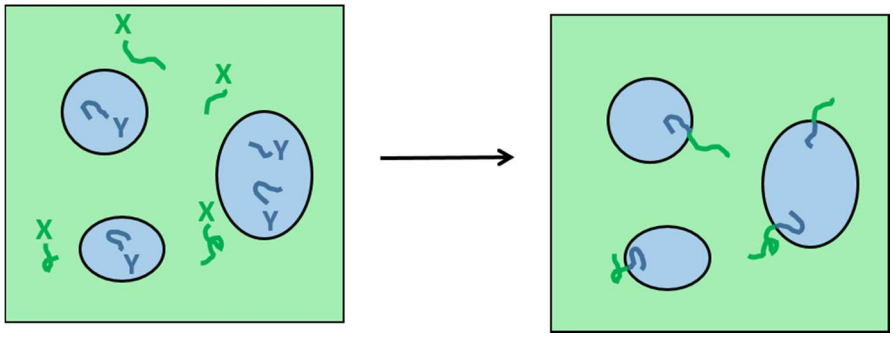

Figure 1.7. Schematic for reactive compatibilization. X and Y represent complementary functional groups that react at the interface in melt processing to form block copolymer

1.4 Applications of reactive compatibilization

Reactive compatibilization has been used widely in industry. Several reviews have been written, with a focus on reaction kinetics and development of applications.[2–5,8,29] A famous example is super-tough nylon (e.g., Zytel, Ultramid).[1–3,7,24,30] The most popular reactions are amine/anhydride (e.g., maleated rubber and nylon in supertough nylon[1,24,30]) and epoxy/acid (e.g., polyesters with glycidyl methacrylate copolymers[31–34]). These reactions have very rapid kinetics at melt mixing temperatures. Rapid kinetics are necessary to promote block copolymer formation and interfacial concentration, which has been well-linked to dispersion, adhesion, and macroscopic physical properties of blends.

1.5 Reactive compatibilization kinetics measurements

Kinetics are of paramount importance for reactive compatibilization, and accordingly, are an active area of research. Reaction kinetics are often difficult to measure in reactive compatibilization due to the dilute concentration of functional groups and block copolymer.

Size exclusion chromatography (SEC) is one of the most common methods to determine reactive compatbilization kinetics, as long as a common solvent for both homopolymers is available and conversion is high.[27,35–38] UV and refractive index (RI) detectors are accurate down to 1-2 wt% copolymer. Moon et al. showed that adding fluorescent tags to the functional polymers and using fluorescence detection in conjunction with typical SEC detectors can increase sensitivity by a factor of ~ 100.[39] Peak deconvolution can also be used to separate copolymer signal from homopolymer signal if the two are overlapping. Typical results are shown in Figure 1.8. Amine end functional polystyrene (PS-NH_2) was reacted with anhydride end functional PMMA (PMMA-anh) for various times at 174 °C, and the resultant materials were dissolved in tetrahydrofuran (THF) for SEC measurements. Copolymer concentration was calculated from the relative ratio of the homopolymer peak area (high elution volume, ~ 21.5 mL) and the block copolymer peak area (low elution volume, ~ 20 mL). The block copolymer

peak is clearly growing with respect to the homopolymer peak as reaction time is increased.

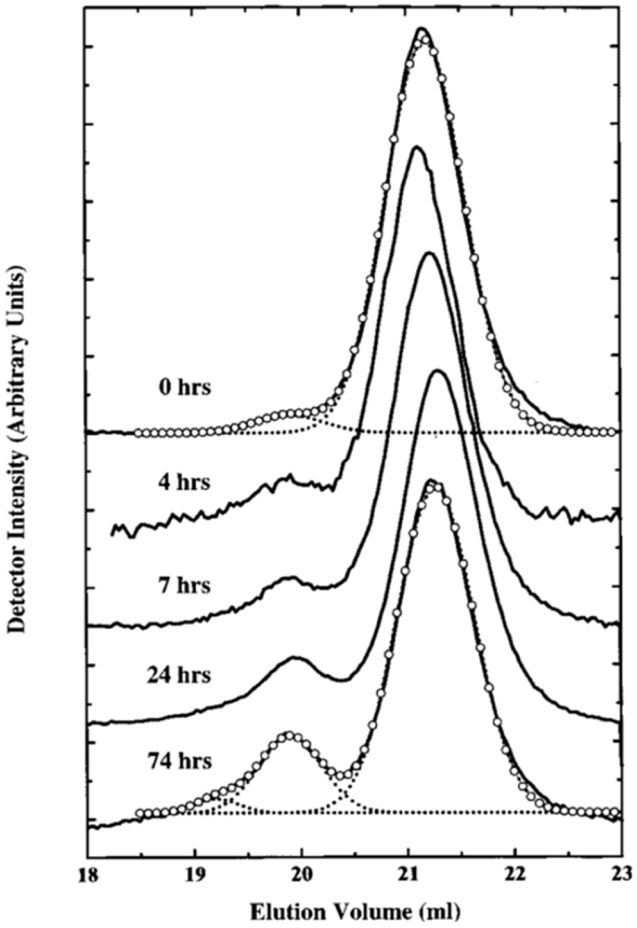

Figure 1.8. SEC traces as a function of reaction time for PMMA-anh and PS-NH_2, reproduced from Schulze et al.[40] Circles indicate peak fits (small dots are deconvoluted peaks) and dark lines are experimental data.

Adhesion is also a sensitive method of detecting copolymer formation at flat interfaces, as described by Creton and coworkers.[20] As described in Section 1.2 and shown in Figure 1.5, $\Sigma \sim G_c$ at low block copolymer areal concentration with chain scission or pullout, and at high copolymer areal concentration $\Sigma \sim G_c^2$ with crazing during failure. Peel tests or asymmetric dual cantilever beam (ADCB) tests are both used to obtain adhesion data (Figure 1.9), where E_1 and E_2 are moduli of the two materials, h_1

and h_2 are thicknesses, a is the distance of crack propagation, Δ is the razor blade thickness, and C_1 and C_2 are geometrical constants based on E_1, E_2, h_1, and h_2. Adhesion itself cannot be used to calculate copolymer concentration, since it is related by scaling, however the correlation between adhesion and copolymer coverage is very strong. In practice, a set of samples is analyzed to determine quantitative conversion by some other technique, which is then related to adhesion. Then, adhesion measurements for a large number of similar samples offers a relatively quick and facile estimate of conversion.

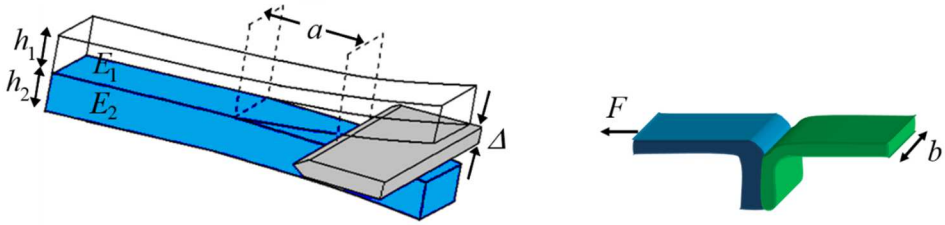

$$G_c = \frac{3\Delta^2 E_1 E_2 h_1^3 h_2^3 \left(C_1^2 E_2 h_2^3 + C_2^2 E_1 h_1^3\right)}{8a^4 \left(C_1^3 E_2 h_2^3 + C_2^3 E_1 h_1^3\right)^2} \qquad \text{Peel strength} = F / b$$

Figure 1.9. Schematic for ADCB test (left) and t-peel test (right).

Blends themselves have been tested qualitatively for copolymer formation using secondary methods such as rheology. Zero shear viscosity increases have been detected, due to increased molecular weight and increased droplet elasticity.[41] The low frequency regime (0.1 – 0.001 rad/s) of the elastic modulus (G') in frequency sweeps can show an upturn compared to non-compatibilized blends, based on increased droplet elasticity arising from Marangoni stresses and/or increased interfacial elasticity.[42–46] The Palierne model can be used to fit this upturn for surface tension (low surface tension is a sign that block copolymer surfactant has formed and is at the interface).[44,47] Also, during batch mixing or extrusion, qualitative rheological measurements of torque, pressure, and normal forces can be used to detect copolymer formation.[31,48–51]

Reduced surface tension is a hallmark of compatibilized blends, which can also be detected through morphology, specifically in smaller droplet sizes[45,52–56] or rougher

interfaces[57–59]. These morphological tools provide screening methods that are quite sensitive to block copolymer conversion. Figure 1.10 shows TEM images of PS/PMMA reactive and non-reactive blends, with the reaction and formation of block copolymer reducing particle size substantially.[27] Figure 1.11 shows interfacial roughness of PS-NH_2/PMMA-anh bilayers as a function of reaction time from atomic force microscopy (AFM).[57] Block copolymer formation decreases surface energy, allowing for more fluctuations and roughness at the interface. There is no quantitative link between morphology and block copolymer concentration to date, so it is a comparative method requiring appropriate non-reactive controls.

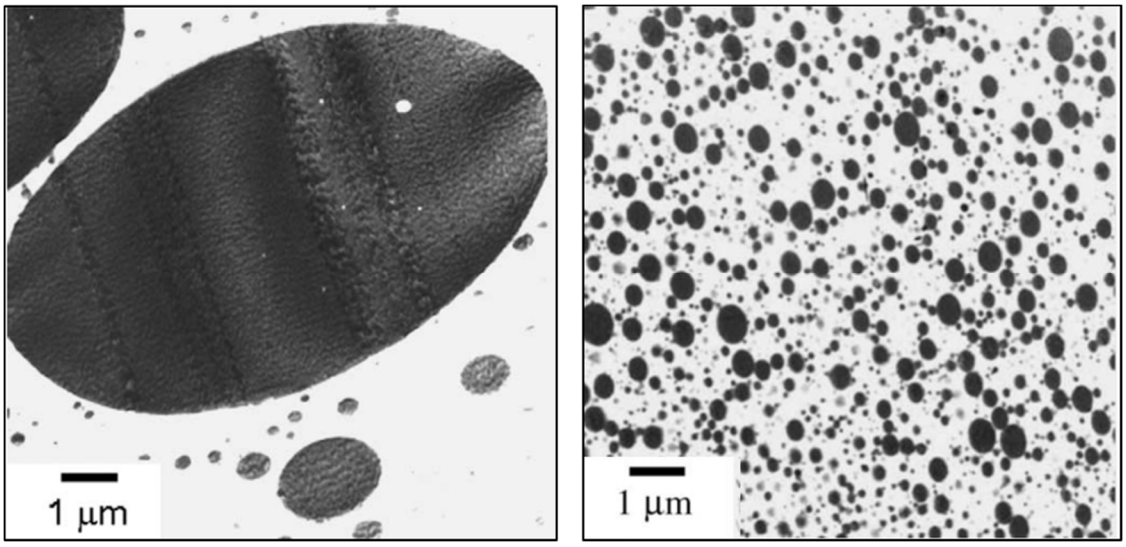

Figure 1.10. TEM images of (left) non-reactive and (right) reactive PS/PMMA blends, reproduced from Jeon et al.[27] The reactive blend image was obtained after 10 min mixing, at approximately 9 wt% block copolymer (determined by SEC).

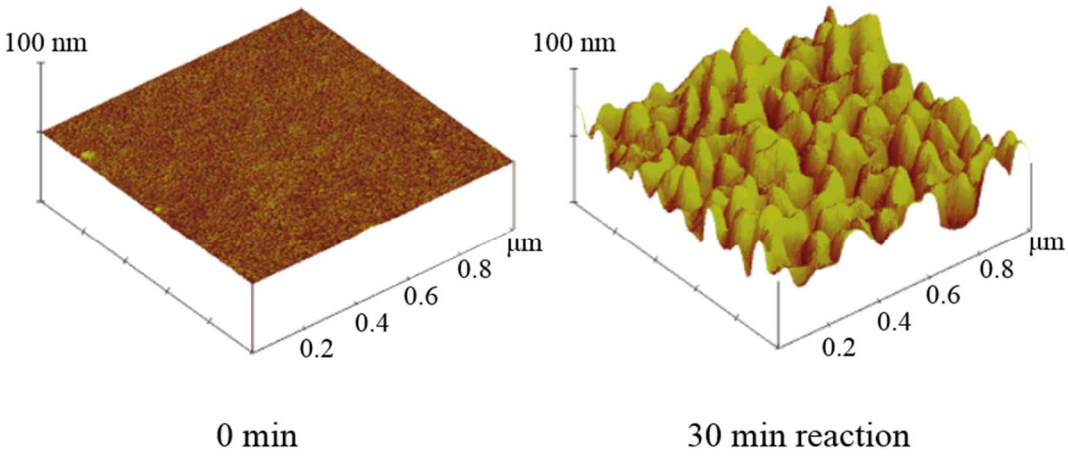

Figure 1.11. AFM of PS-NH_2 / PMMA-anh interface before and after reaction, reproduced from Zhang et al.[57]

1.6 Factors influencing interfacial reaction kinetics

Several general factors that influence reaction kinetics include (1) reaction chemistry, (2) functional polymer molecular weight, (3) functional group location on the polymer, (4) thermodynamic interactions of the homopolymers, (5) flow, and (6) catalysts. Each is explained in the following paragraphs.

Not surprisingly, reaction chemistry is one of the strongest factors influencing reactive compatibilization kinetics. Orr et al.[36] synthesized a series of narrow dispersity polystyrenes with different functional end groups. These were melt blended in different combinations (homogeneously), and SEC was used to measure conversion to copolymer. The authors reported similar rankings in kinetics to small molecule reactions. Aliphatic amines and cyclic anhydrides showed the highest reaction rates (k ~ 1,400 kg mol^{-1} min^{-1}), with the next fastest reaction almost three orders of magnitude slower. This study shows the strong role of functional groups in reaction kinetics, and explains why a select few reactions are used commercially (i.e., kinetics are too slow for most reactions).

Molecular weight of the reactive polymers has a moderate role in reactive compatibilization kinetics.[60,61] Functional polymers that are too large can sterically hinder placement of the functional groups for reaction and occupy a large amount of interfacial

area (or volume) once reacted. However, at low molecular weights, the functional polymers may not be able to entangle sufficiently to improve adhesion. This balance has led some authors to suggest molecular weights in the 20 – 40 kg/mol regime to be optimal.[8]

Functional group location is important for reactive compatibilization kinetics. Jeon et al. compared the effect of end-functional groups versus mid-functional groups on reaction rates.[38] Amine end functional polystyrene (PS-NH_2) and amine functional PMMA (PMMA-NH_2) were reacted with anhydride functional PMMA (end-functional, PMMA-e-anh, and mid-functional, PMMA-m-anh) in melt blending, static bilayers and in solution. The conversion was measured for each system using SEC with a fluorescence detector, and relative reaction rates between end and mid functional polymers (k_E/k_M) were determined (Table 1.1). From kinetic excluded volume theory, the expected k_E/k_M is 2.1. The solution and homogeneous melt cases are in reasonable agreement with theory. This difference in end versus mid-functional reaction rates is due to higher diffusivity (mobility) of chain ends, and steric interactions with the polymer chain. In all cases end-functional polymers have higher reaction rates than mid-functional.

Table 1.1. Ratio of end- to mid-functional reaction rates for PMMA-anh and PS-NH_2

reaction condition	k_E/k_M
static bilayer	> 10
heterogeneous melt	3.2
solution	2.8
homogeneous melt (PMMA)	1.7
theory	2.1

Thermodynamics plays a relatively strong role in conversion during reactive compatibilization, in that it dictates the interfacial volume in which the reaction typically occurs. Generally, as the Flory-Huggins interaction parameter (χ) increases, the overall reaction rate decreases. This comes about for two reasons. First, during blending, high χ raises the energy necessary to create more surface area, leading to coarser morphologies with reduced surface area. Secondly, interfacial thickness is decreased at increased χ, as

described by Helfand and others and shown in equation (2), where χ_c is the interaction parameter at the critical point, b is the geometric average statistical segment length between the homopolymers, and w is the interfacial width.[13,62,63]

$$w = \frac{b\sqrt{2}}{3\chi_c^{0.5}}\left(\frac{\chi}{\chi_c} - 1\right)^{-0.5} \quad (2)$$

Experimentally, the effect of χ on interfacial reaction rate has been observed by Jones et al., by making a series of amine end-functional polymers at similar molecular weight but with different homopolymers to react with PMMA-anh.[64] The polymers were spin-coated to form a bilayer and heated for various reaction times. The bilayers were dissolved for SEC, and the corresponding conversion versus time plot is shown in Figure 1.12. Since the functional group location, temperature, and reaction are the same, differences in conversion can be mostly attributed to χ. As χ increases from 0.017 (PS/PMMA) to 0.32 (polydimethylsiloxane (PDMS)/PMMA) conversion at a given time decreases.

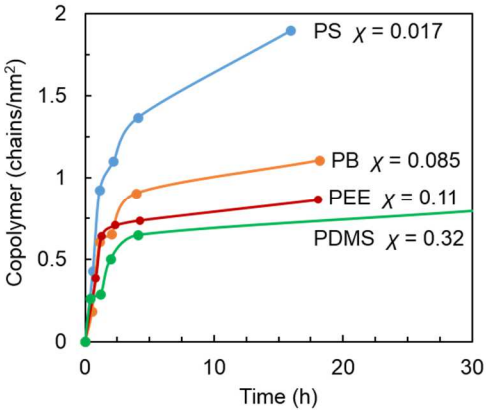

polymer	χ (175 °C)	Σ (chains / nm^2, 4 h)	initial rate (chains / nm^2 hr)
PS	0.017	0.78	0.25
PB	0.085	0.42	0.30
PEE	0.11	0.33	0.32
PDMS	0.32	0.32	0.81

Figure 1.12. Effect of χ on interfacial copolymer conversion for PMMA-anh/x-NH_2 bilayers, reproduced from Jones et al.[64]

Flow also has a strong effect on reaction rate.[26,38,65] Jeon et al. reported a ~1,000-fold increase in the reaction rate between static interfaces and heterogeneous melt mixed blends, based on estimated interfacial volume in the blends.[38] Zhang et al. expanded this

work to coextrusion with a PS-NH_2/PMMA-anh system, which also showed ~1,000-fold faster kinetics than at static interfaces. Examining the same amine/anhydride reaction, Song et al. compared constant thickness (non-compressive) and compressive flow dies in coextrusion and showed that the constant thickness die had similar reaction rates to static interfaces (Figure 1.13).[26] The compressive die reaction rate was ~100-fold faster than static interfaces and the non-compressive die. From these studies, compressive flow toward the interface (in the z-direction in Figure 1.13) emerges as the cause for the elevated reaction rates. This work is particularly promising, since small changes to a production process can lead to very large changes in copolymer formation, adhesion, and final film properties. More work is necessary to determine the mechanism of reaction rate increase from compressive flow.

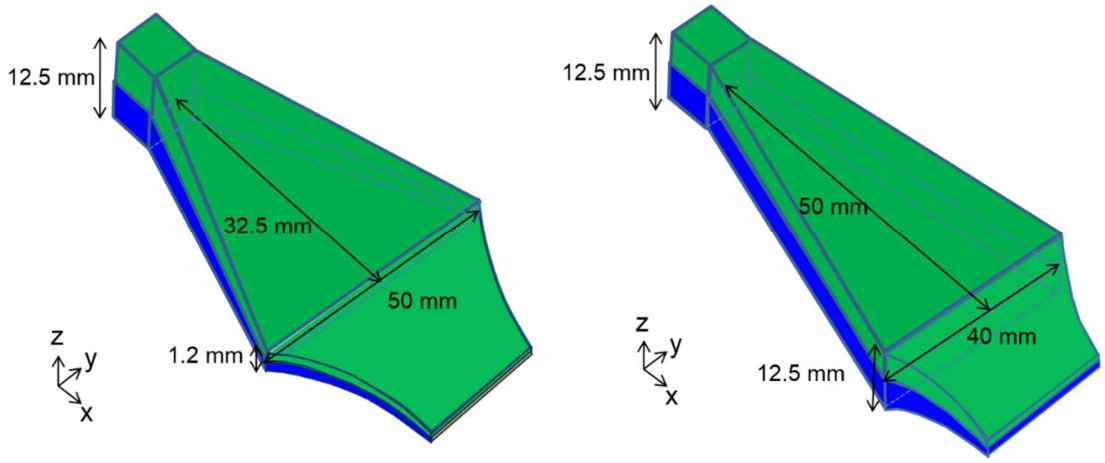

Figure 1.13. Compressive and non-compressive coextrusion dies (left and right, respectively) from Song et al.[26] Compressive die shows ~100-fold reaction rate increase over static lamination and the non-compressive coextrusion die.

Catalysts offer another means of increasing reaction rate without changing the type of reaction or reactive group concentration. Pillon et al. showed transesterification catalysts promoted transreactions in blends of polyesters and polyamides in the 1980s.[66,67] More recently, Feng et al. used N,N-distearylamine to catalyze epoxy/acid reactions in PE/polylactide (PLA) blends.[68] Catalyst localization has been hypothesized to be important for promoting interfacial reactions.[35] The first paper to detect catalyst

localization was Legros et al., who used an electron microprobe to discover that tin distannoxane preferred the poly(butylene terephthalate) PBT portions of reactive PBT/PE blends.[69] This thesis shows an interfacially localized catalyst is even more effective, despite having lower activity, than a non-localized catalyst in reactive PE/PLA blends.[54] Therefore, catalysts should be chosen to have high activity towards the specific coupling reaction, and have surface energies that lead to interfacial localization.

1.7 Kinetics models

There has been controversy in literature over the correct model for reactive compatibilization kinetics in immiscible blends. Most view reactive compatibilization as a diffusion-reaction process, with either diffusion or reaction being limiting. Recent work has argued instead for an interface-limited kinetics model. All three of these models are explored in the following paragraphs.

1.7.1 Diffusion-limited reaction

A summary of the diffusion-limited model of reactive compatibilization is described in Fredrickson and Milner.[70] In this model, there are three stages. The initial stage is described by equation (3), where K_0 is a function of reptation time, the longest Rouse time, and radius of gyration of the functional polymer, and ρ_0 is the concentration density of functional polymer chains. Σ grows linearly with t.

$$\frac{d\Sigma}{dt} = K_0 \rho_0 \tag{3}$$

The second stage involves center of mass diffusion as the limiting step in reaction, with the scaling for $\Sigma \sim t^{1/2}$. This is shown in equation (4), where D_0 is the diffusion coefficient of the functional polymer in the melt state.

$$\Sigma(t) \approx \frac{2}{\pi^{1/2}} \rho_0 \left(D_0 t\right)^{1/2} \tag{4}$$

The final stage is when copolymer has built up at the interface and chains have a difficulty finding space on the interface to react, characterized by a $\Sigma \sim [\ln(t)]^{1/2}$ scaling. Most experimental observations occur in the second and third stages. Muller's Monte-

Carlo simulations showed diffusion-controlled kinetics, but higher rates than expected from the theory of Fredrickson.[71]

Several experimental observations disagree with the diffusion-controlled model. First and foremost, the strong dependence of reactive group type on copolymer conversion is a good indication that reaction controls the rate of this process (Section 1.6). Second, Schulze et al. showed reaction conversion did not scale with diffusion coefficients or molecular weights in reactive PS/PMMA bilayers.[64] Third, Song et al. estimated a Damkohler number (defined as reaction rate/diffusion rate) for a fast amine/cyclic anhydride reaction. The highest possible Damkohler number was orders of magnitude less than 1, indicating reactive compatibilization is always reaction limited in the melt state.[72] Fourth, Schulze et al. synthesized deuterated functional polymers to study their position in a bilayer system as a function of reaction time.[40] Deuterated amine end functional polystyrene (dPS-NH_2) and PMMA-anh were spin coated into thin layers, then heated to react. Forward recoil elastic scattering (FRES) showed no depletion zone for dPS-NH_2 near the interface, which provided direct evidence that reactive coupling is not diffusion-limited, even with the fastest known reaction for reactive compatibilization (Figure 1.14). These observations (and others) have led many authors to adopt a reaction-limited kinetics model.

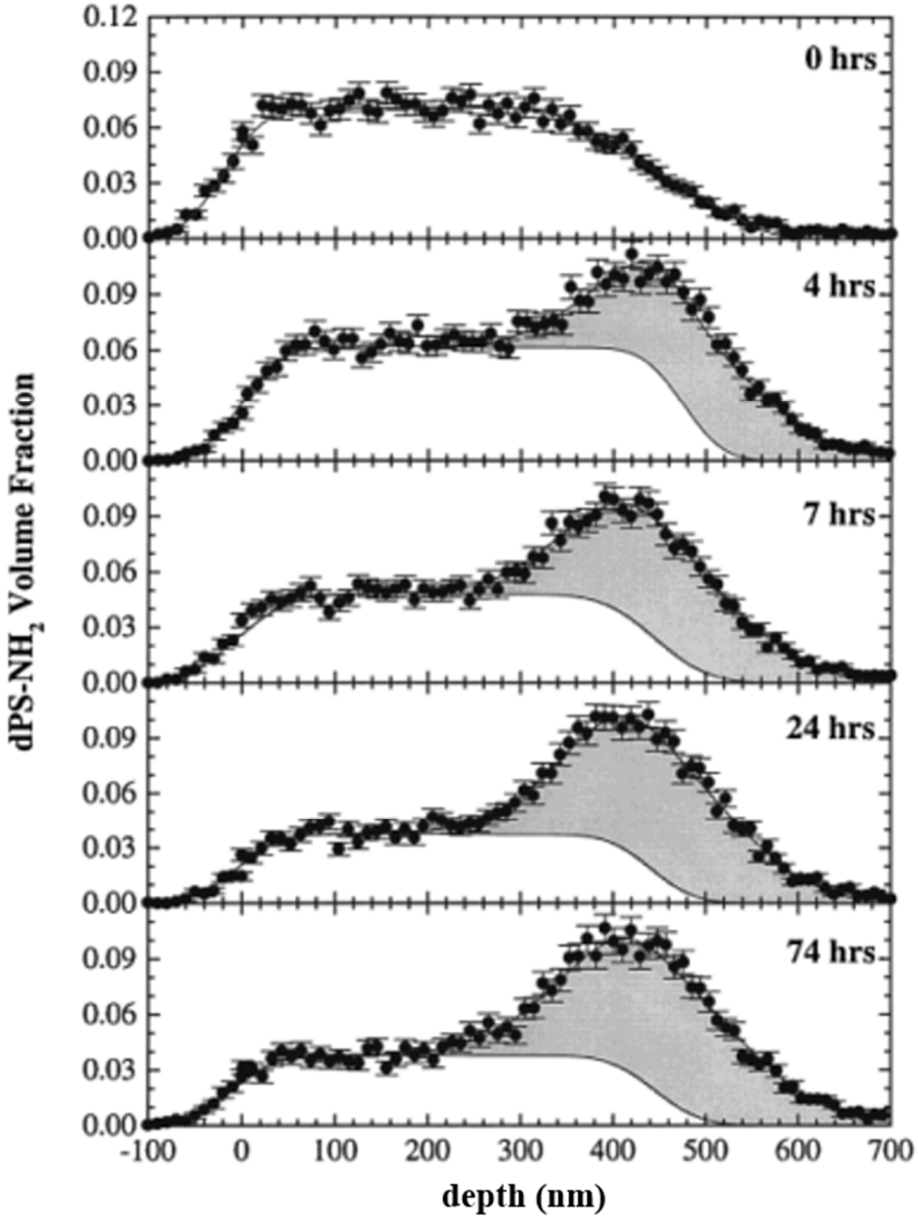

Figure 1.14. FRES signal as a function of depth and time for dPS-NH_2+PS/PMMA-anh bilayer, from Schulze et al.[40] dPS-NH_2 volume fraction is plotted as a function of depth into the film (originally, the dPS-NH_2/PS layer ended at 450 nm, at the interface with PMMA-anh). Interfacial excess of dPS-NH_2 (dark grey shading) is interpreted as reacted copolymer, which matches with SEC results of the same films.

1.7.2 Reaction-limited models

Reactive compatibilization can be viewed as a simple A + B → C reaction. In a reaction limited system, these kinetics are described by the elementary rate law in equation (5).

$$\frac{dC_{copolymer}}{dt} = kC_A C_B \tag{5}$$

Schulze et al. fit second order reaction kinetics to PS/PMMA reactive bilayers, with copolymer conversion determined by FRES.[73] The interfacial excess (which can be qualitatively interpreted as copolymer conversion) is plotted against time in Figure 1.15 for three molecular weights of functional PS. In the left panel, the solid line fits are based on a second order, reaction limiting model, which fit the data fairly well. The right panel shows diffusion-limited fits based on the Fredrickson/Milner theory, which poorly represents the data. In general, the diffusion models overestimate conversion, suggesting that diffusion is not the limiting step.

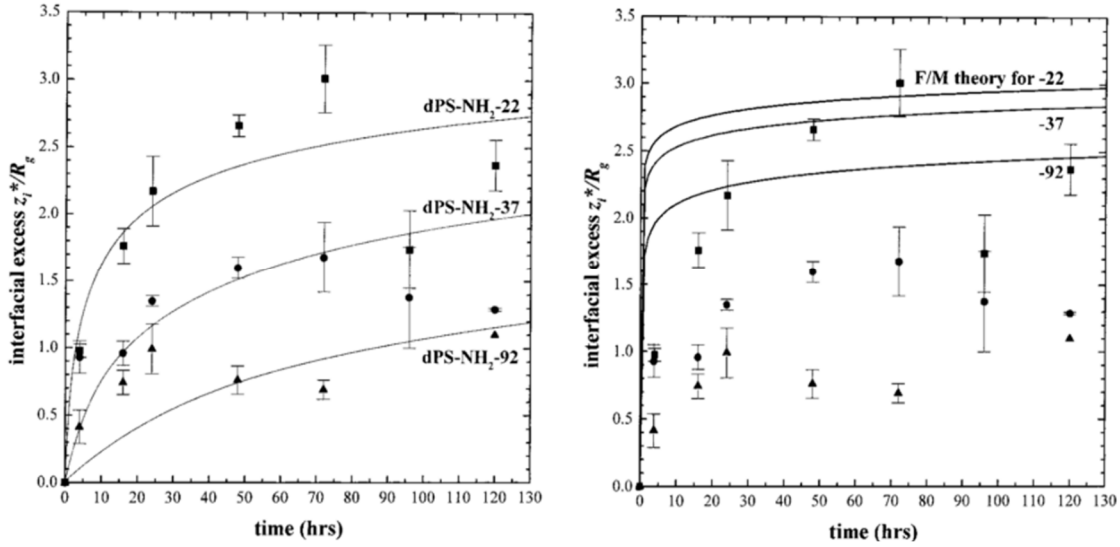

Figure 1.15. Kinetics data for PS/PMMA bilayers from Schulze et al., with second order kinetic fittings (left) and diffusion, first order kinetic fittings (right).[73]

Many other examples of second order kinetics fitting experimental data are present in the literature. Jeon and Kim showed that the reactive blend of acid functional

PS (PS-*g*-COOH) and a random copolymer of methyl methacrylate and glycidyl methacrylate (PMMA-*co*-GMA) is fit well by second order kinetics, but not first order (diffusion-controlled).[74] Jeon et al. showed that second order kinetics fitting adequately described reaction kinetics between PMMA-anh and PS-NH_2.[38] Also, Hu and Lambla were able to fit hydroxyl functional PS (PS-OH)/poly(ethylene-*co*-vinyl acetate) (EVOH) kinetics with a second order, reaction limited model.[75] However, second order kinetics models break down at high interfacial coverage, when reaction is hindered by a crowded interface.

1.7.3 Interface limited model

Authors have erroneously adopted a diffusion-limited model for two reasons: (1) increasing reactive polymer molecular weight slows down kinetics (Schulze et al.,[64] hypothesizes this is due to more interface being covered), and (2) first order kinetics are observed for some systems, particularly at long timescales or high block copolymer surface coverage. Oyama and Inoue reconciled these observations with second order kinetics (reaction limited) by proposing an interface-limited kinetics model where the rate is controlled by the amount of interface available to reactive groups (similar to gas-solid interfacial reactions in surface science).[76] The reaction rate equation is similar to the elementary second order rate law, but with an additional factor ($\Sigma^* - \Sigma$), where Σ^* is the saturation block copolymer area concentration, as shown in equation (6). This expression applies to most systems, where C_A, $C_B >> C_{copolymer}$.

$$\frac{dC_{copolymer}}{dt} = kC_A C_B \left(\Sigma^* - \Sigma\right) \tag{6}$$

The model results in second-order kinetics at low conversions and first order kinetics at high conversion. Experimentally, this has been observed on many occasions, where the rate of conversion to copolymer slows dramatically over time, despite having an excess of reactive groups available in the bulk. Oyama and Inoue's model assumes a flat interface with monolayer coverage of block copolymer at complete conversion, so it does not account for surface roughness or micelles being ejected from the interface. This

model does, however, manage to capture the time scale differences in reactions at polymer-polymer interfaces, namely that they are reaction limited at early timescales (second order), and interface/site limited at longer timescales (pseudo-first order). This model successfully fits data from several experiments,[77,78] one of which is shown in Figure 1.16. For the reaction between PS-COOH and an epoxy surface, the diffusion limited model from Fredrickson and Milner is inappropriate, but the interface limited model is quite accurate.

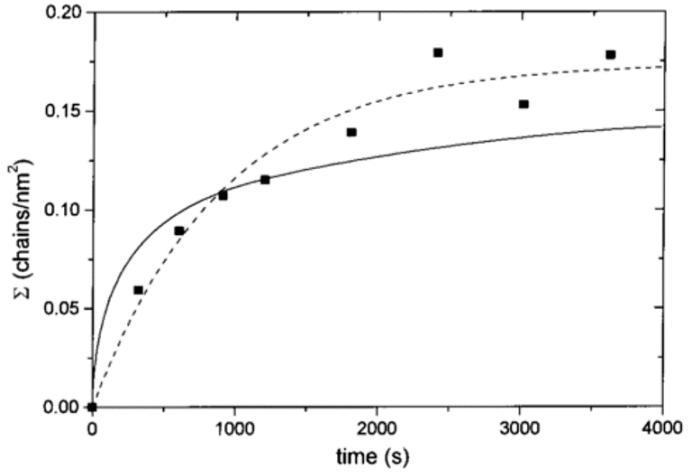

Figure 1.16. Interfacial copolymer coverage versus time for PS-COOH reaction with epoxy interface[78] (■), interface-limited fit (dashed line), and diffusion limited fit[70] (solid line), reproduced from Oyama and Inoue.[76]

Kim et al. also show the transition from second order to pseudo-first order in experiments by reacting PS-*g*-COOH with PMMA-*co*-GMA at a flat interface, and estimating conversion based on complex viscosity values over time. The kinetic data for this reaction are shown in Figure 1.17, with first order (right) and second order (left) fits. Here, M is the initial ratio of epoxy to acid groups, C_{B0} is the starting concentration of epoxy groups, and X_A is the conversion of acid groups at a given time. At low conversion (or time) the second order model fits well, but at longer times the first order model fits better.

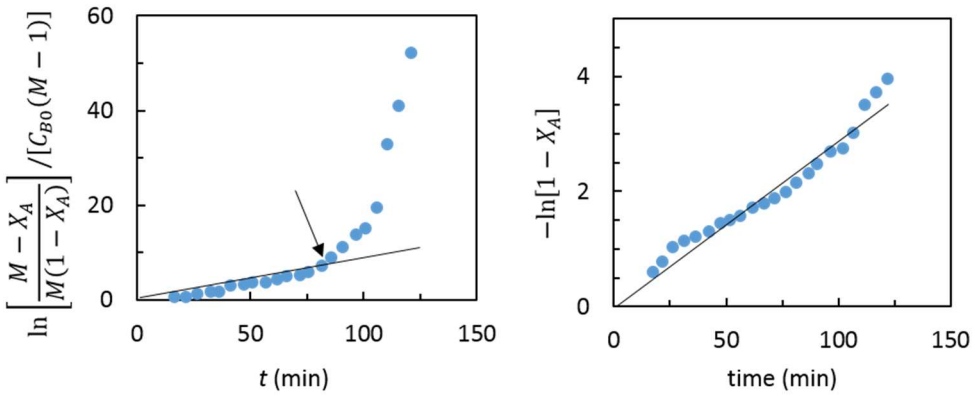

Figure 1.17. Second order and first order kinetic fits for PS-*g*-COOH/PMMA-*co*-GMA reaction, from Kim et al.[59] Arrow indicates transition from second order kinetics to first order kinetics.

1.8 Conclusions

Polymer blending is a practical, economical method employed to obtain useful materials. Most polymer blends are immiscible and require compatibilizer to aid dispersion in the melt state and transfer stress across interfaces in the solid state. Block copolymers have been proven to be successful compatibilizers, both premade and reactively formed. The reaction at immiscible polymer interfaces is reaction and interface limited, so faster reactions are desired for applications. Work is ongoing to understand the effects of compressive flow and catalysts on reaction rate.

Chapter 2. Reactive compatibilization of polyolefins and poly(methyl methacrylate) (PMMA)

2.1 Summary

This work attempts to compatibilize polyolefins and PMMA using reactive compatibilization. Previous co-authored work examined reactive compatibilization between various functional polyolefins and PMMA[55] and the effects of PE-*g*-PMMA[11] and PMMA-*b*-PE-*b*-PMMA[12] on mechanical properties of PE/PMMA blends.

In this chapter, early attempts to blend ATRP synthesized amine functional PMMA (PMMA-NH_2) and commercial maleic anhydride graft functional isotactic polypropylene (iPP-g-MA) showed some positive results, including decreased droplet size and increased complex viscosity of reactive blends compared to non-reactive blends. PMMA-NH_2 has been used previously for reactive compatibilization and adhesion experiments, but this work reveals that it is thermally unstable. It is suspected that the amine end group may attack PMMA ester groups in a backbiting or grafting reaction. Therefore, efforts were devoted to using a catalyzed ester exchange reaction between hydroxyl-end functional PE (HO-PE-OH) and the methyl ester of PMMA. The catalyzed blends display improved compatibility compared to uncatalyzed blends, but are still limited by slow kinetics and catalyst aggregation.

2.2 Introduction and motivation

Polymers are used in a wide variety of applications, including consumer products, packaging, and construction. Since most polymers are oil derivatives, their value to society is dependent on a non-renewable resource. Therefore, using polymers more efficiently is essential. Also, many polymers are used in vehicles and packaging,[79] so improving strength and reducing weight results in decreased energy consumption.

Two important classes of industrial polymers are polyolefins (especially, iPP and PE) and methacrylates. iPP and PE are the most widely used commodity plastics, at 53

and 78 million metric tons per year in 2012, making up over 60% of global polymer production.[80] They have excellent chemical resistance, thermal stability, and are relatively inexpensive.[81] Polyolefins are typically used in packaging, vehicle parts, fabrics, and as engineering thermoplastics.[79] However, their main drawbacks include low scratch and UV resistances, brittleness, and sensitivity to oxidation.[82] Meanwhile, methacrylates such as PMMA are known for hardness, UV resistance, and excellent optical properties.[79] PMMA is more expensive at about $3.80/kg,[83] and was produced at a mass of 1.1 million tons in 2006.[84] Since PMMA has good attibutes in several areas polyolefins do not (e.g. scratch and UV resistance), blending the two may enhance their physical properties and enable new applications.

In addition to wide applicability and financial incentives to creating improved polyolefin and PMMA materials, there is also potential to improve the fundamental understanding of these types of blends. Although polyolefin and PMMA blends have been reported in the literature,[85–89] their physical property improvements have not been fully exploited or understood.

Compatibilizing iPP/PMMA blends is difficult, due to large viscosity differences, high χ parameter, and difficulty in adding chemical functionality to iPP. Fly ash and carbon black have been used as physical compatibilizers, but only the morphology and thermal properties of the blends were explored.[85,86] Chung et al. made iPP-*g*-PMMA by synthesizing a random copolymer of iPP and a borane-containing monomer, then polymerizing PMMA grafts using oxygen in the presence of methyl methacrylate monomer. This copolymer led to finer morphology in 70/30 blends of iPP/PMMA. Souza et al. showed PP-*g*-PMMA decreased drop size and increased low frequency modulus in rheology as well.[90] To our knowledge, there are no studies demonstrating reactive compatibilization of iPP and PMMA at this time.

PE/PMMA blends have more compatibilizer chemistries available than iPP/PMMA blends. Song et al. used reactive compatibilization between hydroxyl, amino, and cyclic anhydride functional poly(propylene-*co*-ethylene) (PPE) and PMMA.[55] The

amine functional PPE was the most effective at improving adhesion in bilayers and dispersion in blends. The resultant compatibilized blends showed improved modulus, scratch resistance, and hardness compared to the non-reactive blends. The same study found a LLDPE-g-PMMA (made from controlled radical PMMA growth from LLDPE-*g*-hydroxyl) was also an effective adhesion promoter between LLDPE and PMMA. Commercial copolymers of PE with polar monomers, such as poly(ethylene-*co*-vinyl acetate), poly(ethylene-*co*-methyl acrylate), poly(ethylene-*co*-glycidyl methacrylate), and poly(ethylene-*co*-vinyl alcohol), all have the potential to improve compatibility in PE/PMMA blends. Generally these structures are made by high pressure copolymerization, leading to branched structures that are more compatible with LLDPE than HDPE. Badel et al. made LLDPE-*g*-PMMA by reacting polyethylene with a peroxide and methyl methacrylate in melt blending, showing the formation of LLDPE-*g*-PMMA decreased droplet size.[91] Xu et al. synthesized PE-*g*-PMMA and PMMA-*b*-PE-*b*-PMMA compatibilizers, showing that these improved dispersion, hardness, modulus, and scratch resistance of HDPE/PMMA and LLDPE/PMMA blends.[11,12] Despite these advances, there is clearly a need for a reactive compatibilization system with fast kinetics at the interface.

This study creates a reactive compatibilization system for polyolefin/PMMA blends. Section 2.2 describes applies very fast amine/anhydride reactions to iPP/PMMA blends. Section 2.3 uses catalysis to react PMMA ester groups with hydroxyl-functional HDPE.

2.3 PMMA-NH_2 / iPP-*g*-MA blends

The simplest approach to reactive compatibilization is using a fast reaction (namely, amine/anhydride) and commercially available functional polymers. For polyolefins, cyclic anhydride functional compatibilizers are the most common, which react quickly with primary amines. Therefore, a model system was devised for the reactive compatibilization of PMMA and iPP using amine and anhydride functional groups, summarized in Table 2.1. Amine end–functional PMMA (PMMA-NH_2) was

synthesized using atom transfer radical polymerization (ATRP) with a tertbutyloxycarbonyl (t-BOC) protected functionalized initiator, t-BOC-aminopropyl 2-bromoisobutyrate.[92–94] Analogous, non-functional PMMA samples were synthesized using 2-ethyl bromoisobutyrate initiator. Maleic anhydride grafted isotactic polypropylene (iPP-*g*-MA), created through a reactive extrusion process, was obtained from Dupont (Fusabond 613). The objective of this system is to form imide bonds at the interface of blends (from the anhydride/amine addition reaction) to improve compatibility.

Table 2.1. Polymer characteristics for PMMA-NH_2/iPP-*g*-MA system

material	M_n (kg/mol)	$Đ$	T_g (°C)	functionality	source
iPP-*g*-MA	23[a]	3.4[a]	-	0.7 wt %MA	Fusabond 613
PMMA-NH_2	51[b]	1.1[b]	119[c]	One NH_2 per chain	ATRP
PMMA	59[b]	1.1[b]	126 [c]	None	ATRP

[a]High temperature SEC at 160 °C in trichlorobenzene and polystyrene standards. [b]Room temperature SEC in tetrahydrofuran with UV-vis and light scattering detectors. [c]TA Discovery DSC at a ramp rate of 5 °C/min on the second heating. [d]Titration with sodium methoxide in methanol and thymol blue indicator.

2.3.1 Synthesis

The synthesis of t-BOC-aminopropyl 2-bromoisobutyrate was performed as described in Boyer et al.,[93] are shown in Figure 2.1. Further purification was necessary using flash chromatography, as outlined in Still et al. and Weitman et al.[95,96] A 4:1 hexane:ethyl acetate solvent and silica column were used, resulting in three separate products. T-BOC-aminopropyl 2-bromoisobutyrate was the second product from the column, a colorless viscous liquid, as verified by ^{1}H NMR and ^{13}C NMR (300 MHz, $CDCl_3$, Figure 2.2).

ATRP was performed using t-BOC-aminopropyl 2-bromoisobutyrate initiator, as outlined in Robin et al.[94] Molar ratios of monomer:initiator:metal halide:ligand were 100:1:1:0.3. Anisole solvent was stirred with the reagents in a reaction flask, degassed

with bubbled argon for 30 min, and heated to 60 °C for 4 h. The polymer was precipitated in methanol, filtered, dissolved in ethyl acetate, and passed through a silica column to remove copper compounds. Final purification was performed by dropwise precipitation in hexane. The product, a white powder, was verified as PMMA-NH_2 by ^{1}H NMR spectroscopy (Figure 2.3).

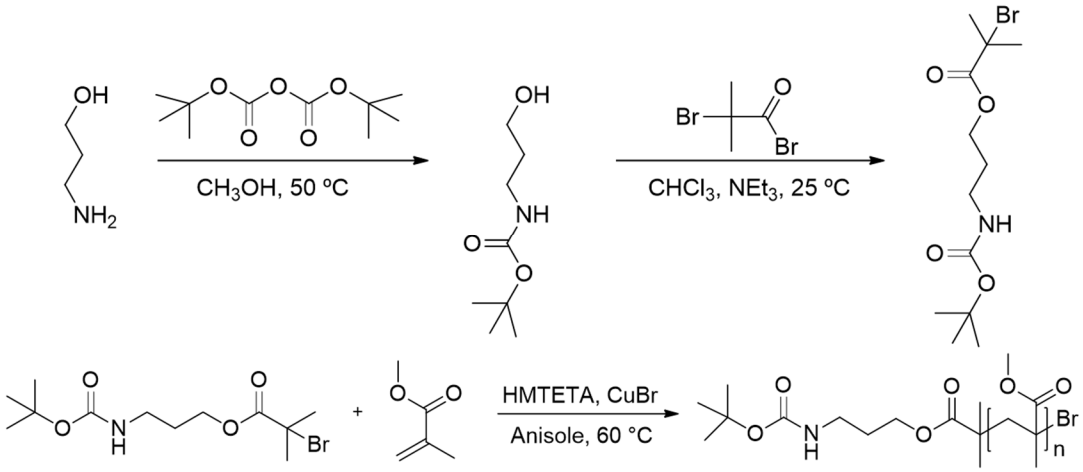

Figure 2.1. Reaction schematics for t-BOC-aminopropyl 2-bromoisobutyrate and PMMA-NH_2 polymerization.

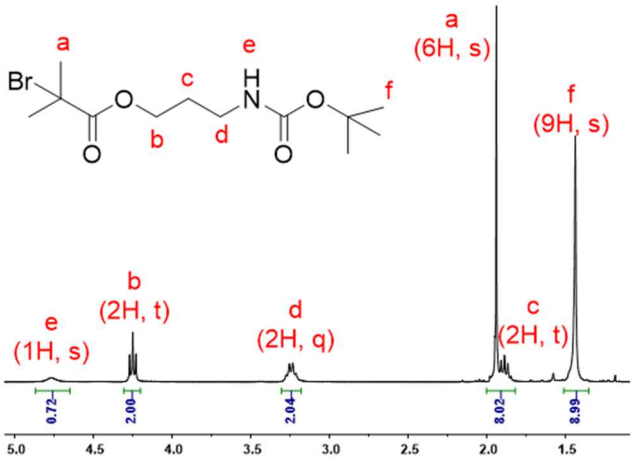

Figure 2.2. t-BOC-aminopropyl 2-bromoisobutyrate ^{1}H NMR spectrum.

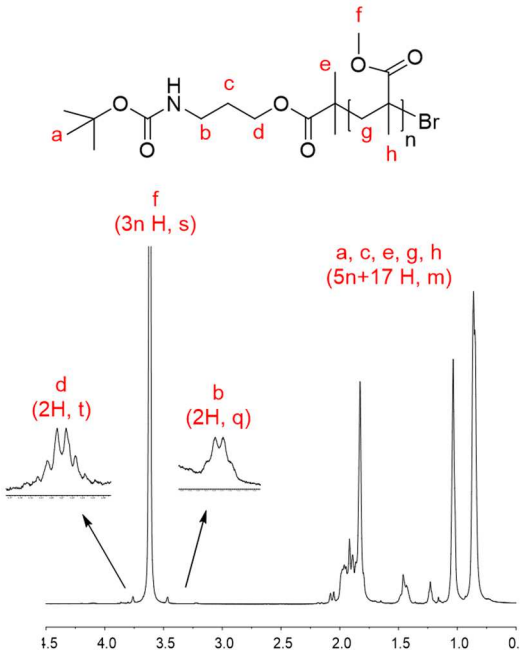

Figure 2.3. ^{1}H NMR of PMMA-NH_2 spectrum ($CDCl_3$, 500 MHz).

T-BOC groups are compatible with radical polymerizations,[97] and are commonly used for amine protection in small molecule synthesis.[92] They are acid labile, but can also be removed with heat. Experimental values for thermal deprotection temperatures range from 65 °C to 270 °C, but are usually around 150 °C for primary amines.[97,98] "Protecting Group Chemistry" describes the decomposition mechanism (Figure 2.4), which occurs around 150 °C and produces carbon dioxide and isobutylene vapors.[99] This is convenient for melt blending, since the protecting group is removed without additional processing steps. If deprotection is desired before heating, trifluoroaceticacid can deprotect the amine in solution.

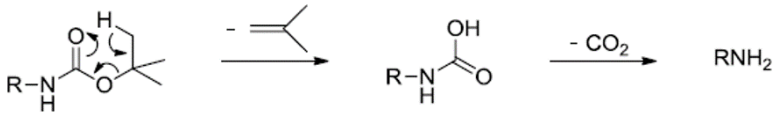

Figure 2.4. Thermal deprotection mechanism for t-BOC protected primary amine above 150 °C. Products are isobutylene, carbon dioxide, and a primary amine. Adapted from "Protecting Group Chemistry".[99]

Identical procedures were followed to obtain a non-reactive control material for PMMA-NH_2. ATRP was performed as in the PMMA-NH_2 synthesis, but t-BOC-aminopropyl 2-bromoisobutyrate was substituted with 2-ethyl bromoisobutyrate. This initiator is commonly used for PMMA ATRP syntheses,[100–102] and has a similar structure to the functionalized initiator. Therefore, the two initiators should have similar kinetics.[103] PMMA was obtained after a reaction time of four hours, verified by ^{1}H NMR spectroscopy.

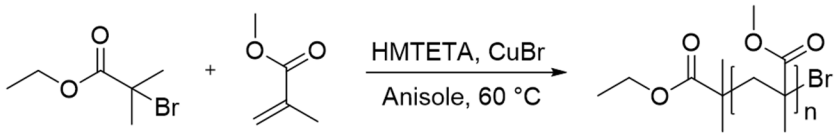

Figure 2.5. ATRP synthesis of PMMA using 2-ethylbromoisobutyrate initiator.

2.3.2 Processing

PMMA and PMMA-NH_2 powders were dried overnight in a 60 °C vacuum oven to remove excess moisture, and iPP-g-MA was dried in a room temperature vacuum oven for two hours before use. Subsequent drying was performed at these conditions between each processing step and before characterization, to remove absorbed water.

Blends of PMMA and PMMA-NH_2 with iPP-g-MA were prepared in a small batch DACA mixer at 210 °C and 200 rpm, mixing for 5 min. Both blends are approximately 80:20 iPP:PMMA by weight. These were then pressed into 25 mm disks using a hot press at ~2 MPa and 210 °C for 3 min.

2.3.3 Characterization

Thermal properties of the pure materials and blends were probed with DSC (Figure 2.6). The glass transitions for PMMA materials are around 120 °C, which is reasonable based on literature values.[79] iPP-*g*-MA shows multiple melting peaks on second heating, which indicates multiple crystal forms, matching previous results.[104] Blends yielded similar results to iPP-*g*-MA, which is expected since it is the majority component.

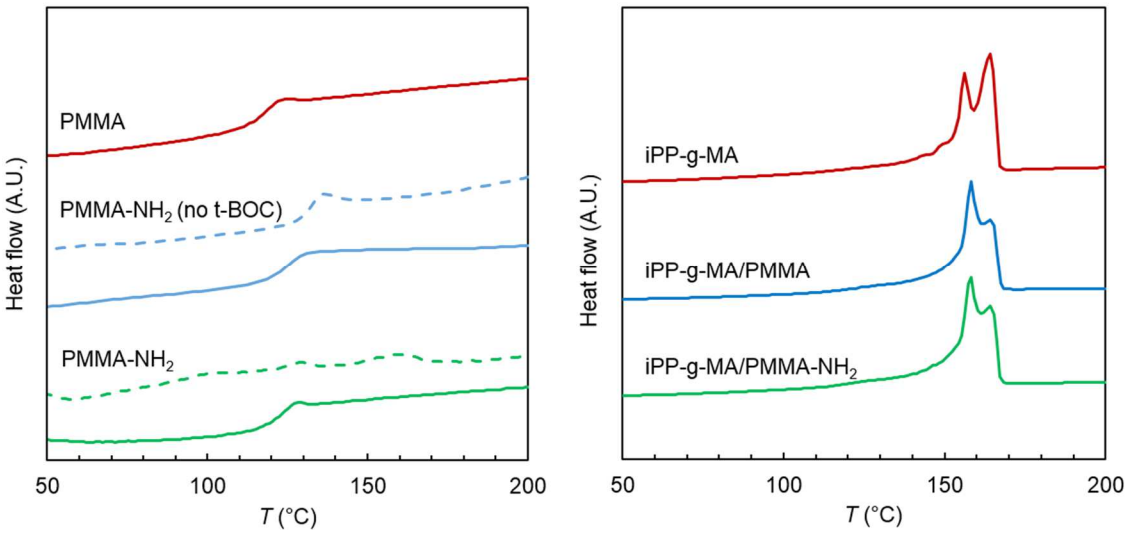

Figure 2.6. DSC of iPP/PMMA blends and neat materials. (left) DSC heating curves for PMMA and PMMA-NH_2, before and after deprotection (dashes are first heating, solid lines are second heating). (right) DSC second heating curves for iPP-*g*-MA, iPP-*g*-MA/PMMA, and iPP-*g*-MA/PMMA-NH_2. All data shifted vertically for presentation. Data was obtained on a TA Discovery DSC at a heating and cooling rate of 5 °C/min.

To verify the loss of the t-BOC protection groups during processing, the first heating cycles of the materials were examined. The t-BOC protected materials showed an increase in heat flow around 150 °C, suggesting successful deprotection of the amine groups. This peak was not shown in second heating of the same material. To verify the peak at 150 °C is associated with deprotection, the t-BOC group was cleaved with weak acid, as described by Robin et al.[94] The deprotected PMMA-NH_2 showed no exotherm at 150 °C on first heating, verifying the t-BOC group is thermally labile. The exotherm at 100 °C (green dashed line) is attributed to absorbed water.

Rheology data were obtained to determine viscosities and moduli of neat materials and blends. Pressed discs were loaded on an ARES rheometer with 25 mm parallel plates at 210 °C. Strain sweeps indicated the linear viscoelastic region (where G′ and G” are 90% or greater of their small strain limit), setting a maximum strain for future tests. A dynamic frequency sweep was performed at 210 °C (Figure 2.7). As expected, PMMA has a much higher viscosity than iPP-g-MA. The iPP-*g*-MA/PMMA-NH_2 blend

has a higher viscosity than the iPP-*g*-MA/PMMA blend, possibly indicating an increase in stress transfer across the interface with the addition of amine groups. This is an indication of increased compatibility between phases.

Rheology data suggest there is another reaction occurring in the pure PMMA-NH_2, even after removal of the t-BOC group. Samples on the rheometer foamed visibly at early times, rendering data not usable. After re-pressing and loading the same material, foaming was reduced, but the viscosity and stiffness was high (data shown in Figure 2.7). After re-pressing several times, the slopes for G' and G" were nearly flat, suggesting crosslinking is occurring. Small bubbles were still forming after many hours at 210 °C. These observations can be explained by amine end groups reacting with ester groups on other PMMA chains, releasing methanol gas.

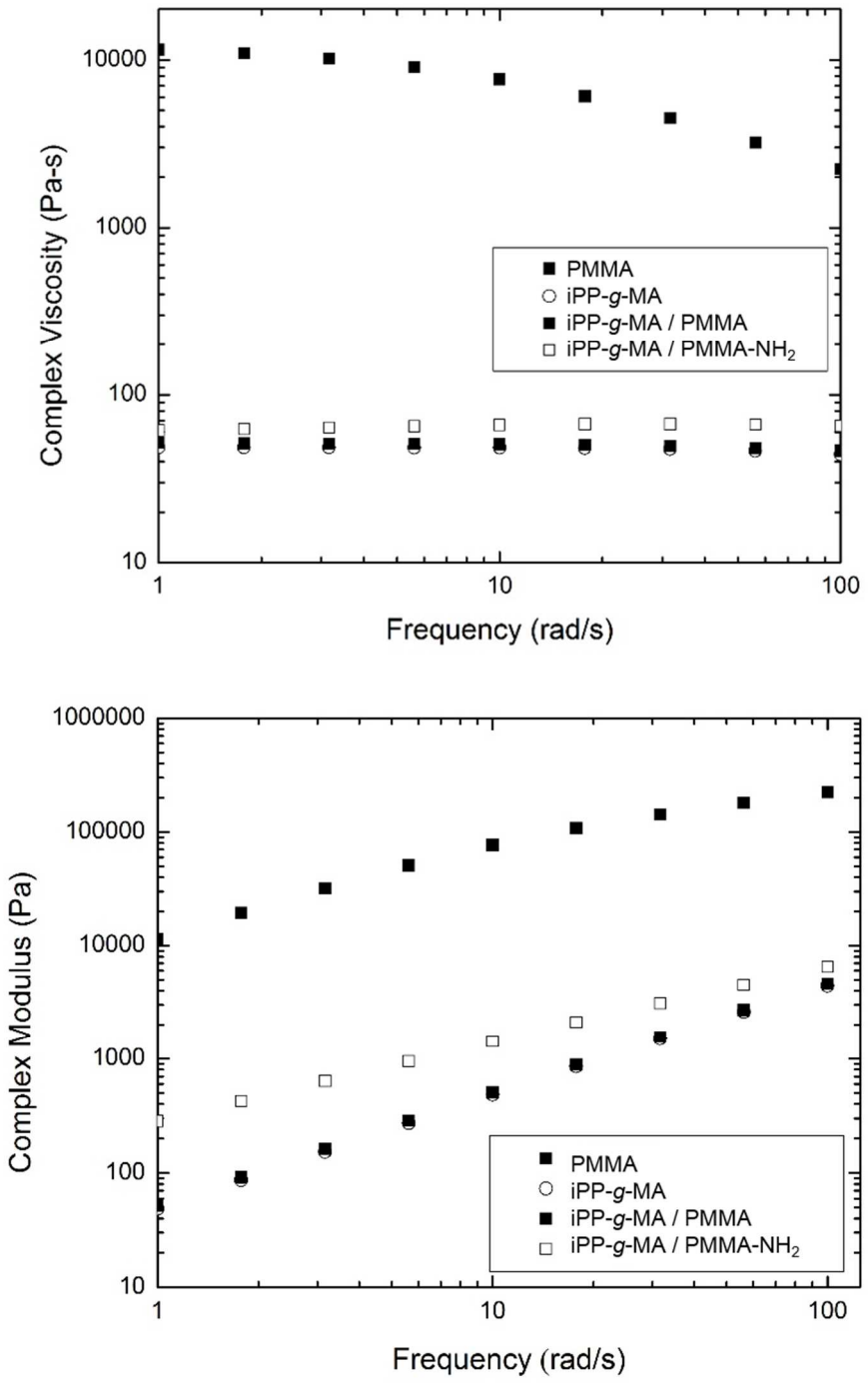

Figure 2.7. iPP/PMMA system rheology. (left) Complex viscosity of neat materials and blends as a function of frequency. (right) Modulus as a function of frequency.

It is interesting that amines have been used in reactive compatibilization studies with the ester groups on PMMA,[55] but amine terminal PMMA has also been used for reactive compatibilization.[36,94] It is possible that the maleic anhydride/amine reaction dominates, since it has faster kinetics and is more thermodynamically favored.

SEM images of the droplet blends were obtained from a JEOL 6500 FEG-SEM after microtoming and washing out PMMA droplets with acetone, then coating the surface with 50 Å Pt. Particle sizes were measured with ImageJ software (NIH) and analyzed in JMP fit distribution platform. Representative images of iPP-*g*-MA/PMMA and iPP-*g*-MA/PMMA-NH_2 blends are shown in Figure 2.8. When both amine and maleic anhydride functional groups are present, the number average particle size is markedly smaller. The compatibilized particles are still larger than one micron, but this is likely due to the large viscosity differences between the two phases.

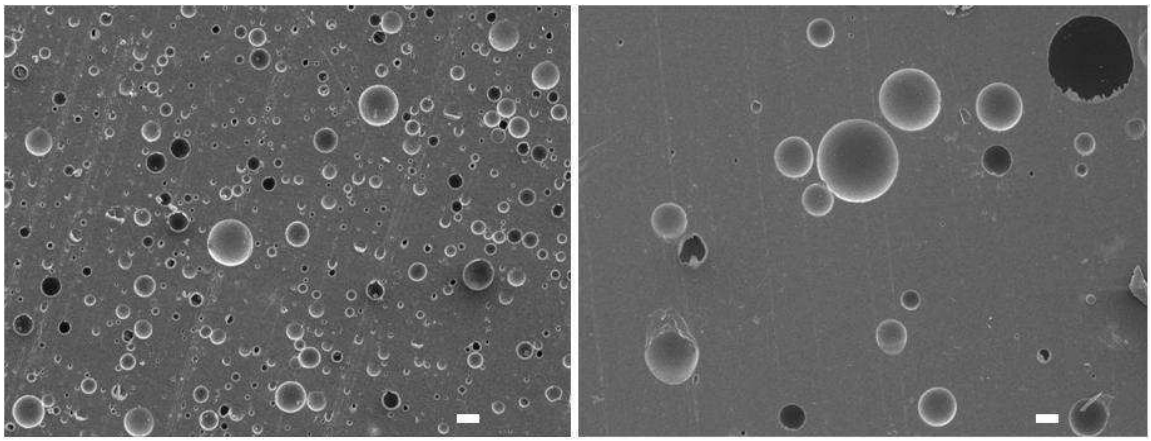

Figure 2.8. SEM images iPP/PMMA blends. (left) iPP-*g*-MA/PMMA-NH_2, (right) iPP-*g*-MA/PMMA (scale bar is 10 µm).

2.3.4 Conclusion

This evidence shows the potential of a maleic anhydride/amine reactive system to improve the compatibility of iPP/PMMA blends. However, the processing stability of

PMMA-NH_2 remains a challenge. We suspect that the amine group reacts with PMMA ester groups at all available processing temperatures (180 – 210 °C).

2.4 HDPE / HO-PE-OH / PMMA / catalysts system

Maleic anhydride or epoxy functional polyolefins are most commonly used for reactive compatibilization with polar polymers. Since neither of these groups reacts with the ester groups of PMMA, and the groups that react most quickly with functional polyolefins cannot be added to PMMA (amine), catalysis is employed to increase the ester reaction rate with more stable functional groups on polyolefins (in this case, hydroxyl). Hydroxyl end–functional polyethylene was created using ring opening metathesis polymerization, and melt mixed with PMMA in the presence of ester exchange catalysts.

2.4.1 Materials

Telechelic α,ω-hydroxyl functional PE (HO-PE-OH) was synthesized to react with the methyl ester of PMMA. HO-PE-OH was synthesized based on the procedure described in Pitet et al.[105] (Figure 2.9). Cis-cyclooctene (Arcos, 95%, stabilized) was dried with calcium hydride and distilled under vacuum to remove impurities. 1,4-diacetoxy-2-butene chain transfer agent (Sigma-Aldrich, 95%) was distilled over calcium hydride. Stannous octoate was distilled under vacuum at elevated temperature. Tetrahydrofuran (FisherScientific, ACS grade) was dried over alumina columns.[106] Grubbs 2nd generation catalyst (Sigma-Aldrich), sodium methoxide (Sigma-Aldrich, 30 wt.% in methanol), decanes (Sigma-Aldrich, anhydrous, 99%), methanol (Sigma-Aldrich, ACS grade), hexadecanoic acid (Arcos, 98%), hexadecanol (Sigma-Aldrich, 99%), and tin chloride dihydrate (Sigma-Aldrich, ≥99.99%) were used as received. PLA (Natureworks 2003D) and HDPE (Dow Chemical Co, DMDA 8904 NT-7) were dried for 12 hours under vacuum at 60 °C and stored in air-tight containers. Synthesis of hydroxyl functional polyethylenes are described below.

Synthesis of PCOE was performed as follows. Approximately 200 mL dry THF was added to a 500 mL reaction flask with 0.31 mL 1,4-diacetoxy-2-butene and a stir bar. 15 mg Grubbs' 2nd generation catalyst was dissolved in 1 mL THF and added by gas tight syringe. 40 g *Cis*-cyclooctene was slowly added at a rate of 1 mL/min at 35 °C, and was left stirring overnight. Diacetoxy-functional poly(cyclooctene) was precipitated in cold methanol and dried under vacuum overnight (white powder, 37.1 g, 93% yield, Figure 2.10).

HO-PCOE-OH was synthesized as follows. The dried PCOE product was dissolved in 300 mL THF at 35 °C and reacted with 14 mL sodium methoxide solution (2.5 × stoichiometric) over six hours. Hydroxyl-telechelic poly(cyclooctene) (HO-PCOE-OH) was precipitated and dried under vacuum (white powder, 34.8 g yield, 94% yield, 93% conversion to –OH, Figure 2.11).

HO-PE-OH was synthesized as follows. 7.0 g HO-PCOE-OH was added to a high pressure hydrogenation reactor with 800 mL cyclohexane and 1.5 g Pt-Re/SiO_2 catalyst (provided by Dow Chemical Co.). 600 psi hydrogen was introduced, and the reactor was heated to 90 °C for 24 hours while stirring. After cooling and venting, the solvent was removed by filtration (Millipore, product GVHP09050) and replaced with decanes. The heterogeneous catalyst was subsequently removed by filtration at 140 °C (Millipore, product GPWP09050). Upon cooling, HO-PE-OH precipitated from decane in the filtrate, and the final polymer was separated from decane by vacuum filtration (white powder, 4.9 g, 70% yield, ~0.8 double bonds remaining per chain, Figure 2.12).

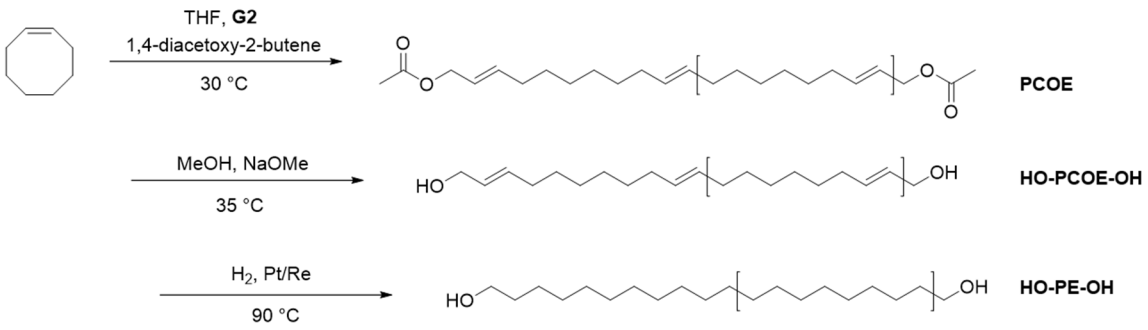

Figure 2.9. Synthetic route to HO-PE-OH

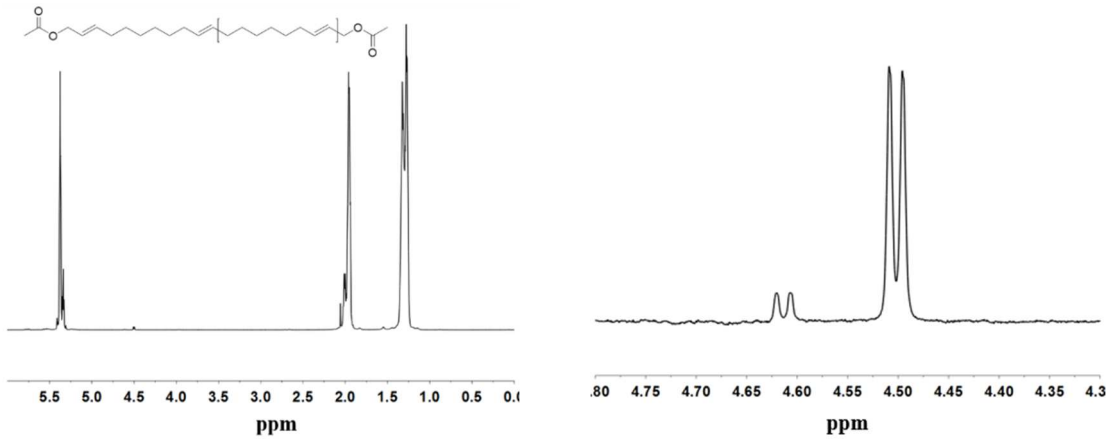

Figure 2.10. PCOE room temperature ^{1}H NMR spectrum (Bruker 500 MHz, $CDCl_3$, *d1* = 20 sec, *at* = 6 sec, *n* = 32 scans). Doublets at 4.62 and 4.50 ppm represent *cis* and *trans* hydrogens next to end groups, respectively. Integration for end group analysis estimates $M_n \approx 22$ kg/mol.

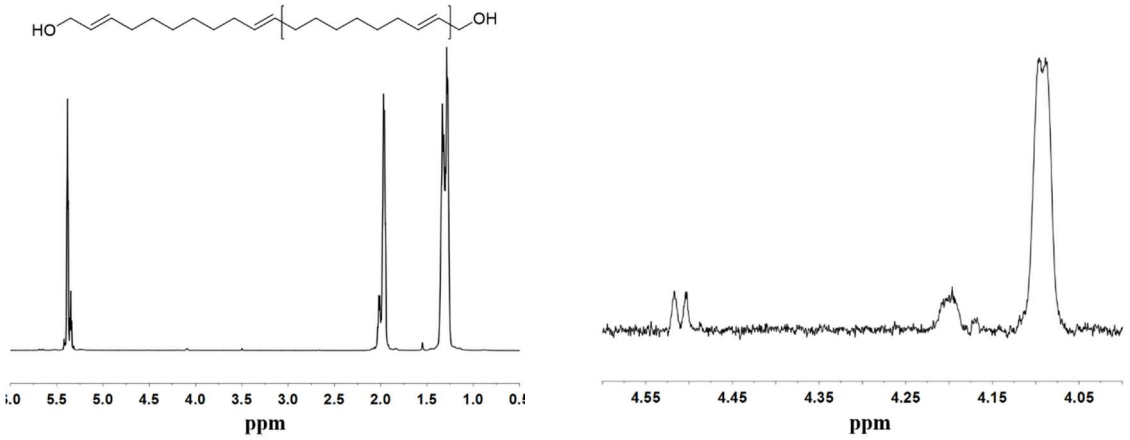

Figure 2.11. HO-PCOE-OH room temperature ^{1}H NMR spectrum (Bruker 500 MHz, $CDCl_3$, *d1* = 20 sec, *at* = 6 sec, *n* = 32 scans). Doublet at 4.50 ppm represents *cis* hydrogens next to unreacted end groups. Comparing the integration of these peaks to those at 4.20 and 4.08 ppm shows 93% conversion to –OH end groups. End group analysis estimates $M_n \approx 23$ kg/mol.

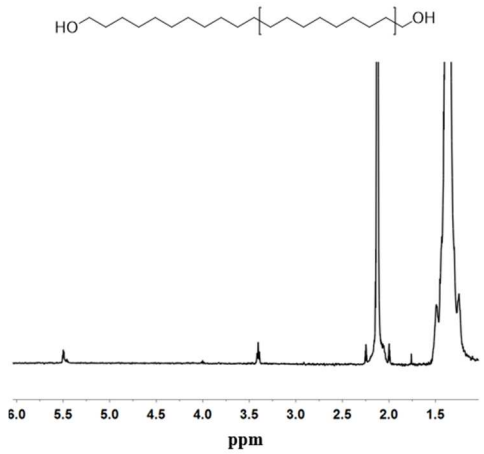

Figure 2.12. HO-PE-OH 100 °C ^{1}H NMR spectrum (Bruker 500 MHz, *d*-toluene, *d1* = 20 s, *at* = 6 s, *n* = 32). End group analysis estimates $M_n \approx 27$ kg/mol, confirmed by high temperature SEC (M_n = 28 kg/mol, $Đ$ = 1.7). Integration of the peak at 5.49 ppm indicates approximately 0.9 double bonds left per chain.

Extrusion grade HDPE was graciously provided by Dow Chemical (DMDA 8904 NT-7) to act as a diluent for HO-PE-OH. Low molecular weight PMMA was purchased from Sigma-Aldrich, for viscosity matching to HDPE. The summary of polymer characteristics is shown in Table 2.2.

Table 2.2. Polymer characteristics for HDPE/HO-PE-OH/PMMA system

polymer	M_n (kg/mol)	$Đ$	η_0 [c] (Pa s)	T_m [d] (°C)	T_g [d] (°C)
HDPE	32[a]	2.4 [a]	2600	132	-
PMMA	21[b]	1.6[b]	3600	-	115
HO-PE-OH	27 [a]	1.7 [a]	190	130	-

[a]High temperature SEC (135 °C, trichlorobenzene, RI detector, PS standards). [b]Room temperature SEC (THF, UV-vis and LS detectors). [c]Dynamic frequency sweep at 200 °C, Cross model fit, Cox-Merz rule applied. [d]TA Discovery DSC at a ramp rate of 5 °C/min on the second heating.

Rheological measurements were performed to ensure droplet breakup and coalescence will occur in melt blending (roughly, η of all components within one order of magnitude). Time sweeps were performed for over an hour to ensure stability and strain sweeps were performed to determine the limit of the linear viscoelastic regime (LVE). Frequency sweeps were performed in the LVE (Figure 2.13) at the melt blending temperature, 200 °C, using parallel plates on a strain controlled ARES rheometer. HDPE and HO-PE-OH are expected to be miscible, with their combined viscosity (estimated by log volume fraction mixing rule) within an order of magnitude of PMMA.

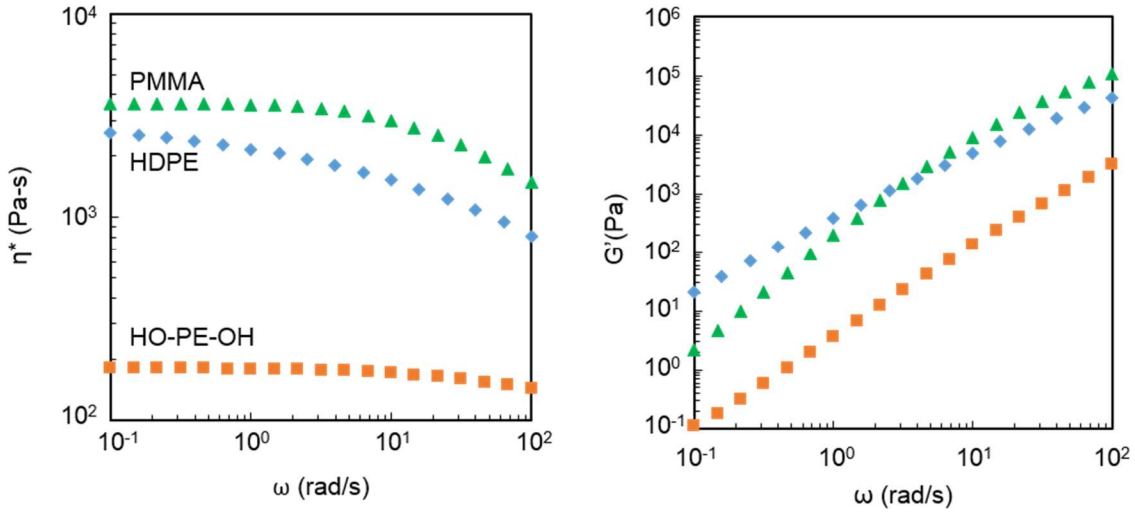

Figure 2.13. Frequency sweep data for PMMA / HDPE / HO-PE-OH / catalyst system. (left) Viscosity as a function of frequency, (right) elastic modulus as a function of frequency.

2.4.2 Catalysts

The hydroxyl/ester reaction is known to be slow. Orr et al. reported no conversion for an alcohol/acid reaction in homogeneous end-functional polystyrene blends,[36] and esters are typically less reactive towards hydroxyl groups than acids. Therefore, transesterification catalysts will be necessary to improve reaction kinetics. Catalysts were chosen based on (1) degradation temperature (above melt blending temperatures), (2) known activity towards ester exchange, (3) vapor pressure and melting temperature (liquid at melt blending temperatures), and (4) solubility parameter/surface energy. The catalysts need to be stable, active, and able to flow, and the hypothesis for this work is that catalysts need to localize at the interface to be effective. Therefore, catalysts that wet PE/PMMA interfaces are desirable. Table 2.3 summarizes the catalysts used in this study.

Stannous octoate (or tin (II) ethylhexanoate) has been used in reactions over 200 °C, suggesting it is stable at melt mixing temperatures.[107] All materials should be liquids at the melt processing temperature, except for $Zn(Ac)_2$. All catalysts were ordered from Sigma-Aldrich, and used as received.

Table 2.3. Catalysts properties summary

catalyst	abbr.	T_{deg} (°C)	T_m (°C)	δ ($MPa^{1/2}$)	appearance
stannous octoate	$Sn(Oct)_2$	N/A	< 25	20.0[b]	clear liquid
tin chloride dihydrate	$Sn(Cl)_2$	N/A	38[a]	48.9[b]	white solid
stannous stearate	$Sn(St)_2$	N/A	< 25	~22 [b]	grey solid
zinc acetate	$Zn(Ac)_2$	237[a]	N/A	~25[c]	white powder
zinc acetylacetonate hydrate	$Zn(Acac)_2$	N/A	135[a]	~24[c]	white solid

[a]Sigma-Aldrich MSDS. [b]Estimated from Fedors[108] lyoparachor method. [c]Estimated from Fedors[108] energy of vaporization method.

2.4.3 Small molecule model reactions

Small molecule model reactions were performed to evaluate catalyst activity, and determine if this reaction generates enough product for reactive compatibilization. Hexadecanol was reacted with methyl stearate (HO-PE-OH and PMMA analogs, respectively) in a 100 mL 3-necked flask equipped with condenser at 200 °C at 5 mL

scale (miscible reactants in bulk). The proposed reaction is an ester exchange, shown in Figure 2.14, which gives off methanol vapor. Water above the vaporization temperature of methanol was used in the condenser to allow methanol to leave, driving the reaction to completion. It is expected that the long hydrocarbon tails on the reagents will be similar to the solvent quality in melt mixing. Hexadecanol was chosen as the limiting reagent, to further emulate the melt reaction between HO-PE-OH and PMMA.

Figure 2.14. PMMA/HO-PE-OH small molecule model reaction scheme

An example reaction procedure follows. An oil bath was heated to 200 °C, using foil for insulation. 1.254 g hexadecanol, 3.094 g methyl stearate (2:1 molar ratio), and 0.011 g tin chloride dihydrate (0.01 M) were added to a reaction flask, using rubber stoppers on the side necks. A 50 °C water bath was used to heat the mixture above the melting point of the reagents. Immediately after melting, the flask was transferred to hot oil bath. Small aliquots were removed by gas tight syringe every 5 min, dispensing into a glass vial to quench the reaction.

Samples were dissolved in $CDCl_3$ for ^1H NMR spectroscopy (n = 16, $d1$ = 6 s, at = 2 s, 500 MHz, example spectra shown in Figure 2.15). Expected peaks for hexadecanol (t, 3.65 ppm) and methyl stearate (s, 3.68 ppm, d, 2.28 ppm) were observed for all samples. In addition, peaks of hexadecyl hexadecanoate product (t, 4.07 ppm, d, 2.28 ppm) appeared after reaction occurred. Conversion was calculated by comparing the integrations of peaks a, b, and c (equation (7), where $C_{MS,0}$ and $C_{HD,0}$ are the initial molar concentrations of methyl stearate and hexadecanol, respectively). This uses peak c as a basis, since it stays constant throughout the reaction, to eliminate concentration or signal differences between NMR samples.

$$X = \frac{\text{int}(H_b)}{\text{int}(H_c)} \times \frac{C_{MS,0}}{C_{HD,0}} \tag{7}$$

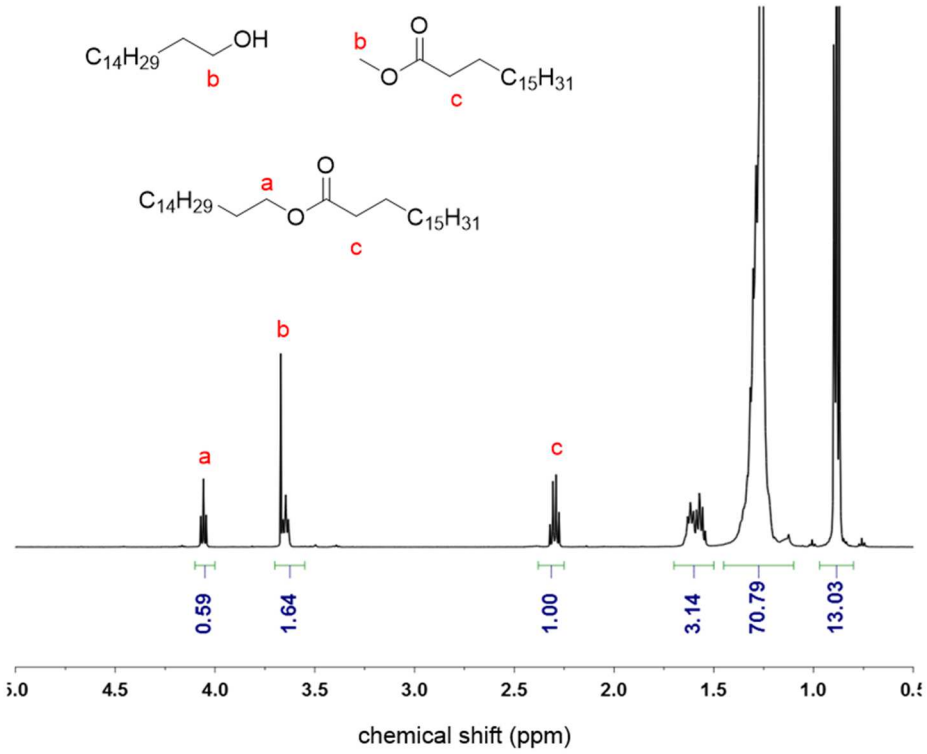

Figure 2.15. Sample ^{1}H NMR spectrum of catalyzed ester exchange reaction.

Second order equilibrium batch reactor kinetics apply to this situation, so equation (8) applies, where $X_{A,e}$ is the equilibrium conversion based on species A, X_A is the conversion based on species A at time t, C_{A0} is the initial concentration of limiting reagent A, and k is the second order reaction rate constant.

$$\ln\left(\frac{X_{A,e} - X_A(2X_{A,e} - 1)}{X_{A,e} - X_A}\right) = 2k\left(\frac{1}{X_{A,e}} - 1\right)C_{A0} \qquad (8)$$

Results are shown in Figure 2.16 (●) with lines showing kinetics least squares fits for $X_{A,e}$ and k. The second order equilibrium batch kinetics fit well, with equilibrium conversion constant around 0.8. $Sn(Oct)_2$ may be degrading during the reaction, lowering its efficacy over time, as shown by a reaction mixture color change to light yellow during the course of the reaction. This results in lower equilibrium conversion. $Sn(St)_2$ and uncatalyzed reactions show no conversion up to 1 hr.

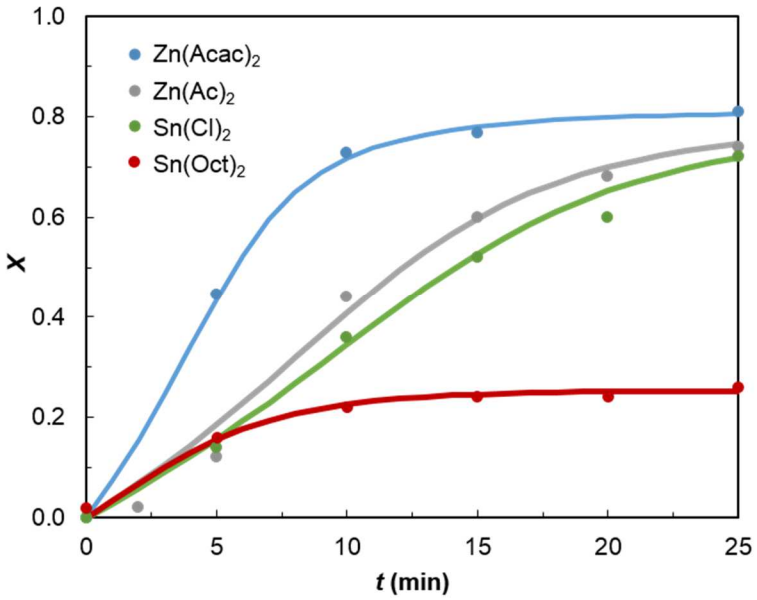

Figure 2.16. Small molecule reaction conversion and kinetic model fits

Fit parameters are shown in Table 2.4. $Zn(Acac)_2$ and $SnCl_2$ were heterogeneous (did not dissolve by eye, cloudy mixture), whereas all the other catalysts were miscible. $Sn(St)_2$ was eliminated due to no conversion. $SnCl_2$, $Zn(Ac)_2$, and $Zn(Acac)_2$ all show enough conversion that reasonable interfacial coverage could be achieved in melt mixing, given the same reaction rate constant (for uniform 1 μm diameter drops, same rate constant, and homogeneous reaction, surface coverage is estimated < 0.3 nm^2/chain in catalyzed blends).

Table 2.4. Ester/alcohol reaction rate constants

catalyst	k (M^{-1} min^{-1})
None	0
$Zn(Acac)_2$	0.19
$Zn(Ac)_2$	0.15
$SnCl_2$	0.14
$Sn(Oct)_2$	0.07
$Sn(St)_2$	0

2.4.4 Processing

Melt mixing was performed in a 500 mL Minimax cup and rotor mixer (Custom Scientific Instruments) with two ¼" diameter ball bearings added to improve mixing.[109,110] 90/10 PE/PMMA samples by weight were blended at 200 °C and 310 rpm for 5 min. Rheology samples were created in a twin screw 5 mL batch mixer (DACA Instruments) at 200 rpm and 200 °C, because larger samples were needed.

Table 2.5. HDPE / HO-PE-OH / PMMA / catalyst blend compositions

Blend	Composition HDPE/HO-PE-OH/PMMA/catalyst (wt fraction)
Non-reactive (NR), uncatalyzed	90 / 0 / 10 / 0
Reactive (R), uncatalyzed	60 / 30 / 10 / 0
Non-reactive (NR), $SnCl_2$	90 / 0 / 10 / 0.4
Reactive (R), $SnCl_2$	60 / 30 / 10 / 0.4
Non-reactive (NR), $SnOct_2$	90 / 0 / 10 / 0.8
Reactive (R), $SnOct_2$	60 / 30 / 10 / 0.8
Non-reactive (NR), $Zn(Ac)_2$	60 / 30 / 10 / 0.3
Reactive (R), $Zn(Ac)_2$	60 / 30 / 10 / 0.3
Non-reactive (NR), $Zn(Acac)_2$	90 / 0 / 10 / 0.5
Reactive (R), $Zn(Acac)_2$	60 / 30 / 10 / 0.5

2.4.5 Blend morphology

Droplet size in SEM is used as a screening method to determine if a compaibilization reaction is successful. Samples were quenched in liquid nitrogen immediately after blending to preserve morphology, and cryo-fractured to obtain a surface for imaging. Then, the PMMA was removed using a selective solvent (acetone or tetrahydrofuran for 24 h). The fractured surfaces were mounted on a carbon-tape covered SEM stub and coated with 50 Å Pt before imaging in a JEOL 6500 SEM (5 kV). Representative SEM images for all blends are shown in Figure 2.17.

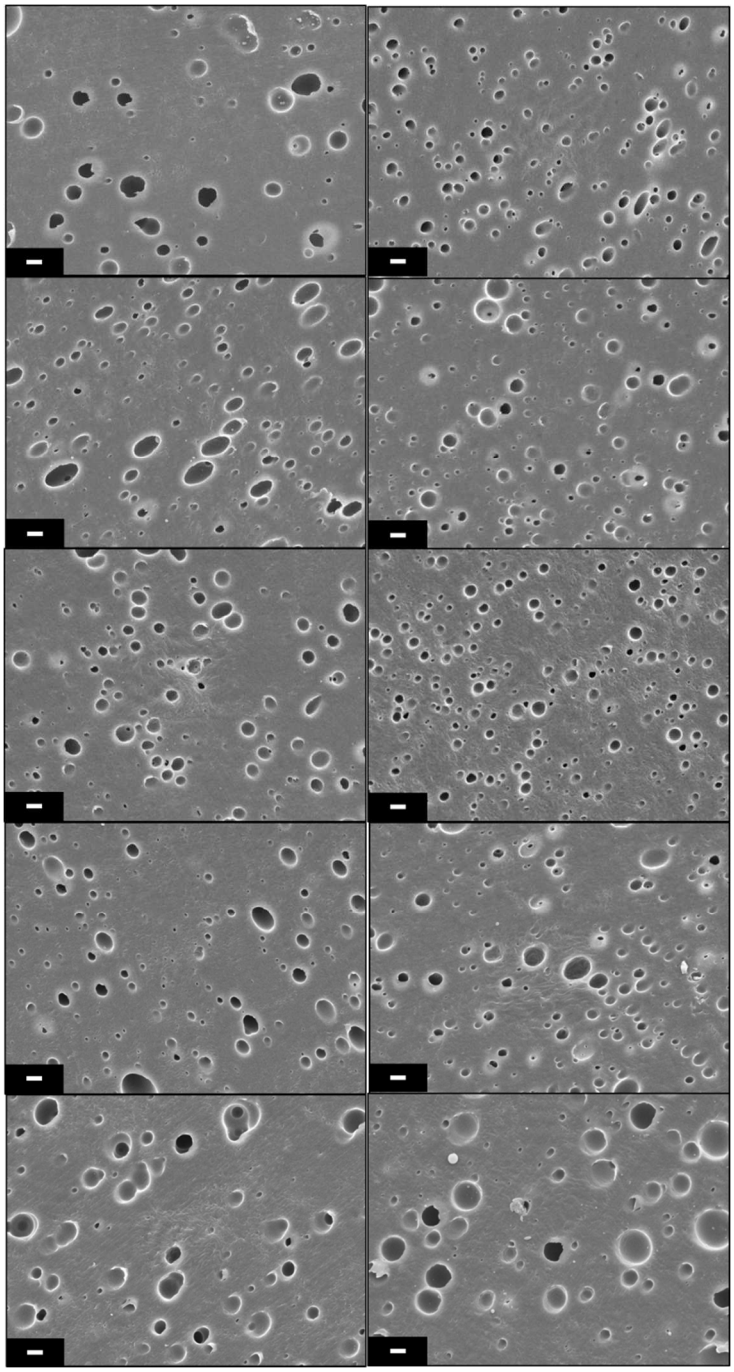

Figure 2.17. SEM images of PMMA / HDPE / HO-PE-OH / catalyst blends. Non-reactive blends (left), and reactive blends (right). Catalyst level on decending rows: neat, $SnCl_2$, $SnOct_2$, $Zn(Ac)_2$, $Zn(Acac)_2$. Scale bars are 1μm.

Droplet sizes were measured from at least four 5000x images in ImageJ software (NIH), and analyzed in Excel and JMP (Table 2.6). Two diameters were measured per drop, and each reported diameter is a number average of the two. All standard deviations were between 0.6 and 0.8 μm.

Table 2.6. Blend number average droplet diameters

catalyst	non-reactive blend $<d_n>$ (μm)	reactive blend $<d_n>$ (μm)
none	2.1	1.6
$SnCl_2$	1.6	1.0
$SnOct_2$	2.1	2.0
$Zn(Ac)_2$	1.7	1.8
$Zn(Acac)_2$	3.1	2.3

Droplet sizes are generally reduced for functional blends, suggesting that reaction or polar-polar interactions are reducing surface tension. $SnCl_2$ seems to reduce particle size for reactive blends, whereas $Zn(Ac)_2$ and $SnOct_2$ do not change size much, and $Zn(Acac)_2$ actually increases droplet size for non-reactive blends. This suggests a very weak reaction for $SnCl_2$ blends, and no significant change otherwise.

2.4.6 Blend rheology

Further evidence of reaction was sought from rheology, examining low frequency elastic moduli for increases. G' can be viewed as a sum of contributions from the blend components and the interface. At low frequency, elasticity is enhanced by the presence of copolymer at the interface.[42,47] Comparing non-reactive blends to reactive blends for an upturn in G' at low frequency is an established method for verifying reaction.

Blends were pressed (25 mm dia. cylinders, 200 °C, 5 min, ~3 MPa) to form discs, which were subsequently loaded on an ARES rheometer at 200 °C. Strain sweeps were performed to determine the LVE regime, and time sweeps were performed to ensure material thermal stability. Frequency sweeps with autostrain were collected, as shown

Figure 2.18. There is a clear upturn in G' at low frequency for the $SnCl_2$ catalyzed reactive blend (R, $SnCl_2$), evidence suggestive of reaction.

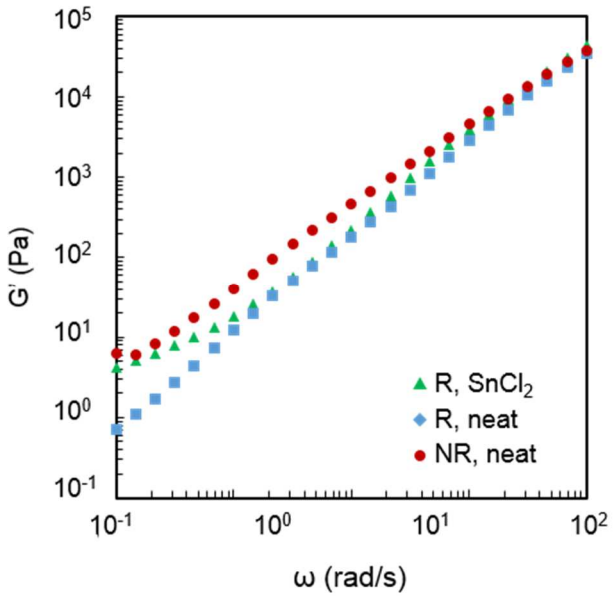

Figure 2.18. $SnCl_2$ catalyzed PMMA blends storage moduli.

2.4.7 Catalyst localization

Despite reduction in droplet size and suggestive rheology evidence, the catalyzed hydroxyl/methyl ester reaction does not seem to be rapid (or producing much copolymer). To investigate why this is so, TEM EDS was performed to examine catalyst localization in blends. Thin sections (~50 nm) were cryo-microtomed at −160 °C using a Leica EM UC 6 instrument and Microstar 45° diamond knife, then transferred to a copper-Formvar grid (300 mesh). No staining was necessary to obtain contrast. Samples were imaged on a T12 TEM at 120 kV, and EDS spectra were obtained for observed aggregates, droplets, and matrix. Only $SnCl_2$ and $Zn(Acac)_2$ blends were tested due to time constraints.

Images of $SnCl_2$ blends show light droplets (PMMA, some pulled out) in a dark HDPE matrix (Figure 2.19). Small, dark aggregates are observed in both the PMMA

drops and HDPE matrix in $SnCl_2$ blends, suggesting catalyst aggregation. The gradient dark and light regions in HDPE are attributed to differences in thickness and crystallinity

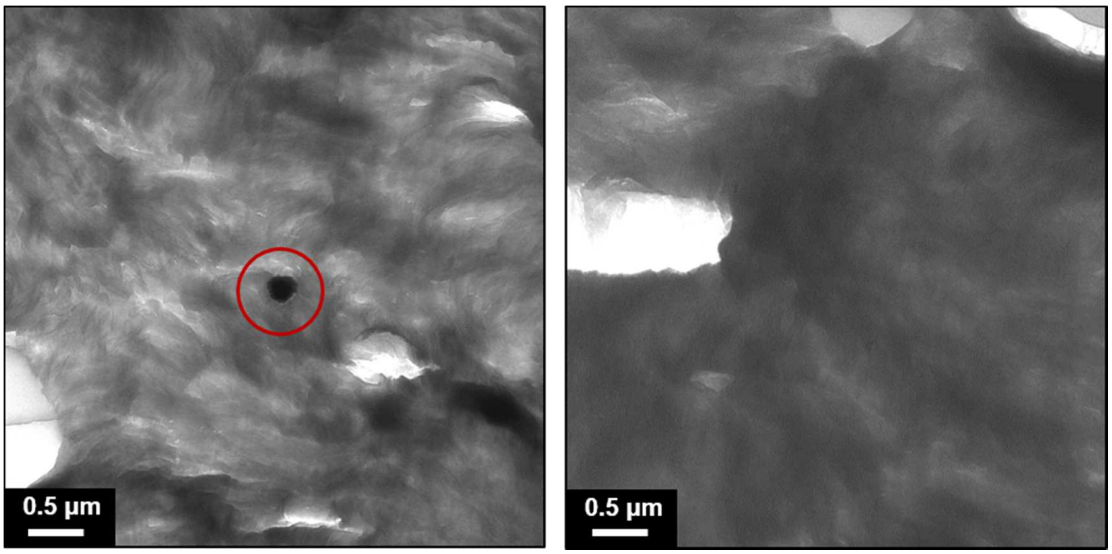

Figure 2.19. TEM of reactive $SnCl_2$ blend and reactive uncatalyzed blend (left and right, respectively). Small dark aggregates are observed only in the $SnCl_2$ blend (highlighted by red circle). Similar aggregates noted in the non-reactive $SnCl_2$ blend.

EDS was performed to verify the presence of tin in these aggregates, and to test for tin in other locations in the blend (microprobe mode, estimated spot size shown on image). The presence of tin is confirmed in the aggregates (Lα transition, ~3500 eV, Figure 2.20), whereas signal was much lower at the interface, in PMMA droplets, and in the HDPE matrix. Multiple droplets and aggregates were tested, with the same conclusion.

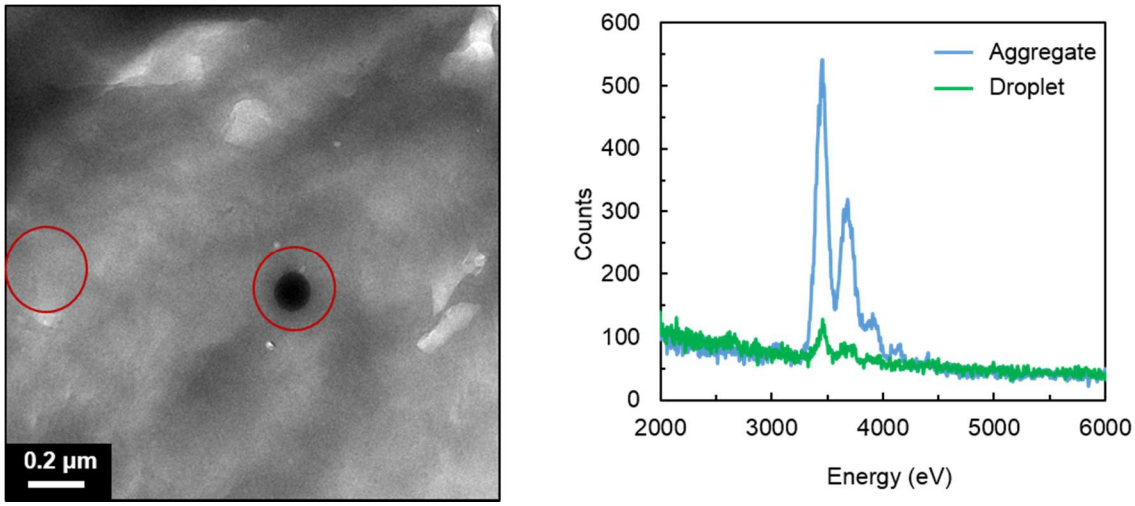

Figure 2.20. TEM image and EDS spectra for reactive, $SnCl_2$ blend.

Likewise, TEM shows distinct dark aggregates for $Zn(acac)_2$ blends, whose EDS spectra confirm the presence of tin (Figure 2.21). The matrix spectra were taken away from the image location. Estimated spot sizes are shown in red circles on the image. Expected Zn transitions are shown for the aggregates at 2200 eV (Mβ, in plot below), as well as in the 8000-9000 eV range (Lα, Lβ, partially overlapping Cu peaks from grid, not shown). No areas outside the aggregates show these transitions, indicating the $Zn(Acac)_2$ catalyst almost exclusively aggregates.

Localization offers a clear explanation for why the catalysts are not more effective: they are not localized at the interface, where reaction primarily occurs.

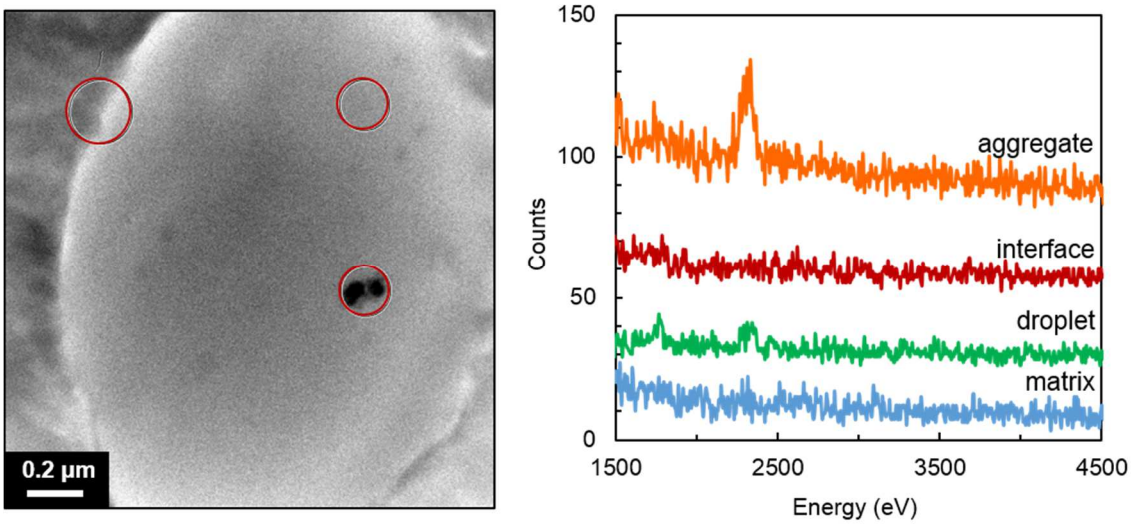

Figure 2.21. TEM image and EDS spectra for reactive $Zn(Acac)_2$ blend.

2.4.8 Conclusion

Hydroxyl-telechelic polyethylene was synthesized using ROMP with chain transfer agent to react with the methyl esters of PMMA, with the goal of compatibilizing HDPE/PMMA blends. Small molecule reactions show the feasibility of this reaction at elevated temperatures in the presence of catalysts. Small improvements to compatibility were observed in droplet size and rheological measurements, but were not as strong as anticipated. TEM EDS detected aggregates of tin chloride dihydrate and zinc acetylacetonate catalysts in blends, suggesting that localization of catalyst is very important for copolymer formation and improved compatibility. New catalysts and more reactive functional groups will be explored in Chapters 3 and 4.

Chapter 3. Accelerating reactive compatibilization of PE/PLA blends by an interfacially localized catalyst and hydroxyl functional PE

This work is reproduced in a large measure from "Accelerating Reactive Compatibilization of PE/PLA Blends by an Interfacially Localized Catalyst" (ACS Macro Letters, 2015, 4, 30-33).[54]

3.1 Summary

We show that catalyst localized at the interface can compatibilize polyethylene (PE) and polylactide (PLA) blends. Telechelic hydroxyl functional PE was synthesized by ring opening metathesis polymerization, and it reacted with PLA in melt mixing (shown by increased adhesion and droplet size reduction). Lewis acid tin catalysts were examined as interfacial reaction promoters, with the goal of interfacial localization. Stannous octoate was shown to localize at the interface by transmission electron microscopy with energy dispersive X-ray spectroscopy. This catalyst improved dispersion of PLA in PE as compared to both uncatalyzed materials and a nonlocalized tin chloride dihydrate catalyst.

3.2 Introduction

Immiscible blends represent a growing fraction of advanced polymeric materials but require compatibilizers to achieve stable morphologies and superior mechanical properties.[8,29] Reactive compatibilization is the preferred approach, as block or graft copolymers are formed in situ, thereby avoiding loss of compatibilizer to micellization. However, few reactions (e.g., primary amine plus anhydride) are sufficiently rapid without a catalyst. Suitable catalysts could greatly expand the palette of accessible reactive groups, but to be efficient, they should be localized at the interface. In this report we demonstrate directly that interfacial localization is crucial by preparing novel blends

of biorenewable polylactide (PLA) in a majority polyethylene (PE) matrix using esterification of hydroxyl-functionalized PE.

Reactive compatibilization leads to improvements in adhesion,[20,21] processing stability,[53] and bulk mechanical properties (impact strength,[111,112] tensile toughness,[48,113] hardness,[55] scratch resistance[11,12]). Interfacial coupling kinetics determines the amount of copolymer formed, and therefore, final material properties. Past work has identified variables that strongly affect coupling kinetics, including the Flory-Huggins interaction parameter between the blend components,[64] flow,[65,72] coupling reaction type,[36] and catalyst. Several reports have utilized catalysts to improve conversion to copolymer, but results have been mixed.[35,66–69,114–118] Most studies select catalysts based on their activity toward analogous small molecule reactions and stability at melt processing temperatures, with little regard for surface activity or localization. The sole report of catalyst localization came from Legros et al.,[69] where tin distannoxane catalyst preferentially localized in poly(butylene terephthalate) (PBT) portions of PE/PBT reactive blends. However, in that work a relationship between localization and compatibility was not determined. Guegan et al. reported that N,N-dimethyldodecylamine catalyst had no effect on conversion in acid functional polystyrene (PS-COOH)/epoxy functional polystyrene miscible blends, but adding the same catalyst to an analogous immiscible blend, PS-COOH/epoxy end-functional poly(methyl methacrylate), resulted in a 250% increase in reaction rate.[35] This suggests that the presence of an interface, or localization, might be critical for catalyst performance. This concept finds a precedent in small molecule chemistry with catalyst-combined-surfactants from Kobayashi and co-workers.[119–121]

Reactive groups on PLA homopolymers have recently been used in catalyzed reactive compatibilization schemes. PE-co-ethyl acrylate-co-glycidyl methacrylate (EMA-GMA)/PLA blends catalyzed with N,N-dimethylstearylamine resulted in higher conversion to graft copolymer, finer dispersion, and increased impact strength of PLA.[68] Sadik et al. also compatibilized poly(ethylene-co-vinyl alcohol) (EVOH) and PLA with stannous octoate catalyst, demonstrating copolymer formation by NMR, SEC, and

rheology.[118] However, these studies used undiluted functional PE copolymers with many functional groups per chain, in order to obtain improved properties and conversion. Also, the miscibility of these functional PE copolymers with neat PE may limit applications.

In this work, compatibilized blends of HDPE (high density PE) and PLA are created using modest amounts of hydroxyl functional PE. PLA is chosen to blend with PE for its high modulus (~3 GPa) and renewable nature.[112] This particular PLA/PE system may have applications in food packaging since stannous octoate catalyst is FDA approved[122] and the chemistry is less hazardous than maleic anhydride or epoxy functional PEs. The effect of catalyst localization on blend compatibility and adhesion is examined. This work develops a method of locating catalyst in reactive polymer blends and, thereby, potentially expands the number and types of interfacial reactions with sufficient rates for applications.

3.3 Synthesis

Telechelic α,ω-hydroxyl functional PE (HO-PE-OH) was synthesized using ring opening metathesis polymerization with a chain transfer agent, followed by hydrolysis and hydrogenation, as pioneered by Pitet and co-workers and described in Chapter 2.[105] This serves as a high density PE analog to commercial EVOH. HO-PE-OH was diluted with commercial HDPE (DMDA 8904 NT-7, Dow Chemical Company) and reacted with PLA (Natureworks 2003D) during compounding. Polymer characteristics are shown in Table 1. Tin chloride dihydrate ($SnCl_2$; Sigma-Aldrich) and stannous octoate ($SnOct_2$; Sigma-Aldrich) were used to promote interfacial reaction.

Table 3.1. Polymer characteristics for the HDPE/HO-PE-OH/PLA system

polymer	M_n (kg/mol)	$Đ$	η_0 [c] (Pa s)	T_m [d] (°C)
HDPE	32[a]	2.4 [a]	2600	132
PLA	190[b]	1.5[b]	5700	150
HO-PE-OH	27 [a]	1.7 [a]	190	130

[a] 135 °C trichlorobenzene SEC, RI detector, [b] 30 °C $CHCl_3$ SEC, [c] shear rheology with Cox-Merz and Cross model fit, [d] second heating DSC at 10 °C/min.

3.4 Results and discussion

3.4.1 Small molecule model reactions

Catalysts were screened for activity toward esterification and ester exchange reactions using model small molecules. Kinetic rate constants from small molecule reactions generally compare well to those found for homogeneous polymer blends, in terms of ranking relative rates.[8] Hexadecanol was reacted with either methyl stearate (ester exchange) or hexadecanoic acid (esterification) at 180 °C. Conversion with and without catalyst was monitored with ^{1}H NMR spectroscopy. $SnCl_2$ and $SnOct_2$ showed similar, significant activity toward both esterification and ester exchange. This will prove important in isolating the effect of catalyst localization from catalyst activity.

Hexadecanol (4.40 g, ~3.24 M), hexadecanoic acid (0.11 g, ~0.08 M), catalyst (0.04 M), and a stir bar were introduced to a three-necked 100 mL reaction flask with a condenser. Dilute hexadecanoic acid was used to minimize the self-catalytic activity of the carboxylic acid. The reactor was placed in a preheated 180 °C oil bath. The reaction time was recorded from the moment all reagents had melted. After 25 min, the product was quickly cooled and dissolved in $CDCl_3$, and the composition was measured by ^{1}H NMR spectroscopy using a 500 MHz Bruker NMR spectrometer (RT, $CDCl_3$, n = 16, d1 = 6 s, at = 2 s, Figure 3.1). Conversion was determined by comparing the integrations of the α-hydrogens of hexadecanol (3.65 ppm) to α-hydrogens of the hexadecyl hexadecanoate product (4.07 ppm). Conversion was calculated as shown in equation (9). Both catalysts increase conversion to ester at melt blending temperatures, with $SnCl_2$ having higher conversion than $SnOct_2$ (Table 3.2). The reagents were homogeneous at 180 °C; $SnOct_2$ was soluble but $SnCl_2$ was not (cloudy mixture).

$$X = \frac{\text{int}(4.07\,\text{ppm})/\text{int}(3.65\,\text{ppm})}{1+\text{int}(4.07\,\text{ppm})/\text{int}(3.65\,\text{ppm})} * \frac{3.24\,\text{M}}{0.08\,\text{M}} \qquad (9)$$

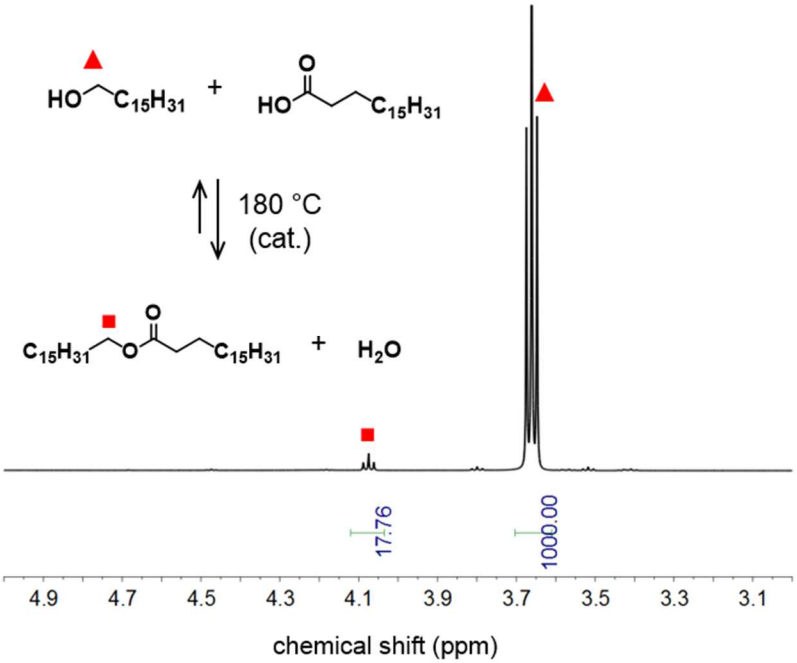

Figure 3.1. Small molecule model esterification reaction and sample ^{1}H NMR spectrum ($SnCl_2$, 25 min)

Table 3.2. Small molecule reaction conversion between hexadecanol and hexadecanoic acid

catalyst	fractional conversion with respect to palmitic acid at 25 min
None	0.08
$SnCl_2$	0.71
$SnOct_2$	0.26

Hexadecanol (1.254 g, ~1.0 M), methyl stearate (3.094 g, ~2.0 M), catalyst (~0.02 M), and a stir bar were introduced to a three-necked 100 mL reaction flask with a condenser. The reactor was placed in a preheated 180 °C oil bath. The reaction time was recorded from the moment all reagents had melted, and aliquots were removed every five minutes to determine conversion to hexadecyl hexadecanoate. Aliquots were dissolved in $CDCl_3$ and the composition was measured by ^{1}H NMR spectroscopy using a 500 MHz Bruker NMR spectrometer (n = 16, $d1$ = 6 s, at = 2 s). Conversion was determined by comparing the integrations of the α-hydrogens of methyl stearate and hexadecyl

hexadecanoate product (2.32 ppm) to the hydrogens vicinal to the oxygen in the hexadecyl hexadecanoate product (4.05 ppm). Conversion was calculated as shown in equation (10). Both catalysts increase conversion to ester at melt blending temperatures, with $SnCl_2$ having higher conversion than $SnOct_2$. Similar solubilities were noted as in the esterification small molecule model reactions.

$$X = \frac{\text{int}(4.05\,\text{ppm})}{\text{int}(2.32\,\text{ppm})} * 2 \tag{10}$$

Scheme 1. Small molecule model ester exchange reaction

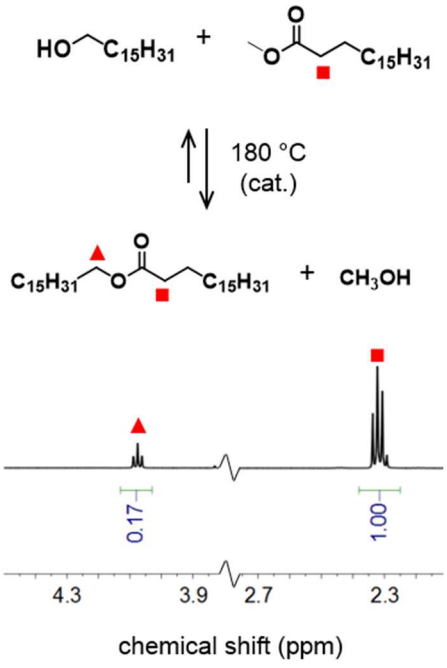

Figure 3.2. Small molecule model ester exchange reaction and sample ^1H NMR spectrum ($SnCl_2$, 25 min)

Table 3.3. Small molecule reaction results between hexadecanol and methyl stearate

catalyst	fractional conversion with respect to hexadecanol at 25 min
None	0.00
$SnCl_2$	0.34
$SnOct_2$	0.20

3.4.2 Rheology

Shear rheology was used to determine the viscosity of HDPE, HO-PE-OH, and PLA. A strain controlled ARES rheometer (Rheometrics Scientific) was equipped with 25 or 50 mm parallel plates at 180 °C for all experiments. The linear viscoelastic regime (LVE) was determined by strain sweeps (ω = 1 rad/s), defined by $G'(\gamma) > 0.90\ G'(0)$. Frequency sweeps with autostrain were performed in the LVE from 100 rad/s to 0.01 rad/s. Cross model fits were performed to minimize summed error. To perform Cross model fits, the Cox-Merz relationship was assumed to be valid ($\omega = \dot{\gamma}$) and η_∞ was assumed to be zero.

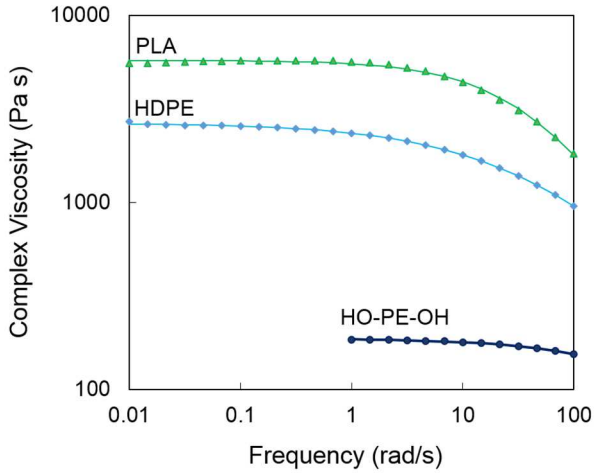

$$\frac{\eta - \eta_\infty}{\eta_0 - \eta_\infty} = \frac{1}{1 + (K\dot{\gamma})^{1-n}}$$

material	η_0 (Pa-s)	n	K (s)
PLA	5700	0.14	0.025
HDPE	2600	0.43	0.027
HO-PE-OH	190	0.34	0.001

Figure 3.3. Complex viscosity as a function of frequency in small amplitude oscillatory shear for PLA/HDPE system. Points indicate experimental data, lines indicate Cross model fits.

3.4.3 DSC

Thermal properties were determined using a TA Q1000 DSC. Samples were heated from 40 °C to 180 °C, then cooled to 40 °C, then heated a second time to 180 °C (all at 10 °C/min). Enthalpy of melting (ΔH_m) was determined by integration of the melting peak on second heating. In the case of PLA, the integration of the cold crystallization peak was subtracted from the melting peak area.

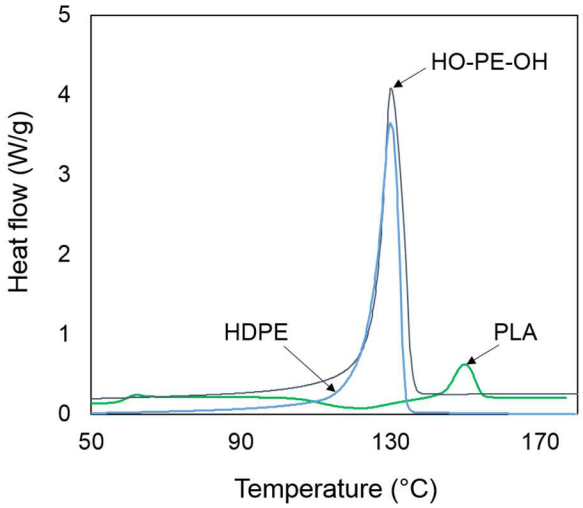

Figure 3.4. DSC second heating curves for HDPE/HO-PE-OH/PLA system (10 °C/min).

3.4.4 Melt mixing

Melt mixing was performed in a Minimax cup and rotor mixer (Custom Scientific Instruments) with two ¼" diameter ball bearings added to improve mixing.[109,110] Samples were blended at 180 °C and 310 rpm for 5 min, then removed and quenched in liquid nitrogen. All blends contained 90 wt% PE, 10 wt% PLA, and 0.01 M catalyst (0.4 wt% $SnCl_2$ or 0.8 wt% $SnOct_2$) for 0.50 g total material.

3.4.5 SEM for droplet size

Blends were cryo-microtomed at –160 °C, washed with acetone overnight to remove PLA, coated with 50 Å Pt, and imaged on a JEOL 6500 scanning electron microscope (Figure 3.5). Droplet sizes were measured using ImageJ software (NIH) and are compared in Table 3.4. Formation of copolymer reduces surface tension in mixing, resulting in decreased droplet size.[90,123,124] The reduction in droplet size with addition of HO-PE-OH suggests interfacial reaction. Addition of $SnCl_2$ did not appreciably reduce droplet size, despite evidence from small molecule model reactions and literature showing it is an effective catalyst for esterification and ester exchange.[125–127] In contrast, $SnOct_2$ was effective at reducing droplet size further than HO-PE-OH alone.

Table 3.4. Droplet sizes of blends

blend (weight fraction of component)	droplet size (μm, $< d_n >$ ± S.D.)	number of droplets sized
HDPE / PLA (90 / 10)	0.77 ± 0.20	189
HDPE / HO-PE-OH / PLA (60 / 30 / 10)	0.44 ± 0.07	861
HDPE / HO-PE-OH / PLA / $SnCl_2$ (60 / 30 / 10 / 0.4)	0.53 ± 0.30	412
HDPE / HO-PE-OH / PLA / $SnOct_2$ (60 / 30 / 10 / 0.8)	0.26 ± 0.04	1514

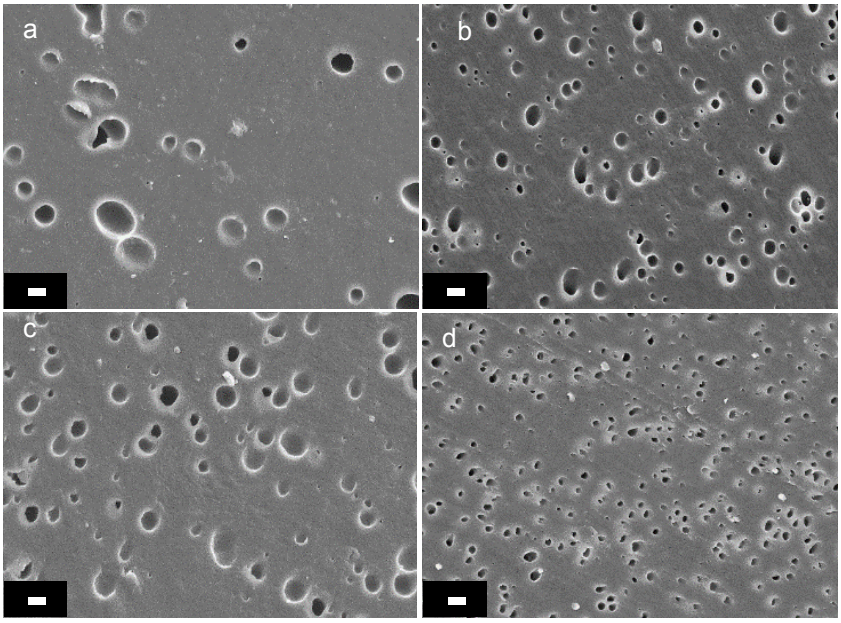

Figure 3.5. Representative SEM images of HDPE/PLA blends, with 1 μm scale bars. (a) PE/PLA (90/10) (b) PE/HO-PE-OH/PLA (60/30/10) (c) PE/PLA/HO-PE-OH/$SnCl_2$ (60/30/10/0.4) (d) PE/PLA/HO-PE-OH/$SnOct_2$ (60/30/10/0.8)

3.4.6 Adhesion

Adhesion measurements were used as a secondary, macroscopic method to verify interfacial reaction at the interface of HO-PE-OH and PLA. PLA was compression molded (60 mm × 7.5 mm × 0.34 mm) between Teflon sheets (McMaster Carr), at 180 °C for three minutes and 0.3 MPa. The surfaces were wiped using a chloroform soaked

kimwipe to remove residual Teflon. HDPE was pressed at 150 °C in the same size mold as the PLA. 0.50 g HO-PE-OH was blended with catalyst (0.4 mg $SnCl_2$ or 0.8 mg $SnOct_2$) at 180 °C and 310 rpm for 5 min, and pressed between Teflon sheets at 150 °C and ~2 MPa for 3 min. The final films were between 0.05 and 0.10 mm thick. All samples were cut from the molds with razor blades, and edges were trimmed. Laminated tri-layers were created in 60 mm x 7.5 mm x 1 mm molds by sandwiching the HO-PE-OH/catalyst layer between PLA and HDPE (PLA on bottom). These filled molds were placed between Teflon sheets with light pressure (< 0.1 MPa) at 180 °C for 1 h, then quickly cooled to room temperature. Samples were removed from the molds using a razor blade and edges were trimmed prior to peel testing. The samples were initially split between the HO-PE-OH and PLA using a razor blade, then mounted in a Shimadzu-AGX tensile tester. Force versus displacement was measured at a constant 5 mm/min extension rate, and a steady-state force was determined for each sample (F, in N). Sample widths (b) were an average of three micrometer measurements. F/b values are reported as peel strengths in Figure 3.6.

The specific adhesion rankings are not clear from this data, due to large uncertainties at low peel strengths. However, this verifies reaction occurs with and without catalysts.

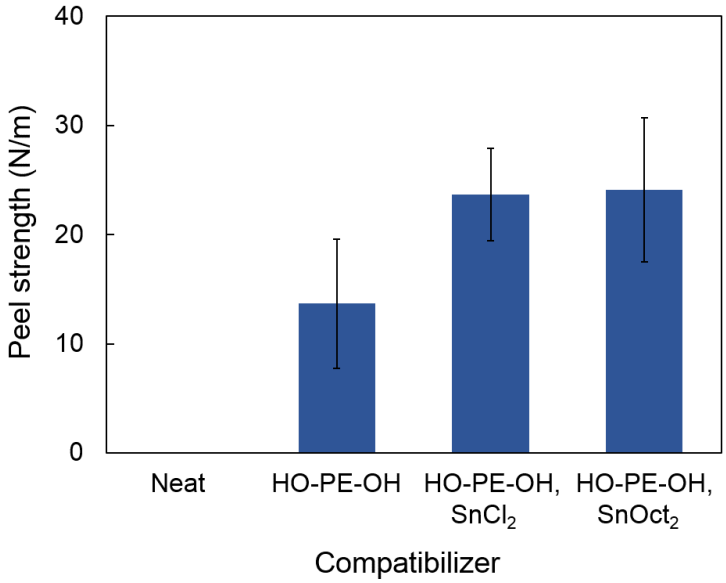

Figure 3.6. Peel strength of PE/PLA laminates by compatibilizer layer.

Samples without HO-PE-OH showed no adhesion, delaminating before removal from the mold. HO-PE-OH samples displayed lower adhesion than reported for most reactive systems[22,72,128] but appreciably higher than most nonreactive laminates[129] and even some reactive ones.[130] When 0.01 M catalyst is blended into the HO-PE-OH compatibilizing layer before lamination, adhesion values increase further. Adhesion shows that reaction occurs with or without catalyst, and that the droplet size decrease seen in SEM is from reaction, not from catalyst acting as a surfactant.

3.4.7 SEC of low molecular weight polymers to verify reaction in melt mixing

To further verify reaction was occurring, low molecular weight PE-OH and PLA were melt mixed (in 50/50 blend, and 50/50 blend with $SnOct_2$) and analyzed by SEC. Mono-end-functional PE-OH was purchased from Baker-Hughes (UNILIN 700) and used as received. PLA 5k was synthesized and provided by Tessie Panthani (M_n = 4700 g/mol by $CDCl_3$ 500 MHz ^{1}H NMR, $Đ$ = 1.4). The Minimax was used at the same blending conditions (310 rpm, 180 °C, 5 min) before quenching in liquid nitrogen. Each sample

was dissolved in 1,2,4-trichlorobenzene and tested by high temperature SEC (135 °C, RI detector, PS standards).

The summarized SEC results are shown in Table 3.5 and Figure 3.7. In the 50/50 blend, two peaks are still visible, but the PLA peak has shifted to higher molecular weight (shorter retention time) and has a higher intensity than the PE-OH peak, compared to the predicted signal. This is a sign of reaction between the PLA and PE-OH even without catalyst. In the catalyzed 50/50 blend, the PE-OH peak disappears, evidence that $SnOct_2$ is an effective catalyst in melt mixing. The 50/50/1 blend peak is also shifted to slightly lower molecular weight. We hypothesize this is caused by some PE-OH reacting with esters of the PLA backbone (ester exchange reaction). This would indicate some ester exchange occurs in the melt, along with esterification.

Table 3.5. SEC results for PLA 5k, PE-OH reaction

material	M_n (g/mol)	M_w (g/mol)	$Đ$	peak maximum retention time (s)
PE-OH	580	1100	1.8	1450
PLA	3100	4400	1.4	1350
50/50 (wt%) blend	540	1000	1.8	1430
	4000	4500	1.1	1350
50/50/1 blend with $SnOct_2$	2525	4100	1.6	1350

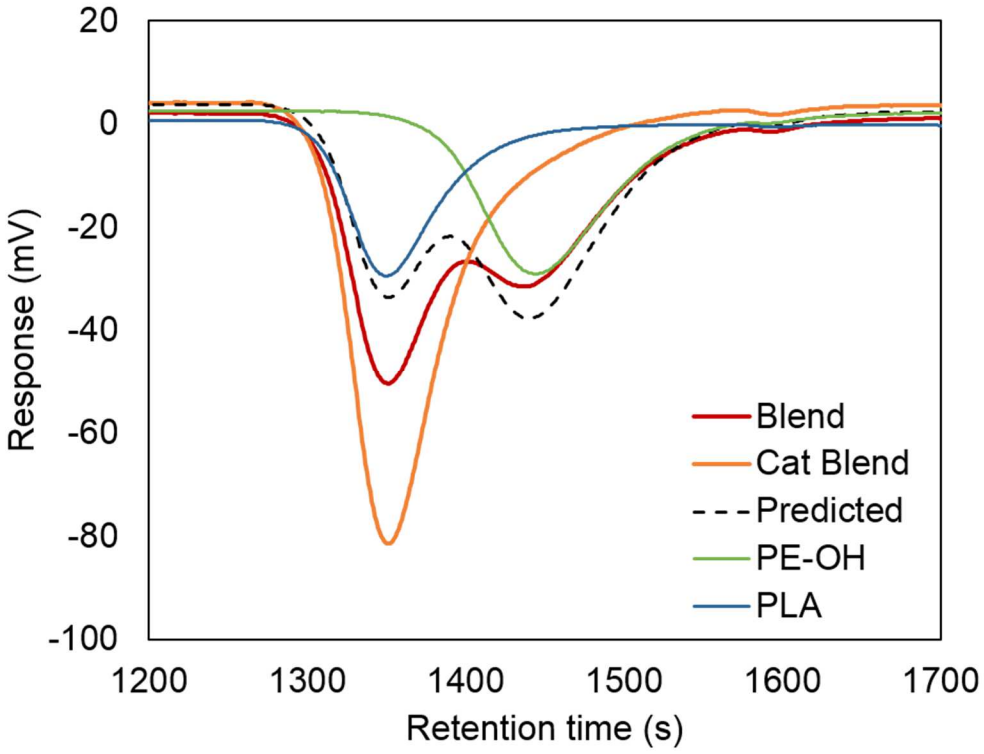

Figure 3.7. SEC traces to show melt mixing reaction between PE-OH and PLA. Traces of neat materials, 50/50 blend, 50/50/1 blend with $SnOct_2$, and predicted curve for 50/50 blend based on concentration normalized addition of the PE-OH and PLA curves are shown.

3.4.8 Degradation of PLA in melt mixing

Control studies were performed to determine the extent of transesterification and degradation of PLA during melt mixing. Pure PLA was mixed for 5 min at 180 °C, the same conditions as blending. Also, PLA was mixed with 5 wt% $SnOct_2$ under the same conditions. The three samples (as received, after 5 min mix, and after 5 min mix with $SnOct_2$) were dissolved in chloroform and tested with room temperature chloroform SEC. Dispersity increases slightly after mixing, an indication of some transesterification or degradation. However, M_w is similar whether blended with catalyst or without. Therefore, PLA rheological changes during blending cannot account for particle size reduction in blending with catalysts.

Table 3.6. Molecular weights before and after blending in Minimax mixer (in kg/mol)

sample	trial 1		trial 2	
	M_n	M_w	M_n	M_w
as received	190	270	190	270
after 5 min mix	170	250	170	250
after 5 min mix with $SnOct_2$	170	250	160	240

3.4.9 Catalyst localization

Transmission electron microscopy with energy dispersive X-ray spectroscopy (TEM EDS) was used to determine $SnOct_2$ catalyst localization in the blends (FEI Tecnai T12, 120 kV). This technique is used to give elemental information as a function of position.[131,132] Blends were cryo-microtomed to 50 nm sections and transferred to a Formvar-coated copper grid (Ted Pella) for imaging. Figure 3.8 and Figure 3.9 show representative PLA droplets (light) in the HDPE matrix (dark). The dark inclusions in the PLA droplet are presumably HDPE. The contrast gradients in the HDPE are attributed to thickness or crystallinity variations.

EDS spectra were obtained inside droplets, in the nearby matrix, and on the interface for several drops. The minimum spot size is approximately 50 nm. Spectra were analyzed for expected Sn Lα and Lβ transitions around 3500 eV. The $SnOct_2$ blend interface (or inclusion interface) spots consistently showed Sn peaks, whereas the matrix, droplet, and $SnCl_2$ blend interface spots did not (Figure 3.8b and Figure 3.9b). To our knowledge, this represents the first direct evidence of interfacial localization of catalyst in reactive compatibilization.

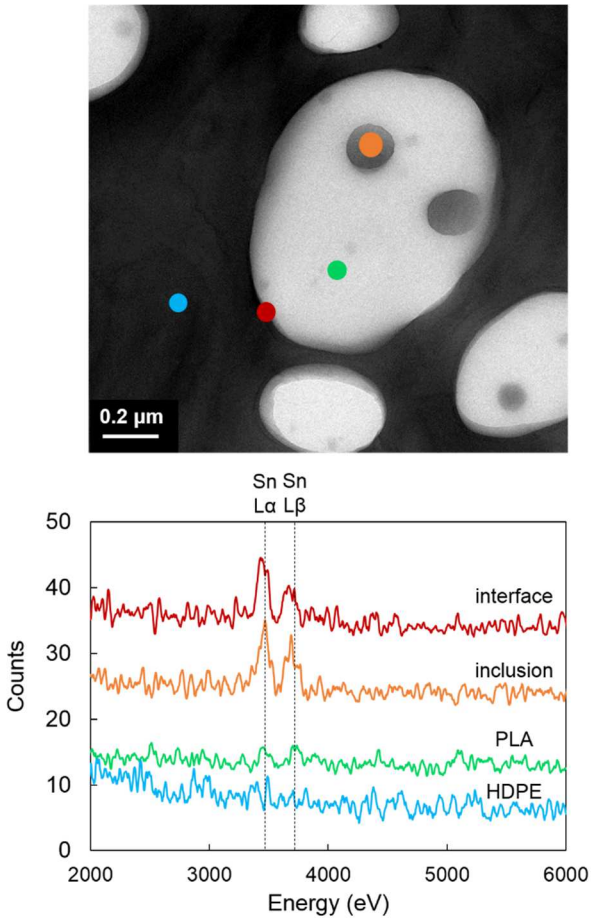

Figure 3.8. Representative TEM image and EDS spectra of HDPE/PLA/HO-PE-OH/ $SnOct_2$ blend, with estimated EDS spot size (color coded).

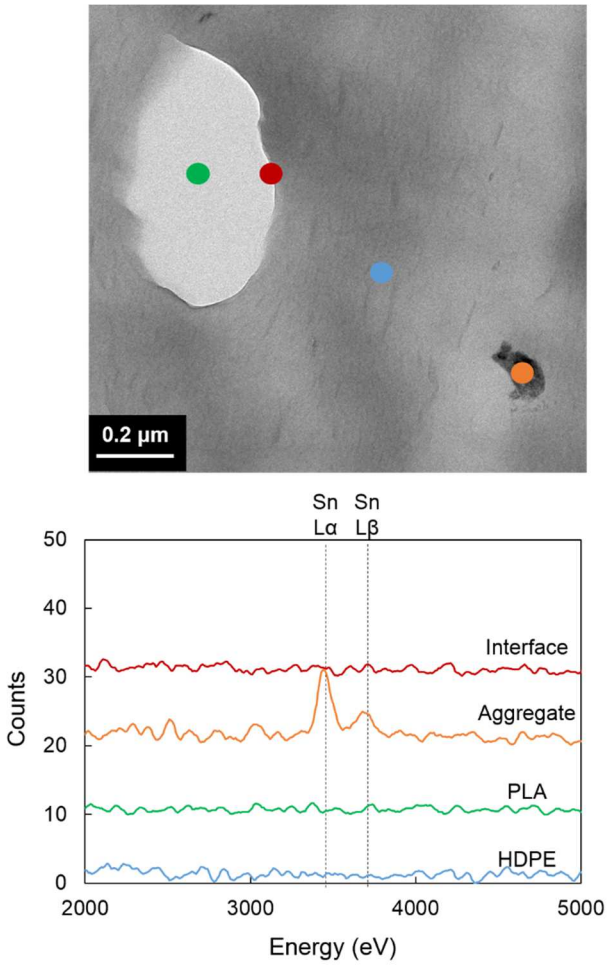

Figure 3.9. Representative TEM image and EDS spectra of HDPE/PLA/HO-PE-OH/ $SnCl_2$ blend with estimated EDS spot size (color coded).

Localization demonstrates why $SnOct_2$ is more effective than $SnCl_2$ at reducing droplet size in reactive blends, and can be explained in part through solubility parameter analysis. The catalyst solubility parameter should lie between those of the homopolymers for interfacial localization. In this case, $SnCl_2$ (δ = 42.3 $MPa^{1/2}$) has a higher solubility parameter than PE (δ = 17 $MPa^{1/2}$) or PLA (δ = 20.5 $MPa^{1/2}$; all values at 25 °C)[79,133] leading to catalyst aggregation. In contrast, δ is estimated to be 20.0 $MPa^{1/2}$ for $SnOct_2$[108] (between that of PE and PLA), which localizes on the interface. It is apparent that

catalyst localization can be roughly predicted by solubility parameters and is important in catalyzed reactive blending.

It is possible to estimate an interfacial coverage for $SnOct_2$ based on droplet size and catalyst loading, assuming all of the catalyst is on the interface. Equation (11) describes the total blend interfacial area assuming a monodisperse droplet size, where A_{blend} is interfacial area of the blend, A_{drop} is the interfacial area of a single droplet, n is number of droplets, $<d_n>$ is the average droplet size, V_{blend} is the volume of the entire blend, V_{drop} is the volume of a single droplet. For $<d_n> = 0.5$ μm, $V_{blend} = 5 \times 10^{-7}$ m^3, $V_{drop} = (4\pi / 3)(<d_n> / 2)^3 = 6.54 \times 10^{-20}$ m^3, and $x_{PLA} = 0.073$ (based on $\rho_{PLA} = 1.27$ g/cm^3 and $\rho_{HDPE} = 0.95$ g/cm^3),[134] then A_{blend} is ~0.4 m^2. $SnOct_2$ is present at 0.01 M, or ~ 5 μmol/blend. Assuming the interfacial area of a single $SnOct_2$ molecule is order 50 $Å^2$ (based on SDS values, which are expected to be similar in the liquid surface phase due to similar size), the amount of $SnOct_2$ in one blend can cover ~2 m^2 interface. Since the area the catalyst can cover is greater than the interfacial area of the blend, there is an excess of catalyst available to the interface in these blends. Future work should examine the effect of catalyst concentration on localization.

$$A_{blend} = A_{drop} \times n_{drops} = \left[4\pi \left(\frac{< d_n >}{2} \right)^2 \right] \times \left[\frac{V_{blend} x_{PLA}}{V_{drop}} \right] \quad (11)$$

3.5 Conclusions

In summary, interfacially localized catalysts are a promising method of improving conversion in reactive compatibilization. Catalysts that segregate preferentially to the interface can be added in submonolayer quantities to obtain large improvements in adhesion and dispersion. This work examined the effect of two tin catalysts on the reactive compatibilization of telechelic hydroxyl functional polyethylene and PLA. There is a weak reaction, even without catalysts, and improved dispersion and adhesion compared to HDPE/PLA materials. $SnOct_2$ was more effective as a catalyst in blend compatibilization than $SnCl_2$, which is attributed to its interfacial localization, as

confirmed directly by TEM with EDS. Localization was justified by solubility parameter arguments.

Chapter 4. Toughening polylactide with a catalyzed epoxy-acid interfacial reaction

4.1 Summary

Polylactide (PLA) is a promising material, with favorable modulus, renewable sources, and biodegradability. However, its low extension at break (4-7 %) and toughness (notched Izod, 26 J/m) limit its applications.[112] PLA toughening has been the subject of recent reviews,[112,135] and is the basis for several commercial products. This work aims to increase PLA toughness using rubbery linear low density polyethylene (LLDPE), glycidyl methacrylate functional PE compatibilizer (EGMA), and novel catalysts that promote copolymer formation at the interface of immiscible blends of PLA and EGMA/LLDPE. Droplet size was reduced from 2.7 μm to 1.7 μm with addition of 5 wt% EGMA, and further to 1.0 μm with the addition of cobalt octoate catalyst. Extension at break of > 200% is achieved with only 5 wt% reactive compatibilizer, 15 wt% LLDPE, and 0.01 M cobalt octoate.

4.2 Introduction

There are many approaches to toughening PLA, but one of the most prevalent and economical methods is reactive blending with an immiscible minority rubbery component.[16,18,32,33,136–138] A similar approach has been used to toughen other brittle polymers, resulting in super tough nylon,[7,139] high impact polystyrene (HIPS),[140,141] and other toughened polyesters.[142,143]

Deformation and failure mechanisms have been studied for rubber toughened polymer blends. Rubbery droplets can cause multiple crazing, spreading deformation energy to large parts of a glassy matrix, and eventual shear yielding.[144] In addition, Kowalczyk et al. noted PLA blends with poly(1,4-*cis*-isoprene) displayed an extra cavitation step between crazing and shear yielding, resulting in dramatically increased toughness compared to the neat PLA matrix.[145] When interfacial adhesion is strong in

rubber toughened blends, microcrack and void formation also serve to dissipate energy of deformation.[146]

To obtain high adhesion, block copolymers must be at the interface. For PLA and linear low density polyethylene (LLDPE), this usually involves addition of polyethylene-*co*-glycidyl methacrylate (EGMA), which can react with PLA end groups at the interface to form a block copolymer (Figure 4.1). PLA has been toughened using a reactive compatibilization system of LLDPE and EGMA, achieving the best toughness with around 20 wt% additives.[33,68,147–149] Evidence of this reaction was demonstrated by FTIR, SEC, ^{1}H NMR, droplet size, and rheology, leading to improved extension at break (up to 200%) and Charpy impact strength (up to 70 kJ/m^2).[34,68,147]

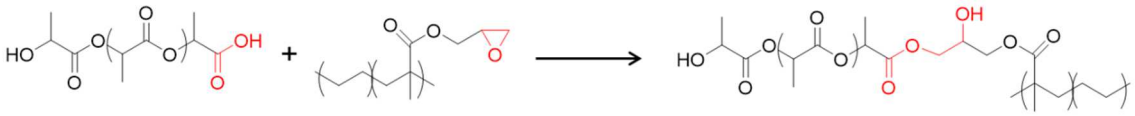

Figure 4.1. The dominant interfacial reaction occurring in EGMA/PLA blends

The amount of copolymer formed is strongly related to adhesion and blend toughness, so rapid reactions are desired.[7,20,21,24,150] Several studies show faster kinetics result in higher toughness of EGMA/PLA blends. Li et al. demonstrated the effect of reactive group concentration of dispersion and toughness.[148] Oyama showed improvement in impact strength and elongation at break for samples prepared with higher extruder screw speeds, possibly from a higher extent of reaction.[147] Reaction rates are most strongly influenced by the reactive groups used, with relative rankings similar to those seen in small molecules.[8] Epoxy–acid reactions are generally fast enough for commercial applications (e.g., Lotader®, Joncryl®, Biomax® Strong), but are almost three orders of magnitude slower than the most common reaction, amine–cyclic anhydride.[36]

Addition of catalysts is a promising method for increasing reaction rates, since catalysts for epoxy-acid reactions have been well-studied.[35,151–153] Feng et al. recently published work on a PLA/PE-*co*-ethyl acrylate-*co*-glycidyl methacrylate (EMA-GMA)

reactive blend, showing improved reaction rate with catalyst incorporation by mixer torque measurements and Fourier transform infrared spectroscopy (FTIR). This led to impressive 50-fold increase in Charpy notched impact strength with the incorporation of 20 wt% EMA-GMA and 0.2 wt % dimethylstearylamine (DMSA) catalyst over neat PLA and ~3-fold increase over the analogous uncatalyzed blend.[68] Bai et al. also blended EMA-GMA with PLA in the presence of DMSA catalyst, successfully creating EMA-g-PLA with high conversion.[149] Faster, catalyzed reactions may preclude the necessity of high functional polymer loadings or long processing times.

This work examines the effect of reaction kinetics and subsequent mechanical property changes of PLA/EGMA/LLDPE blends with the addition of cobalt ethylhexanoate ($CoOct_2$) and N,N-dimethyldodecylamine (DDA) catalysts.

4.3 Experimental

4.3.1 Materials

LLDPE Engage 8200 was generously provided by The Dow Chemical Company. This ethylene-octene random copolymer has 7.3 mol% octene, a melt flow index (MFI) of 5 g / 10 min (190 °C / 2.16 kg) as measured by ASTM D1238 and density of 0.870 g/cm^3 as measured by ASTM D792. PLA Ingeo Bioworks 2003D was purchased from Natureworks LLC (MFI = 6 g / 10 min (210 °C / 2.16 kg) and density = 1.24 g/ cm^3) and dried in a vacuum oven for at least 48 h at room temperature prior to use. EGMA (Lotader AX8840, 8 wt% glycidyl methacrylate, MFI = 5 g / 10 min (190 °C / 2.16 kg), density = 0.94 g/cm^3), DDA, and $CoOct_2$ (65 wt% in mineral oil) were purchased from Sigma Aldrich and used as received.

4.3.2 Size exclusion chromatography (SEC)

PLA 2003D molecular weight distribution was analyzed using room temperature SEC with chloroform eluent and a refractive index (RI) detector. All neat materials and blends were analyzed using high temperature SEC (135 °C, 1,2,4–trichlorobenzene

eluent, RI detector, polystyrene (PS) standards). Reported molecular weights are for equivalent hydrodynamic radius polystyrene.

4.3.3 Melt processing

A 5 mL Xplore twin screw batch mixer made blends comprising 80 wt% PLA and 20 wt% combined LLDPE and EGMA (total mass of 4.00 g). 0.01 M catalyst (mol catalyst / L melt blend volume) was added by syringe to select blends (0.014 g $CoOct_2$ solution in mineral oil or 0.009 g DDA). Catalysts were diluted in acetone to roughly 60 µL solution per batch to reduce viscosity and ease loading. The compounding conditions were 180 °C, 200 rpm (corresponds to average shear rate of about 3.6 s^{-1}), with nitrogen purge, mixing for 5 min before extruding into a liquid nitrogen bath. These samples were used for SEC, rheology, morphology, and catalyst localization tests.

Large sample batches (300 – 500 g) of the same compositions were created for tensile and impact strength tests using a 16 mm twin screw extruder (PRISM, L:D 24:1, four heating zones at 180 °C and a feed zone at 140 °C, 40 rpm screw speed, 3.2 feeder screw speed). Two mixing zones and three conveying zones led to flow rates of 6 – 9 g/min and residence times of about 4 min (residence time distributions ranging from 2 – 7 min for all blends, measured by colored pellets).[154] Outlet pressures ranged from 50 – 350 psi and torques from 5 – 10 N-m. After steady state polymer flow was achieved, a syringe pump was used to dispense liquid catalyst (diluted in acetone to reduce viscosity, roughly 10 wt% catalyst solution) at a controlled rate. Extrudate was chilled in a water bath, dried by air blower, pelletized, and stored in a vacuum oven for 48 h before further processing.

4.3.4 Rheology

Shear rheology was measured on an ARES rheometer with 25 mm parallel plates at 180 °C with gaps between 0.5 and 1.0 mm. Samples were compression molded into disks at 190 °C and 2 MPa for 5 min for loading. Time sweeps were performed at 3% strain and 3 rad/s to determine melt stability. Strain sweeps (3 rad/s) were used to find

the critical strain at the limit of the linear viscoelastic regime, defined as $G'(\gamma) > 0.9 \times G'(\gamma = 0)$, where γ is the strain and G' is the storage modulus. Blends exhibited a critical strain of about 40% and non-reactive blends were stable for over an hour.

4.3.5 Tensile tests

ASTM D638 type V tensile specimens (gage length = 25.4 mm, gage width = 3.15 mm, thickness = 3.2 mm) were created using a Morgan Press injection molder (barrel temperature = 185 °C, nozzle temperature = 220 °C, mold temperature = 60 °C, ram pressure = 3 – 5 kpsi, pilot valve pressure = 100 psi, clamp force = 13 tons, cycle time = 30 s). Samples were aged for at least 48 h in a room temperature vacuum oven. Compression molded samples did not yield consistent tensile results.

An Instron 1101 tensile tester with 5 kN load cell pulled samples to failure at 5 mm/min. Modulus was calculated as the initial slope of the stress-strain curve, yield stress as the maximum stress achieved, and toughness as the integrated area under the stress-strain curve.

4.3.6 Scanning electron microscopy (SEM)

Blends were microtomed using a Leica EM UC 6 and glass knife at −160 °C. The resultant flat surface was coated with 50 Å Pt and imaged using a JEOL 6500 SEM at 5 kV. Droplets were sized at 5000× magnification using ImageJ software (NIH). The average of two diameters were recorded for each droplet. Aggregate statistics were compiled using Excel and JMP 11 software.

4.3.7 Transmission electron microscopy energy dispersive spectroscopy (TEM EDS)

Blends were microtomed at −160 °C using a diamond knife, to create 50 – 70 nm sections for TEM. Sections were transferred to a copper-Formvar 300 mesh grid (Ted Pella, Inc.) using an eyelash tool. Images were obtained using an FEI Technai T12 instrument at 120 kV. Additional images and energy dispersive X-ray spectra (EDS) were collected using an FEI Technai F30 instrument at 300 kV, then analyzed using INCA and DTSA software for the presence of cobalt peaks (0.78 eV Lα, 6.92 eV Kα).

4.4 Results

Material characteristics are listed in Table 4.1. The estimated zero shear viscosities are within an order of magnitude, suggesting droplet breakup and coalescence will occur in blends. All of the polymers used are commercial, with large dispersity ($Đ$).

Table 4.1. Polymer characterization

material	M_n (kg/mol)	$Đ$	T_m (°C)	η_0 (Pa·s)	crystallinity (%)	functionality
LLDPE Engage 8200	33[155]	2.1[155]	66[a]	2500[b]	3[a]	None
PLA Natureworks 2003D	190	1.5	150[a]	5700[b]	< 1[a]	1 –COOH/chain
EGMA Lotader AX 8840	20[49,156]	5.8[c]	104[a]	4300[b]	21[a]	8 wt% GMA ~15 epoxies/chain

[a]from differential scanning calorimetry of as-received pellets, [b]from shear rheology [c]from SEC

4.4.1 Differential scanning calorimetry (DSC)

DSC was used to determine thermal transitions and crystallinity of the neat materials. A TA Q1000 instrument was used with 10 °C/min ramp rate. Second heating curves are shown in Figure 4.2. LLDPE shows a very broad melting transition around 66 °C. EGMA shows a sharper melting peak at 104 °C. PLA shows a glass transition at 60 °C, cold crystallization, and a melting peak at 150 °C. Percent crystallinity was calculated using the difference of the melting and cold crystallization peaks, normalized by the enthalpy of melting of an infinite crystal of PLA or linear PE.

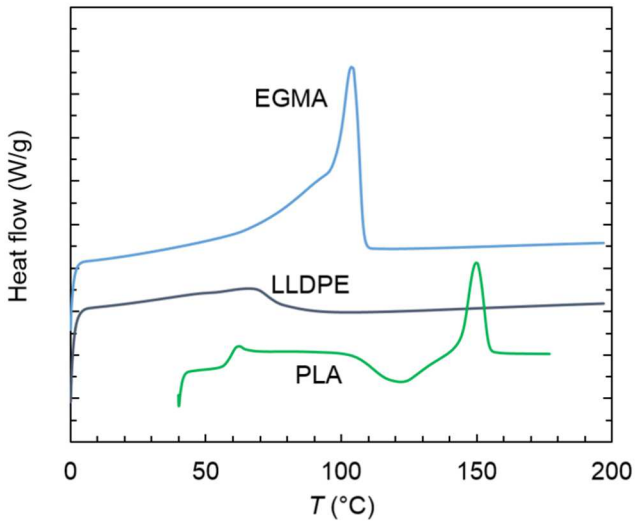

Figure 4.2. DSC second heating curves for EGMA, LLDPE, and PLA at 10 °C/min.

4.4.2 Melt processing

Droplet blends of these materials were made to investigate the effect of epoxy group concentration and catalyst type on reaction kinetics and toughness. All blends had a constant 80 wt% PLA for morphology and mechanical properties comparisons, with compositions shown in Table 4.2. Catalysts (if added) were present at a constant 0.01 M, since an equal molar basis is required for kinetics comparisons.

Table 4.2. Blend composition and nomenclature

blend name	PLA / LLDPE / EGMA / catalyst (wt fraction, 0.01 M catalyst)
0 EGMA	80 / 20 / 0 / 0
1 EGMA	80 / 19 / 1 / 0
5 EGMA	80 / 15 / 5 / 0
20 EGMA	80 / 0 / 20 / 0
DDA, 1 EGMA	80 / 19 / 1 / 0.2 (DDA)
DDA, 5 EGMA	80 / 15 / 5 / 0.2 (DDA)
$CoOct_2$, 1 EGMA	80 / 19 / 1 / 0.3 ($CoOct_2$)
$CoOct_2$, 5 EGMA	80 / 15 / 5 / 0.3 ($CoOct_2$)

4.4.3 Rheology

Frequency sweeps were performed on the pure blend components to estimate zero shear viscosities (via Cox-Merz rule and Cross model fits). Pure material complex viscosities (η^*), storage moduli (G'), and loss moduli (G'') are plotted in Figure 4.3.

Shear rheology was also performed on the blends after mixing. Time sweeps show any time-dependence of viscosity due to reaction or degradation (performed after 5 min melt mixing, 5 min heated on press, and about 10 minutes at heat while loading on the rheometer). Dynamic frequency sweeps were performed after the time sweeps to determine compatibility changes (based on the behavior of G' in the low frequency regime). Viscosity changes with time, and subsequent frequency sweeps are shown in Figure 4.4.

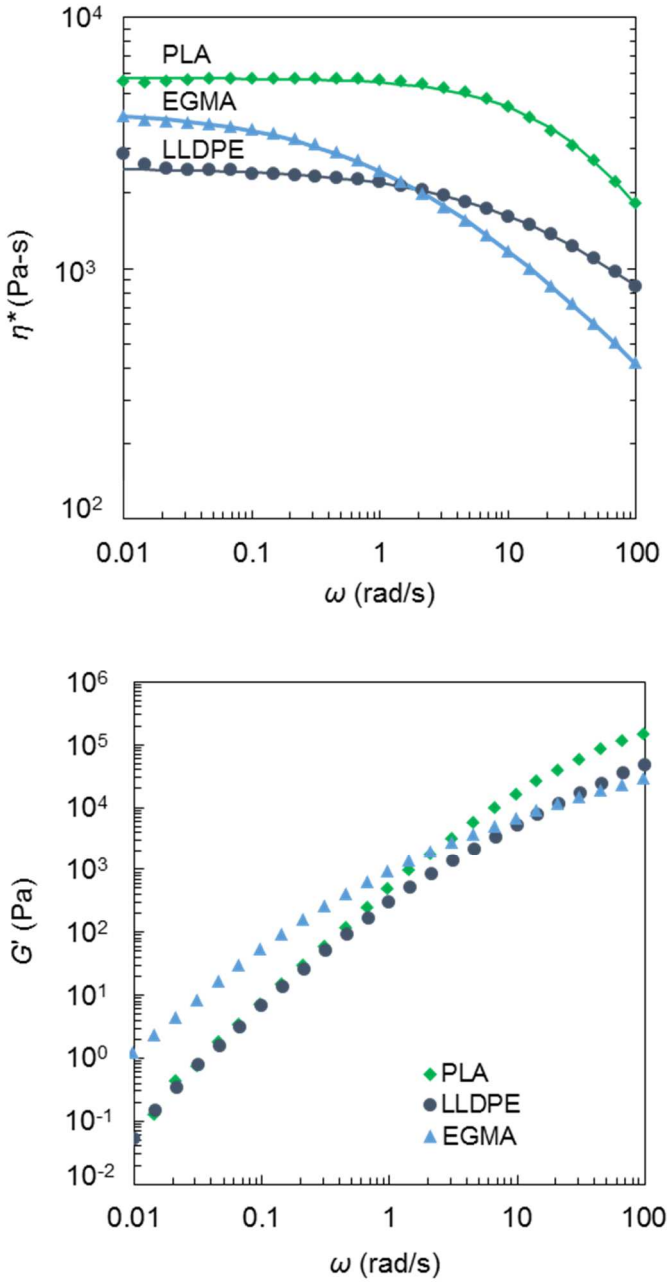

Figure 4.3. Frequency sweeps of pure blend components, on parallel plates at 180 °C in the LVE regime. (top) Complex viscosity plotted versus frequency with Cross model fits (solid lines). (bottom) Storage and loss modulus from frequency sweeps.

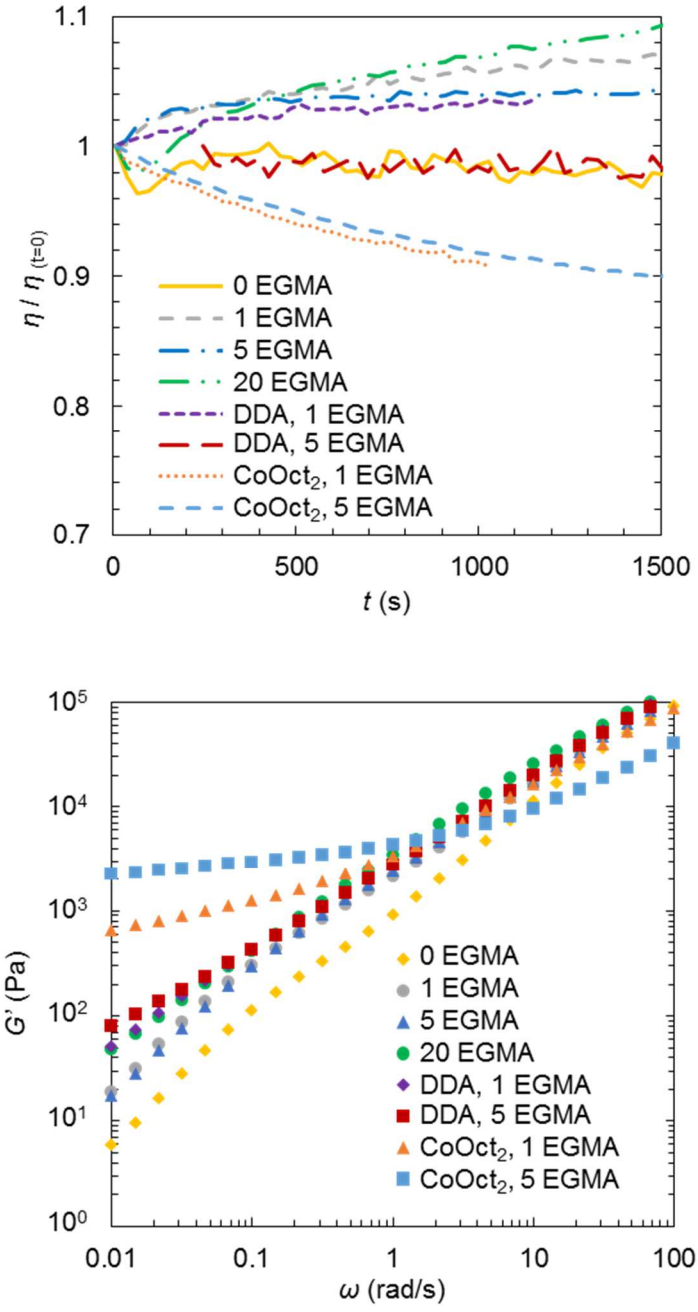

Figure 4.4. Blend shear rheology after mixing, at 180 °C on 25 mm parallel plates. (top) Viscosity changes over time, from time sweeps at 3 rad/s and 3% strain. Viscosity changes indicate if reaction or degradation is occurring. (bottom) G' as a function of frequency. Data was obtained after the time sweeps.

Time sweeps show the competing effects of two reactions: degradation of PLA (which decreases viscosity), and interfacial copolymer formation (which increases viscosity). $CoOct_2$ samples show a decrease in viscosity, attributed to $CoOct_2$ accelerating the degradation of PLA and the epoxy-acid reaction being nearly complete during melt mixing. Viscosity increases for 1 EGMA, 5 EGMA, 20 EGMA, and DDA, 1 EGMA samples, suggesting that interfacial epoxy–acid reactions are still occurring in these blends on the rheometer. 0 EGMA shows very little change, suggesting neither interfacial copolymer formation nor degradation are present. DDA, 5 EGMA was not dried sufficiently before rheology, so it may be showing competing degradation and interfacial reaction effects. The noise in the DDA, 5 EGMA and 0 EGMA blend signals occurred because lower frequency and strain were used (1%, 1 rad/s and 1%, 3 rad/s respectively, compared to 3%, 3 rad/s for all other blends). The $CoOct_2$ sample required about 45 min to load, due to extremely slow relaxation on the rheometer plates (sustained 400 g normal force for this sample through all tests, compared to 0 g normal force for all other blends). However, this sample was not crosslinked, as it dissolved completely for size exclusion chromatography.

Frequency sweeps show an upturn in G' at low frequency for samples with high copolymer formation rates ($CoOct_2$, 5 EGMA > $CoOct_2$, 1 EGMA > DDA, 5 EGMA > 20 EGMA ≈ DDA, 1 EGMA > 5 EGMA ≈ 1 EGMA > 0 EGMA). The high frequency data for $CoOct_2$, 5 EGMA does not match the rest of the blends at high frequency, which is attributed to experimental error deriving from a high normal force for this sample. The trend in G' matches the general trends observed in mixer normal force, SEC, and droplet size measurements, described below.

4.4.4 Size exclusion chromatography (SEC)

SEC was used to verify copolymer formation as a function of EGMA content and catalyst. After mixing, blends were dissolved in 1,2,4–trichlorobenzene at elevated temperatures before injection. A linear baseline was created between retention times of 15 and 25 min, and data are normalized by integrated area. All traces showed one broad

peak, as shown in Figure 4.5. EGMA, PLA, and LLDPE showed integrated changes in RI signal of −2200, −1900, and −2200 mV-s at 1 mg/mL, respectively. Compared to predicted traces (based on blend composition and pure component RI changes) and uncatalyzed blend traces, $CoOct_2$ blend results show a clear shoulder at high molecular weight, suggestive of reaction.

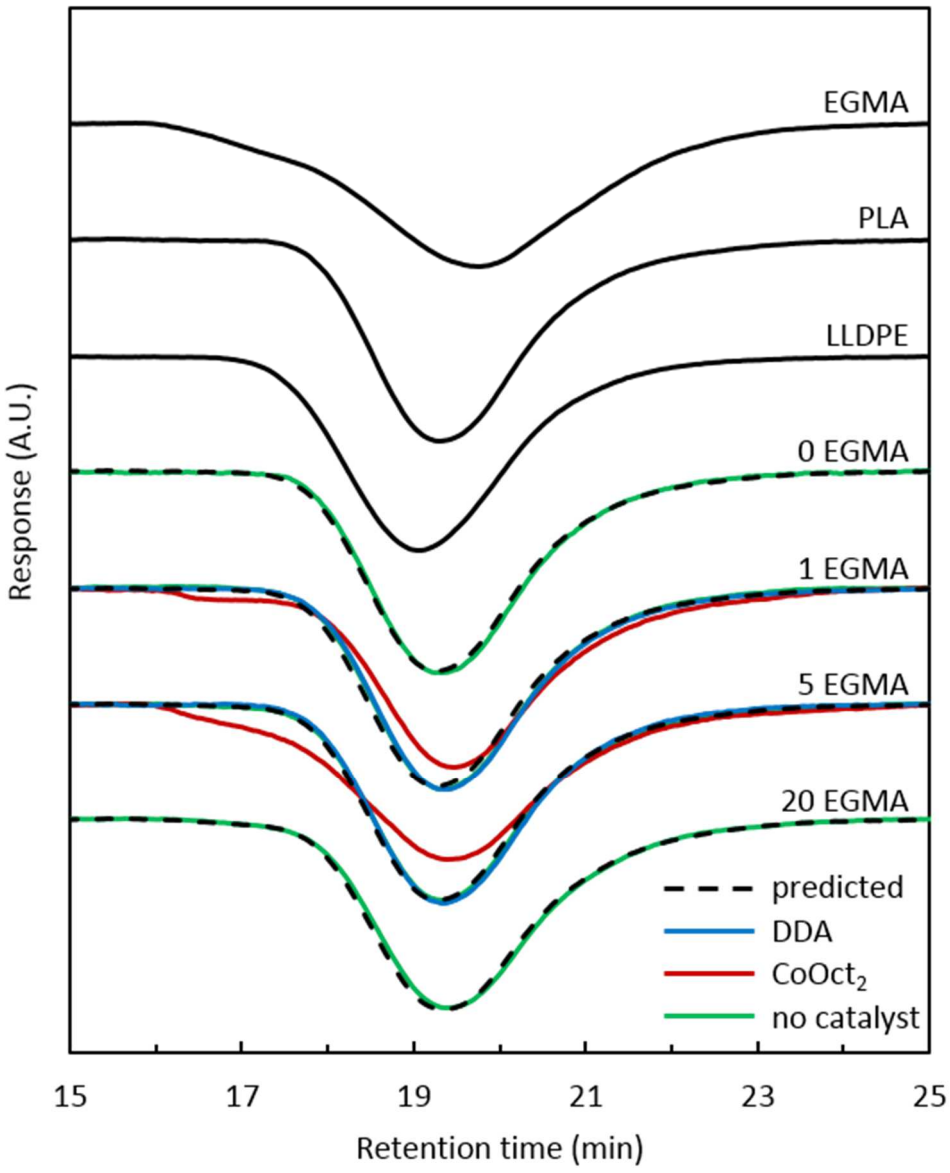

Figure 4.5. High temperature SEC traces for neat polymers and batch mixed blends (135 °C, 1,2,4-trichlorobenzene, RI detector, normalized by peak area, shifted vertically based on compatibilizer content).

Black dashed lines indicate predicted traces if no reaction occurs, based on neat material traces weighted by blend composition.

Polystyrene equivalent molecular weights were calculated, displayed in Table 4.3. M_n is similar for all blends except those containing $CoOct_2$, which were lower. This is due to $CoOct_2$ accelerating the degradation of PLA in melt mixing (discussed further in toughness results section). M_w increases with EGMA content and catalyst, again indicating that reaction occurs more quickly with more functional polymer and in the presence of catalyst. $CoOct_2$ is more effective than DDA for increasing M_w and high molecular weight fractions in SEC.

Table 4.3. Polystyrene equivalent average molecular weights for pure materials and batch mixed blends

material	M_n (kg/mol)	M_w (kg/mol)
PLA	43	130
EGMA	32	190
LLDPE	69	180
0 EGMA	42	130
1 EGMA	42	130
5 EGMA	40	140
20 EGMA	39	140
DDA, 1 EGMA	41	130
DDA, 5 EGMA	39	150
$CoOct_2$, 1 EGMA	34	150
$CoOct_2$, 5 EGMA	33	210

4.4.5 Morphology

Droplet size was measured for all blends, as smaller droplet size is often an indication of copolymer formation and compatibility improvements. Representative SEM images are shown in Figure 4.6 and average droplet sizes in Table 4.4. It should be noted that SEM droplet sizes are accurate only down to about 200 nm, so the smallest droplets are not observed. Also the particle size distribution (d_{vv}/d_n) is quite wide for these samples. Droplet size follows the same general trends as SEC and rheology: higher loadings of EGMA decrease droplet size, and catalysts are effective for reducing droplet

size (with $CoOct_2$ being more effective than DDA). DDA broadens the particle size distribution, making it almost bimodal, which is why its d_{vv} is higher than anticipated for DDA, 5 EGMA in Table 4.4. The $CoOct_2$, 5 EGMA sample seems to have strong adhesion, since very little droplet pullout is observed (Figure 4.6 e,f). Also, this sample has irregularly shaped drops, which suggests a lower interfacial tension in mixing (Figure 4.6 f).

Table 4.4. Droplet size statistics, 5 min batch mixing

blend	droplet size (μm, $< d_{vv} >$)	$< d_{vv} > / < d_n >$	droplets sized
0 EGMA	2.7	5.6	687
1 EGMA	2.2	6.6	870
5 EGMA	1.8	4.7	840
20 EGMA	1.7	5.3	1407
DDA, 1 EGMA	2.4	6.5	826
DDA, 5 EGMA	3.0	10.2	626
$CoOct_2$, 1 EGMA	1.1	3.5	1224
$CoOct_2$, 5 EGMA	1.0	3.2	929

d_{vv} = volume averaged diameter, d_n = number averaged diameter

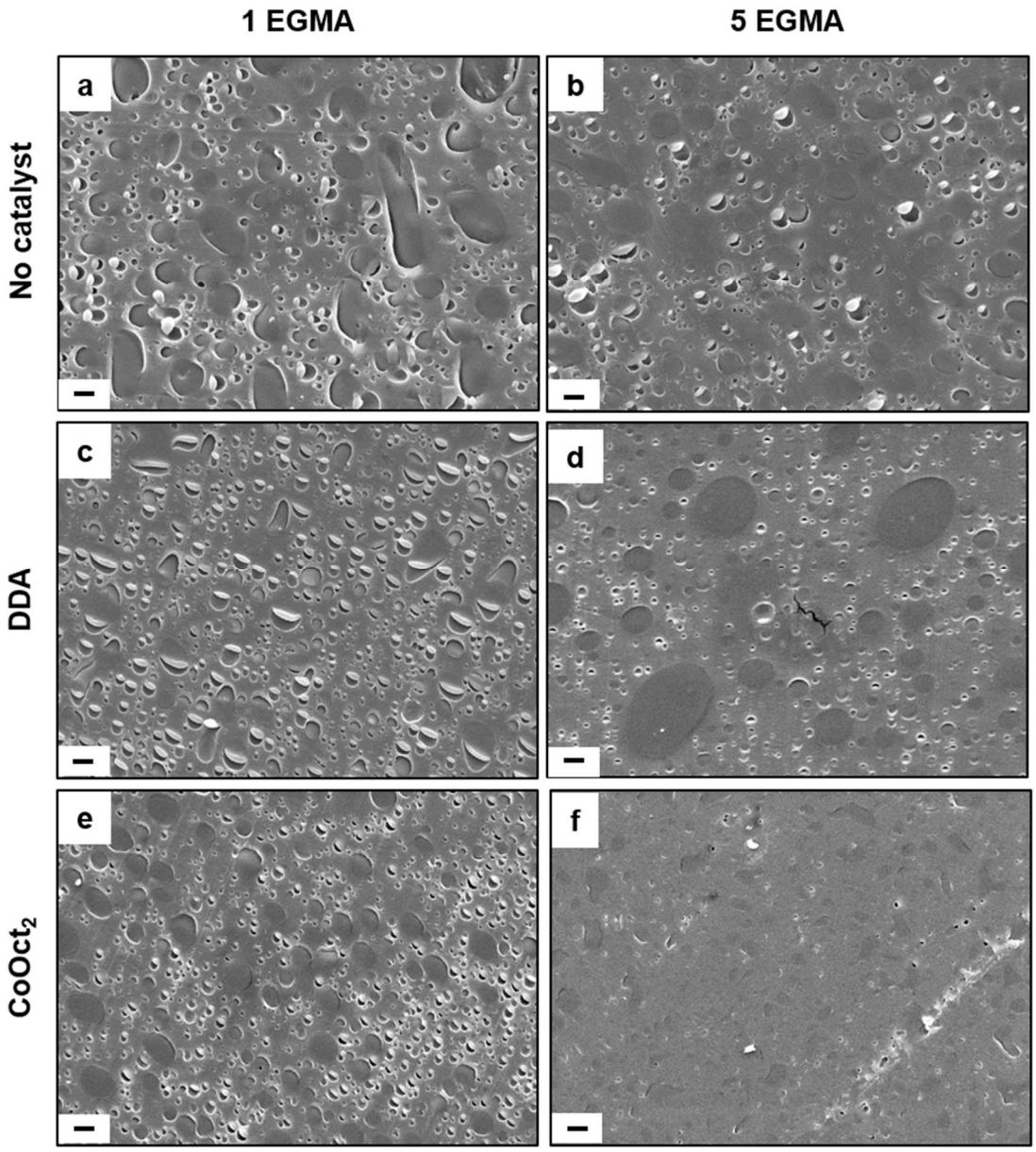

Figure 4.6. Representative SEM images of batch mixed blends, taken at 5000× magnification after cryo-microtoming and coating with 50 Å Pt with 1 μm scale bars. (a) 1 EGMA, (b) 5 EGMA (c) DDA, 1 EGMA, (d) DDA, 5 EGMA, (e) $CoOct_2$, 1 EGMA, (f) $CoOct_2$, 5 EGMA, 0 EGMA and 20 EGMA blend images shown in Appendix 2. Droplet size generally decreases with increasing EGMA content and catalyst addition.

Select blends were also examined by TEM to verify droplet size rankings, and to explore the possibility of micelle formation (Figure 4.7). These low magnification images show a general decrease in average droplet size as EGMA content increases. Also, micelles are observed in the $CoOct_2$, 1 EGMA blend, and a much higher concentration in the $CoOct_2$, 5 EGMA blend. These micelles are likely spherical with an EGMA core and PLA shell. They were not included in the droplet size count for SEM, as they were not visible. Micelles are another indication of very fast interfacial reaction and low surface tension.

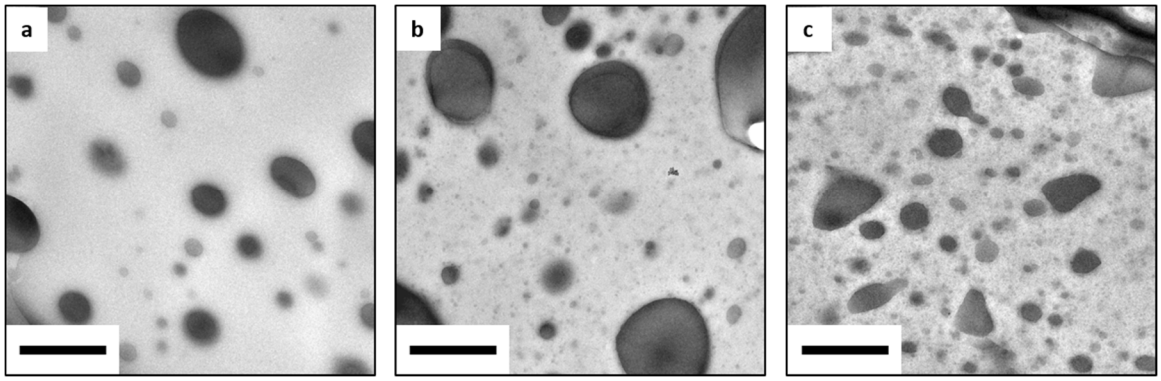

Figure 4.7. TEM images of batch mixed blends at 120 kV. 50-70 nm thick sections created by cryo-microtome then transferred to 300 mesh copper Formvar grids. (a) $CoOct_2$, 0 EGMA, (b) $CoOct_2$, 1 EGMA, and (c) $CoOct_2$ 5 EGMA blends. Droplet size reduction and micelle concentration increase are observed with increasing EGMA content. Scale bars are 1 μm.

4.4.6 Melt reaction kinetics

Mixer normal force (f_N) was used to compare reaction rates between blends. As copolymer is generated at the interface, interfacial slip decreases and average molecular weight (viscosity) increases. This results in an increase in pressure at the bottom of the mixing chamber, due to the drag flow of the screws. This can be measured from the normal force felt between the screws and mixing chamber.

Representative plots of mixer force (f_N) versus time (t) are shown in Figure 4.8. For the first minute, loading causes a large initial increase in f_N for all samples. At the

leftmost arrow, polymer pellet loading is complete. Then catalysts are added (if necessary), which is completed by the middle arrow. Then, there is a steady state region of mixing, followed by extrusion (right arrow). All samples were mixed at least three times and forces were recorded. Small changes in initial forces (f_{N0}) are due to viscosity differences between EGMA and LLDPE.

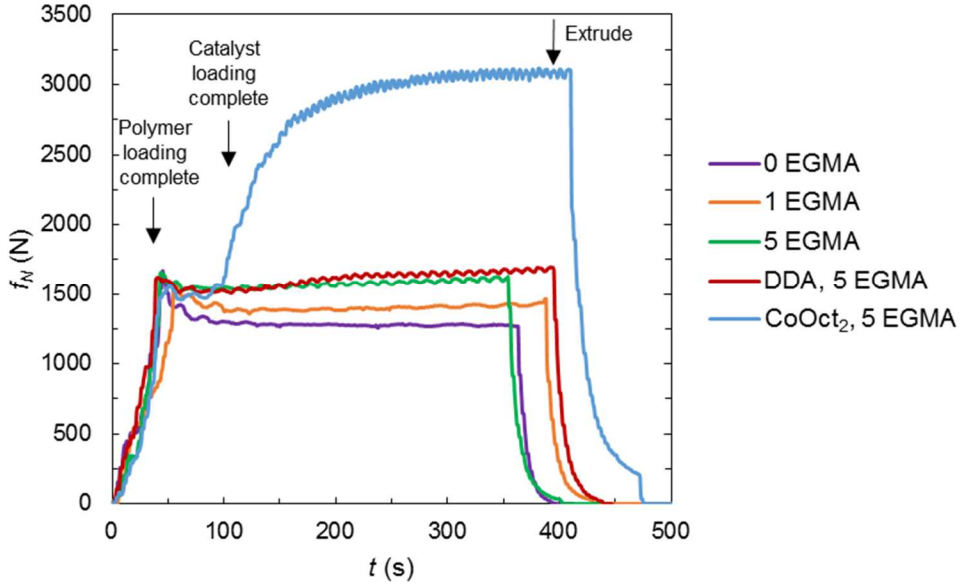

Figure 4.8. Mixer normal force versus time for batch mixed blends, measured by strain gauge between the mixer barrel and screws. Slopes in the steady state portion of blending indicate if reaction is occurring.

There is no exact correlation between f_N and viscosity, molecular weight, or size of the dispersed phase. However, relative reaction rates can be estimated between analogous catalyzed and uncatalyzed blends by assuming the reaction follows the same pathway (rate law) and the force is the same for a given conversion and composition. From batch reactor design equations and a generic rate law,

$$N_{A0}\frac{dX}{dt} = -r_A V = -kC_A^{\alpha}C_B^{\beta}V \qquad (12)$$

where N_{A0} is the initial moles of reactant A, X is conversion, t is time, r_A is reaction rate, k is reaction rate constant, C_A is concentration of reactant A at time t, α is the order of reactant A, C_B is the concentration of reactant B at time t, β is the order of reactant B, and

V is the reaction volume. The reaction takes place almost exclusively at the interface in reactive compatibilization, so V is defined as the interfacial volume (Figure 4.9).

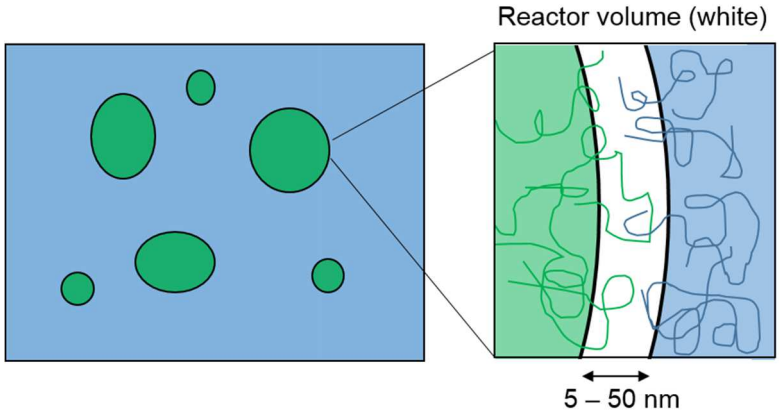

Figure 4.9. Schematic of interfacial reaction volume (white). Blue represents the PLA matrix and green represents the LLDPE/EGMA droplets. Interfacial thickness will increase with graft copolymer formation.

Integrating and rearranging yields equation (13), where kt is some function of V, X, C_A, C_B, α, and β. This assumes the same rate law (i.e., α and β) for catalyzed and uncatalyzed blends.

$$kt = f(V, X, C_A, C_B, \alpha, \beta) \tag{13}$$

For analogous catalyzed and uncatalyzed blends (e.g., 5 EGMA and $CoOct_2$, 5 EGMA), at a specific f_N, given the assumptions stated above, the generic function on the right hand side of Equation 2 is assumed to be constant. Therefore, the times that analogous blends reach a given force can be used to estimate reaction rate constant ratios. For normalized force (f_N / f_{N0}) versus time plots, slopes (m) can also be compared, as shown in equation (14). This method includes data from many time points, and is more robust than comparing individual values.

$$\frac{k_{cat}}{k} = \frac{t\ (f_N/f_{N0})}{t_{\ cat}(f_N/f_{N0})} = \frac{m}{m_{cat}} \tag{14}$$

Plots of f_N / f_{N0} versus time are shown in Figure 4.10, time shifted from Figure 4.8 to eliminate force data during loading. Table 4.5 contains aggregate statistics for the slope of f_N / f_{N0} versus time. It can be inferred that blends with higher slopes have higher

reaction rates, and therefore, higher copolymer contents. For blends that reached a plateau ($CoOct_2$, EGMA 1 and $CoOct_2$, EGMA 5), initial slopes were calculated, avoiding the interface-limited reaction kinetics regime at high conversions.

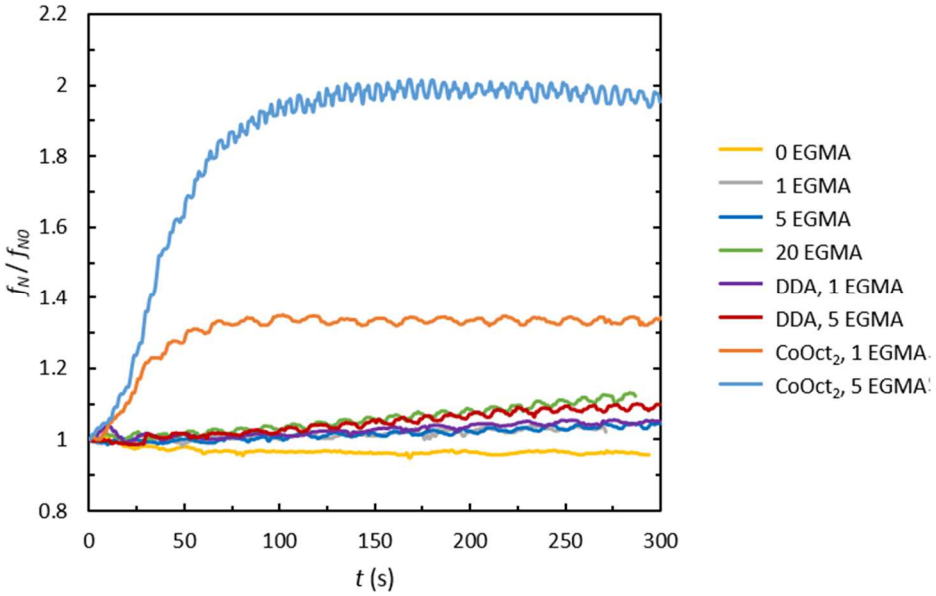

Figure 4.10. Representative curves of normalized mixer normal force versus time. Catalyst and EGMA content changes the slope of these curves, indicative of interfacial reaction.

Table 4.5. Average starting force ($\langle f_{N0} \rangle$) and average slope ($\langle m \rangle$) from mixer normal force plots

Blend	$\langle f_{N0} \rangle$ ± S.D. (N)	$\langle m \rangle$ ± S.D. (10^{-4} s^{-1})
0 EGMA	1310 ± 20	-1.6 ± 0.9
1 EGMA	1420 ± 40	0.8 ± 0.5
5 EGMA	1550 ± 30	1.9 ± 0.6
20 EGMA	1380 ± 20	4.1 ± 0.4
DDA, 1 EGMA	1380 ± 10	1.5 ± 0.5
DDA, 5 EGMA	1530 ± 20	3.2 ± 0.2
$CoOct_2$, 1 EGMA	1390 ± 40	80 ± 11*
$CoOct_2$, 5 EGMA	1550 ± 30	165 ± 27*

Standard error reported; $n > 3$. *Initial slope

EGMA content and catalysts have clear effects on reaction rate. Increasing EGMA content from 0 to 20 wt% increases the slope observed from -1.6×10^{-4} s^{-1} to 4.1×10^{-4} s^{-1}. DDA further increases slope, so that DDA, 1 EGMA has a similar slope to 5 EGMA and DDA, 5 EGMA has similar slope to 20 EGMA. This efficacy of similar alkylamine catalysts for epoxy-acid interfacial reactions is in agreement with previous reports.[35,68] $CoOct_2$ catalyzed blends show a much more dramatic increase in f_N reaching a plateau in under 100 s, suggesting complete conversion on this timescale.

Calculations of reaction rate constant ratios are shown in Table 4.6. DDA catalyst increases reaction rates by less than a factor of two, and $CoOct_2$ increases reaction rate by roughly 90 fold. This dramatic effect agrees with changes seen in SEC and droplet size measurements. Similar values obtained for 1 EGMA and 5 EGMA blends suggest this is a reasonable method for measuring relative reaction rates. $CoOct_2$ is clearly more effective at promoting interfacial reaction rate in this system.

Table 4.6. Estimated ratio of reaction rates between neat and catalyzed blends

ratio	1 EGMA	5 EGMA
k_{DDA} / k	1.8	1.7
k_{CoOct2} / k	96	88

Three weaknesses of this analysis are (1) viscosity cannot be directly related to chemical reaction, (2) interfacial volume is not constant between catalyzed and non-catalyzed blends, and (3) it takes finite time for the catalysts to be dispersed completely in the mixer. The second effect is due to copolymer formation. In blends with faster reactions, copolymer is formed more quickly, reducing surface tension and causing finer dispersion and wider interfaces at any given time. This difference in interfacial reactor volume leads to an overestimation of reactivity ratio. The third effect, time between catalyst addition and having it fully mixed, leads to an underestimation of the reaction rate constant ratio (due to a decrease in effective catalyzed reaction volume at small times). Regardless, this is a useful, fast method for comparing reaction rates, relevant to

processing. It clearly shows the effectiveness of $CoOct_2$ over DDA and uncatalyzed blends.

4.4.7 Tensile tests

Copolymer can facilitate stress transfer across the interfaces of blends, which has potential application in toughening PLA. Tensile and impact strength tests are two of the most common methods for measuring toughness. Tensile data is presented here, and preliminary impact strength data is in the appendices.

Representative stress-strain tensile curves from tensile tests are shown in Figure 4.11. The average yield stress, strain at break, tensile toughness, and modulus are displayed in Table 4.7 ($n = 5$). All blends showed stress whitening at low strain, in accordance with the cavitation stress dissipation mechanism described by Kowalczyk et al.[145] Necking was also observed for all reactive blends, suggesting shear yielding is also a deformation mechanism. The moduli are slightly reduced for all blends compared to neat PLA. DDA catalyst blends show slight improvements to tensile toughness over uncatalyzed blends, in accordance with their relative reactivities calculated from mixer normal force measurements. $CoOct_2$, 5 EGMA shows the best toughness, over an order of magnitude higher than pure PLA and over five times higher than the 0 EGMA blend. The extension at break for this blend is about 200%, comparable to the best PLA blends with 20% additive in current literature.[112,135]

For rubber toughened blends, improvements in tensile toughness generally come at the cost of decreased elastic modulus and yield strength compared to the neat matrix material. Feng et al. noted a decrease in elastic modulus from ~1800 MPa to ~1300 MPa and yield stress from ~73 MPa to ~40 MPa when adding 20 wt% EMA-GMA to PLA.[68] Oyama found ~30% reduction in modulus and ~40% reduction in yield stress when blending 20 wt% EGMA into PLA.[147] Finally, Li et al. added 20 wt% LLDPE+EGMA to PLA, observing decreased modulus (from 3000 to 1800 MPa) and yield stress (from ~69 MPa to ~30 MPa) for the blends compared to neat PLA.[148] Our blends show similar

results, with ~30% reduction in elastic modulus and ~40% reduction in yield stress when adding 20 wt% LLDPE+EGMA.

Table 4.7. Tensile and impact properties of PLA/LLDPE/EGMA/catalyst blends

blend	σ_y (MPa)	ε_b (%)	toughness (MJ/m^3)	elastic modulus (MPa)
PLA	78 ± 1	7 ± 2	3 ± 0.2	2700 ± 160
0 EGMA	36 ± 1	25 ± 3	7 ± 0.4	1800 ± 80
1 EGMA	48 ± 0	47 ± 3	15 ± 1.0	2100 ± 90
5 EGMA	47 ± 1	107 ± 6	16 ± 0.3	2100 ± 100
20 EGMA	54 ± 0	58 ± 12	3 ± 0.5	2300 ± 160
DDA, 1 EGMA	45 ± 1	116 ± 9	15 ± 1.0	1900 ± 70
DDA, 5 EGMA	48 ± 2	140 ± 9	30 ± 2.3	2000 ± 110
$CoOct_2$, 1 EGMA	44 ± 0	21 ± 7	4 ± 2.0	1900 ± 100
$CoOct_2$, 5 EGMA	45 ± 1	199 ± 6	38 ± 1.4	1900 ± 130

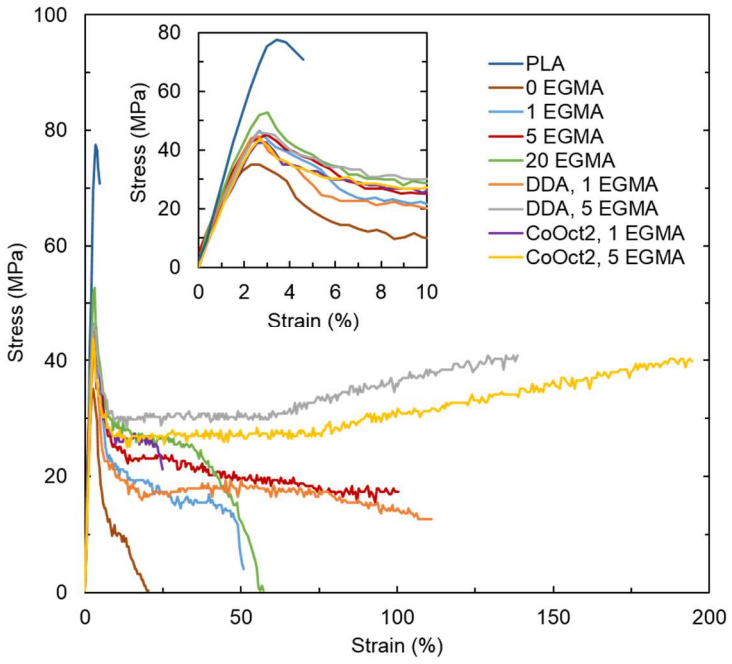

Figure 4.11. Representative tensile stress-strain curves for PLA/LLDPE/EGMA/catalyst extruded blends, obtained at 5 mm/min. Inset highlights the decrease in elastic modulus and yield stress of PLA when LLDPE and EGMA are added.

Interestingly, the $CoOct_2$, 1 EGMA blend shows very poor tensile properties and melt strength, attributed to $CoOct_2$ accelerating PLA degradation in processing. SEC of injection molded and extruded samples are compared in Table 4.8. The extruded and injection molded samples for $CoOct_2$, 1 EGMA show a distinct decrease in molecular weight compared to the batch mixed blend in Table 4.3 (M_w < 90 kg/mol and M_w = 150, respectively). This is ascribed to having a nitrogen blanket in the batch mixer. Assuming similar degradation in the extruded $CoOct_2$, 5 EGMA blend, its improved tensile toughness is even more surprising. If the residence time of in the extruder was shorter, PLA degradation and blend molecular weight reduction should be reduced, possibly leading to even higher tensile toughness for $CoOct_2$ blends compared to non-catalyzed blends. The effect of residence time on tensile properties and degradation is discussed further in Appendix 2.

Table 4.8. SEC results examining degradation in extrusion and injection molding

sample		M_n (kg/mol)	M_w (kg/mol)	$Đ$
PLA	extruded	51	150	2.9
	injection molded	52	140	2.5
0 EGMA	extruded	49	160	3.3
	injection molded	56	160	2.8
1 EGMA	extruded	50	160	3.2
	injection molded	54	160	2.9
5 EGMA	extruded	45	160	3.5
	injection molded	51	160	3.1
20 EGMA	extruded	56	160	3.5
	injection molded	51	170	3.3
DDA, 1 EGMA	extruded	51	160	3.1
	injection molded	49	150	3.0
DDA, 5 EGMA	extruded	48	150	3.2
	injection molded	48	150	3.1
$CoOct_2$, 1 EGMA	extruded	14	86	6.2
	injection molded	19	85	4.6
$CoOct_2$, 5 EGMA	extruded	37	130	3.4
	injection molded	19	100	5.1

4.4.8 Catalyst localization

TEM EDS was performed to determine $CoOct_2$ catalyst localization. Past work has shown localization can play an important role in catalyst efficacy for reactive compatiblization.[35,54] $CoOct_2$ was chosen because it has clear EDS peaks and may have a solubility parameter similar to stannous octoate, which has been shown to localize at the interface in PE/PLA blends (Chapter 3).[54]

EDS spectra were obtained every 36 nm (100 scans, ~20 nm spot diameter). Each spectra was integrated for Co signal (6.8 – 7.1 keV), reported as integrated Co counts as a function of distance along the line scan (Figure 4.12). $CoOct_2$ shows measurable concentration in the PLA matrix, and no noticeable increase in concentration at the interface. This result is consistent for multiple $CoOct_2$ blends (0 EGMA, 1 EGMA, and 5 EGMA) and various EDS collection conditions. Normalizing by Cu or C counts does not change the general results. Therefore, another attribute such as activity is contributing to the superior reaction facilitation of $CoOct_2$, instead of localization. Past work has shown stannous octoate localizes at the interface of PE/PLA blends despite having a solubility parameter close to that of PLA (20.0 $MPa^{1/2}$ estimated by lyoparachor method for stannous octoate versus 20.5 $MPa^{1/2}$ reported experimentally for PLA, from Chapter 3).[54] We hypothesize changing the metal center from Sn to Co increases the catalyst solubility parameter enough for $CoOct_2$ to be miscible in PLA. DDA is composed of light elements, so EDS is not feasible.

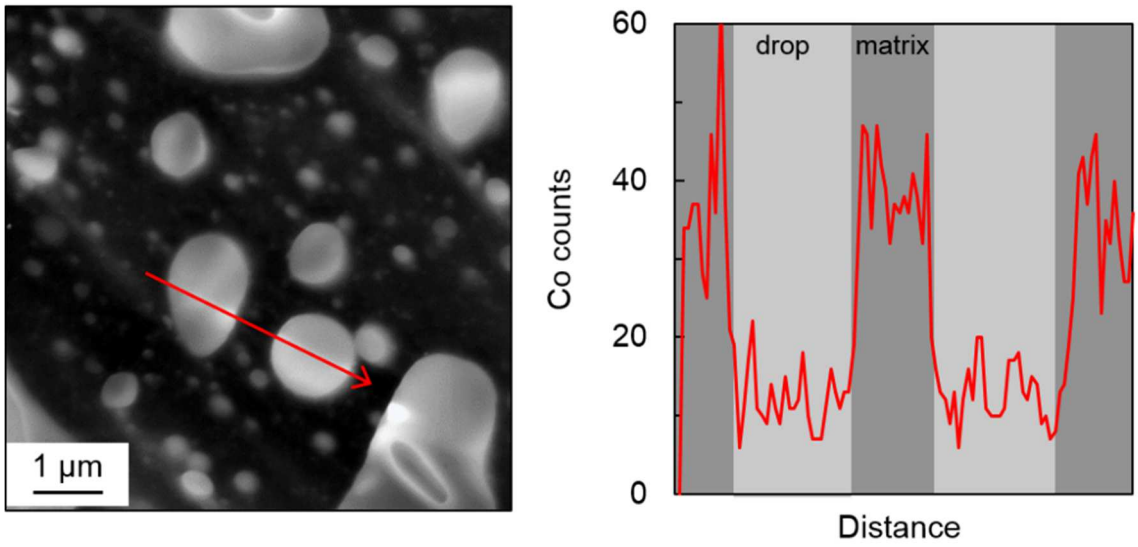

Figure 4.12. TEM EDS line scan of $CoOct_2$, 5 EGMA blend showing that $CoOct_2$ resides in the PLA matrix (120 kV, F30, 70 nm section unstained). (left) STEM image with red arrow indicating location and direction of line scan. (right) Integrated Co counts as a function of distance along line scan. Light and dark background roughly specifies the domains probed in the image.

4.5 Conclusions

PLA was toughened using a commercially available reactive compatibilization system of EGMA and LLDPE. Addition of epoxy–acid catalysts to the system increased copolymer formation rate, leading to higher tensile toughness and notched impact strength. Tensile extension at break was increased ~25 fold for $CoOct_2$, 5 EGMA compared to neat PLA, albeit with ~30% reduction in elastic modulus and ~40% reduction in yield stress. Catalysts reduce the amount of expensive EGMA necessary to obtain a given toughness in PLA/EGMA/LLDPE blends (as compared to previous work[68,149]).

A new method was developed for comparing interfacial reaction kinetics, using mixer normal force. This is a useful tool for quickly screening catalysts and functional groups for reactive compatibilization. It is generally more sensitive than SEC. This method shows $CoOct_2$ catalyst was particularly effective for this system, accelerating

conversion to copolymer by an estimated 90 times over non-catalyzed reactions and 50 times over established alkylamine catalysts.

Future work will include contact angle measurements to estimate catalyst wetting parameters, blending with other catalysts (such as chromium (III) complexes) to achieve higher activity and interfacial localization, and catalyzed adhesion testing of PLA/EGMA bilayers.

Chapter 5. Toughening isotactic polypropylene (iPP) with polyethylene (PE) and iPP-b-PE copolymers

5.1 Summary

PE and iPP are the two largest-volume commodity plastics worldwide.[157] Recycling these materials can be difficult due to iPP impurities in PE or vice versa, since they are difficult to separate.[158] Blending iPP and PE is an alternative to separation, but their blends have poor compatibility and physical properties.[159] This project uses novel iPP-*b*-PE copolymers to compatibilize mixtures of iPP and PE to improve toughness and adhesion. A library of novel iPP-*b*-PE copolymers was made by the Coates and Lapointe groups at Cornell with varied molecular weight, tacticity, PE weight fraction, and PE branching to explore iPP/PE/iPP-*b*-PE blend properties and determine block copolymer architectures that increase toughness and adhesion. Block copolymers with total molecular weight greater than 100 kg/mol improved adhesion between iPP and HDPE laminated sheets, but formed micelles in melt blending leading to little improvement of blend mechanical properties.

5.2 Introduction

This project targets tough blends of recycled PE and iPP, with similar modulus and yield stress to neat iPP. Non-compatibilized blends of the two typically have poor toughness and extension at break compared to the pure materials. An example of this is shown in Figure 5.1, where blends of high density polyethylene (HDPE) and isotactic polypropylene (PP) show lower tensile strength and elongation at break than the substituent homopolymers.[159] This highlights the difficulty in obtaining useful properties from blending mixed recycle streams of these materials.

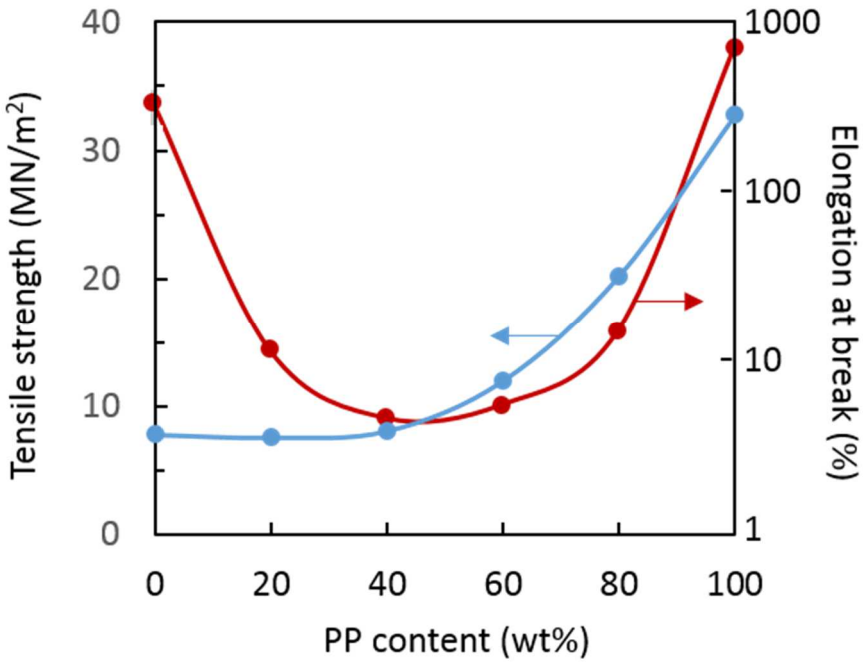

Figure 5.1. Tensile strength and elongation at break of PP/HDPE blends, reproduced from Teh et al.[160] Blends show decreased elongation at break compared to neat materials, and tensile strength is less than weight averaged pure component values.

Compatibilizers are a way to strengthen the interface and improve dispersion in polymer blends. iPP/PE compatibilized blends generally exhibit tensile modulus and yield strength the same or worse than the homopolymers (except low temperature iPP), but the impact strength and elongation at break can be dramatically improved.[146]

PE and iPP have been compatibilized using a variety of random and block copolymers (reviewed by Teh et al.[160]). Random copolymers of ethylene and longer alkenes (e.g., propylene, butylene, hexane, or octene) show good compatibility and sometimes even miscibility with iPP. Therefore, these random copolymers, alone or in blocks with PE-miscible materials, are often effective compatibilizers for PE/iPP blends.[161,162] Nakamura et al. added 3 wt% poly(ethylene-*b*-ethylene/butylene-*b*-ethylene) triblock copolymers from JSR Corporation to increase the extension at break of 70/30 PE/iPP blends from ~140% to almost 1000%.[163,164] Ethylene propylene rubber

(EPR) is one of the most common compatibilizers found in literature. It generally increases impact strength but lowers tensile modulus and yield strength; these changes are attributed to increased interfacial adhesion.[161,165–170] More recently, olefin-based multiblock copolymer compatibilizers have resulted in large improvements in extension at break and impact strength of iPP/PE blends. Multiblock copolymers exhibit super–toughness based on their ability to bridge the interface multiple times and poor packing in micelles. Researchers from The Dow Chemical Company and Case Western Reserve University reported blending iPP and HDPE with a novel olefin multiblock polymer (with HDPE hard blocks and LLDPE soft blocks), resulting in a material with extension at break of almost 900%.[171] The multiblock copolymer also increased adhesion between HDPE and iPP layers and resulted in finer dispersion in blends. Marchand and coworkers developed iPP/ethylene-*ran*-propylene multiblock copolymers for the same purpose, showing decreased droplet size in TEM.[172] Lin et al. compared ethylene/octene multiblock copolymers, ethylene/octene random copolymers, propylene-ethylene block copolymers, and a styrenic block copolymer for toughening in HDPE/iPP blends.[173] While none of the blends were as tough as the pure HDPE or iPP materials in room temperature tensile tests, the toughness of the compatibilized blends was almost an order of magnitude higher than the binary blend. Additionally, the low temperature tensile toughness of the compatibilized blends was higher than pure iPP or the binary blend.

Interfacial adhesion often controls the toughness of blends. Previous work at the University of Minnesota examined failure mechanisms at iPP/PE interfaces and the toughness of iPP/PE blends with and without copolymer.[174] The authors found that crystallite-anchored interfacial entanglements are critical for adhesion and blend toughness. Addition of a block copolymer suppressed these anchored entanglements, decreasing adhesion and toughness. Chaffin et al. studied the adhesion between HDPE and iPP bilayers, noting that metallocene synthesized materials had much higher adhesion than Ziegler–Natta (Z–N) materials, because of low molecular weight fractions in the Z–N materials that went to the interface and could not co-crystallize.[175] Song et al. also

modulated crystallinity in HDPE/iPP bilayers by changing cooling rate of bilayers in coextrusion and lamination, finding that faster cooling and higher crystallinity correlated with higher adhesion.[63] These studies show crystallinity and adhesion are critical parameters for blend toughness. The block copolymers in this study are unique, in that the iPP blocks have higher isotacticities than others reported in literature, making them potentially better at co-crystallizing with the iPP matrix. This may lead to higher adhesion and toughness in blends.

This study focuses on the ability of different architectures of iPP-*b*-PE to compatibilize iPP/PE blends, with the ultimate goal of making a tough iPP/PE blend for recycling applications. Adhesion tests performed on laminated bilayers show the ability of these molecules to increase adhesion at iPP/PE interfaces. TEM shows droplet size changes and detects if block copolymer micelles are formed during melt mixing. Rheology (in conjunction with TEM) helps confirm block copolymer localization. The blend toughness is evaluated by tensile and impact strength tests. Finally, rheology is performed on the pure block copolymers to obtain an estimate of the Flory-Huggins interaction parameter, in order to better understand the phase separation and interactions between PE and iPP (which are not well understood currently[176–180]).

5.3 Materials

The list of iPP-*b*-PE copolymers from Cornell are shown in Table 5.1 and are listed in decending molecular weight. The isotacticities of the iPP block are constant, about 88% [m^4] (i.e., on average 88% of pentads are completely isotactic). Interestingly, some of the copolymers show multiple melting peaks, while most only show one. The cause of this is unknown currently. Total molecular weights range from 10–210 kg/mol, with fairly low dispersities. These copolymers were synthesized using living and chain transfer mechanisms, through a method soon to be published. Wide angle X-ray scattering (WAXS), differential scanning calorimetry (DSC), and size exclusion chromatography (SEC) data will also be presented in a forthcoming journal article.

Table 5.1. Library of iPP-b-PE from Cornell.

iPP-*b*-PE	$M_{n\ iPP}$ (kg/mol)	$M_{n\ tot}$ (kg/mol)	$Đ$	T_m (II) (°C)	PE (wt%)	[m^4] (iPP) (%)
$P_{71}E_{139}$	71	210	1.3	133	66	88
$P_{81}E_{69}$	81	150	1.3	134	47	88
$P_{73}E_{47}$	73	120	1.3	131	37	87
$P_{82}E_{38}$	82	120	1.3	132	30	88
$P_{32}E_{57}$	32	89	1.4	135	63	88
$P_{55}LE_{31}$	55	86	1.2	133	37	-
$P_{31}E_{33}$	31	64	1.4	133	52	88
$P_{32}E_{20}$	32	52	1.3	131	39	89
$P_{29}E_{14}$	29	43	1.3	130	33	88
$P_{26}E_{11}$	26	37	1.4	131	30	88
$P_{15}E_{20}$	15	35	1.4	134	57	88
$P_{21}E_{10}$	21	31	2.0	134	31	88
P_8E_3	7.5	11	2.0	143, 151	26	-

All iPP-b-HDPE except $P_{55}LE_{31}$ (iPP-b-LLDPE, 9% octene content). Materials and information from Coates and Lapointe groups, Cornell University

Table 5.2 shows the characteristics of the homopolymers HDPE, LLDPE, and iPP used in this study. These were chosen to have similar viscosities, so that droplet breakup and coalescence occurs in melt mixing. In particular, HDPE and iPP are very closely viscosity matched, especially at high shear rates.

Table 5.2. Homopolymer charateristics for iPP/PE blends

material	M_n (kg/mol)	$Đ$	T_m (°C)	η_0 (Pa·s)	MFI	crystallinity %
LLDPE Engage 8200	33[155]	2.1[155]	66	2500	5 g / 10 min / 190 °C	< 5
HDPE J-rex HD KF 251A	8.1[181]	14[181]	130	28000	-	53
iPP Dow H314-02Z	61	6.9	163	28000	2 g/ 10 min / 230 °C	37

Rheology data were obtained from an ARES rheometer with a 25 mm parallel plate fixture using small amplitude oscillatory shear. All the materials are stable at 180 °C

based on time sweeps over one hour, confirmed by constant G' and G'' as well as SEC data collected before and after each loading. Frequency sweeps at the processing temperature of interest (180 °C) are shown in Figure 5.2.

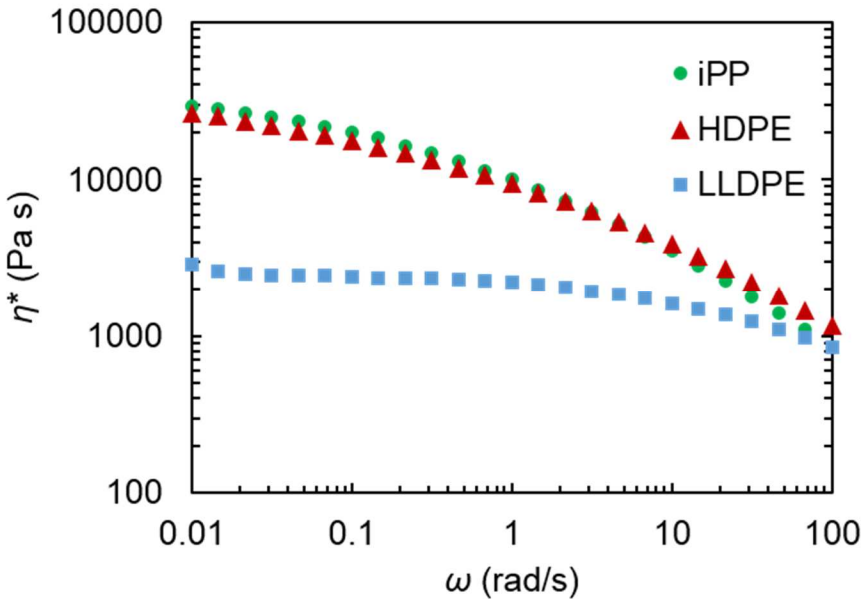

Figure 5.2. iPP, HDPE, and LLDPE viscosity (η^*) as a function of frequency (ω) from frequency sweeps (180 °C, 25 mm parallel plates, LVE regime). Moduli are shown in Figure 5.17 and 5.18.

Second heating curves from DSC are plotted in Figure 5.3. The LLDPE has a broad melting peak and low crystallinity. HDPE shows a sharp melting peak at 130 °C. iPP shows a single melting point at 163 °C. The shape, area, and location of the iPP peak depends on the crystalline structure, and therefore, processing history. The curve shown below is for tensile samples, pressed at 190 °C then cooled at −40 °C/min to room temperature. The crystallinities are noted in Table 5.2

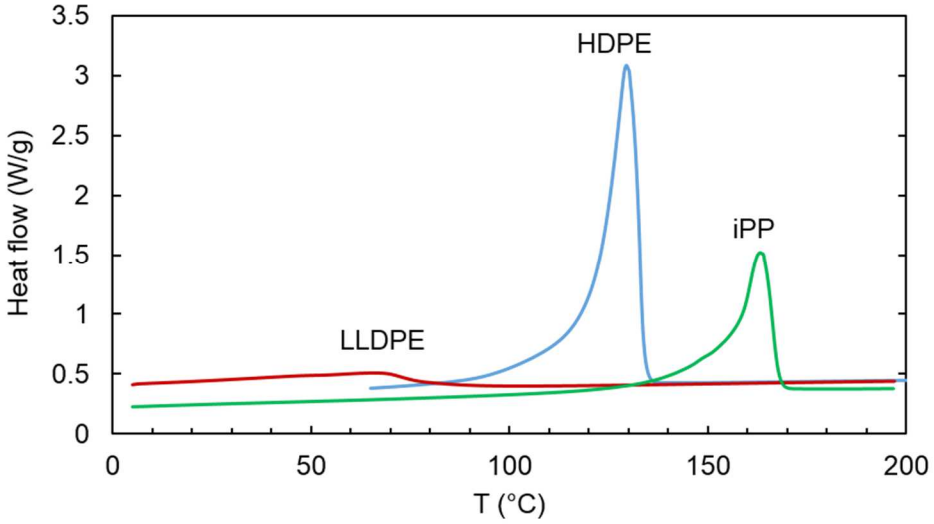

Figure 5.3. DSC second heating curves of LLDPE, HDPE, and iPP homopolymers (10 °C/min, TA Q1000).

5.4 Adhesion

Adhesion tests were performed on laminated iPP/HDPE bilayers. 0.5 mm thick iPP and HDPE sheets were compression molded at 190 °C for 5 min and ~3 MPa (60 mm × 7.5 mm × 0.34 mm mold). iPP-*b*-HDPE (18 mg) was dissolved in xylenes (41 mL) at 130 °C. The iPP sheet was dipped into the iPP-*b*-HDPE solution, removed, shaken to remove excess liquid, and dried for 48 h. A thin, uniform, white layer was observed, possibly an indication that the block copolymer coating is thicker than necessary. The coated iPP was laminated to PE (60 mm × 7.5 mm × 1.00 mm mold) at 180 °C for 5 min. A crack was started at the interface, and partially peeled apart for loading on a Shimadzu-AGX tensile tester. Samples were pulled at 5 mm/min, and peel strengths were recorded as the steady-state force divided by the width of the sample (Figure 5.4).

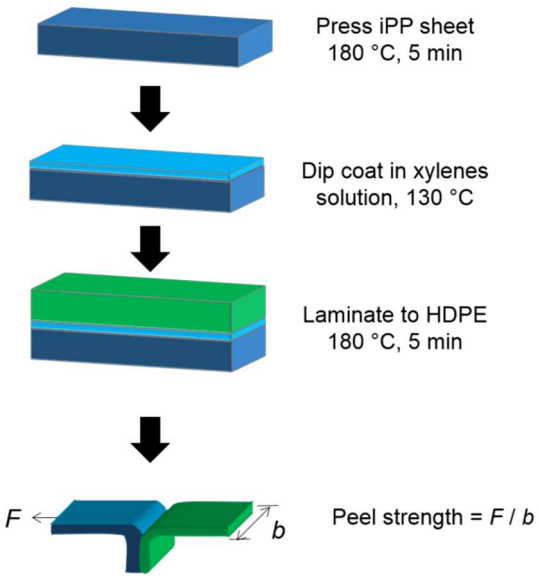

Figure 5.4. Schematic of iPP/HDPE adhesion test. iPP sheets are pressed, then dip coated in a hot solution of xylenes and iPP-*b*-PE before being laminated to HDPE sheets. A crack is started at the interface, then the layers are pulled apart at 5 mm/min in a tensile tester.

Peel strength is reported for the neat and iPP-*b*-HDPE coated interfaces in Figure 5.5. High molecular weight iPP-*b*-HDPE coated interfaces had a higher peel strength than the neat interface, indicating block copolymer spans the interface. The main trend is that increasing block copolymer molecular weight increases peel strength.

Due to the opaque iPP-*b*-PE layer on the dip coated iPP bars, we suspected that the layer is thicker than the desired monolayer. This may lead to cohesive failure in a third block copolymer tie layer, rather than adhesive failure between iPP and PE. To indirectly probe if layer thickness is important, the dip coating solution concentration of $P_{15}E_{20}$ in xylenes was decreased from ~0.4 mg/mL to ~0.05 mg/mL (Figure 5.6). It is clear that decreasing concentration increases adhesion, directing future studies toward more dilute solutions for dip coating.

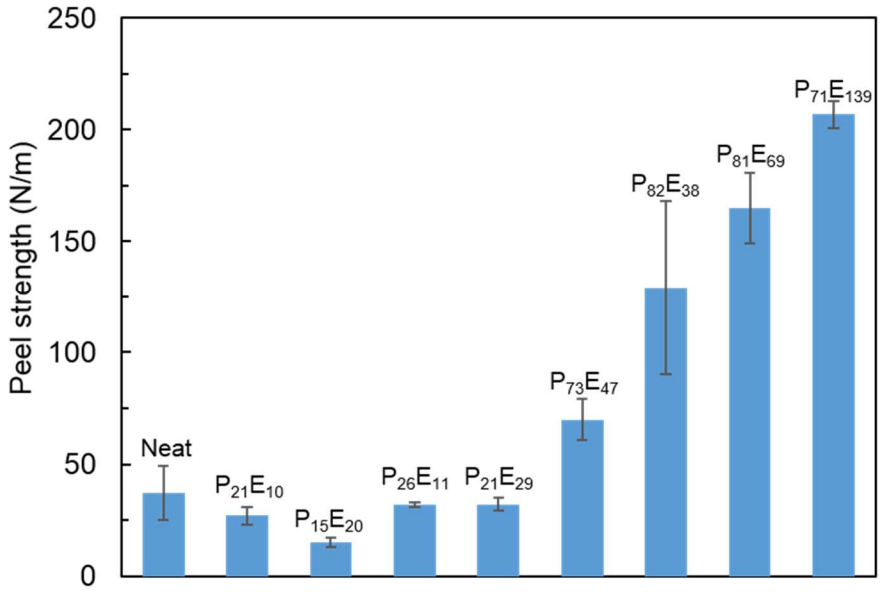

Figure 5.5. Adhesion of iPP/HDPE bilayers with different iPP-*b*-HDPE compatibilizers. Total molecular weight of block copolymer coating increases from left to right. Peel strength increases with copolymer molecular weight.

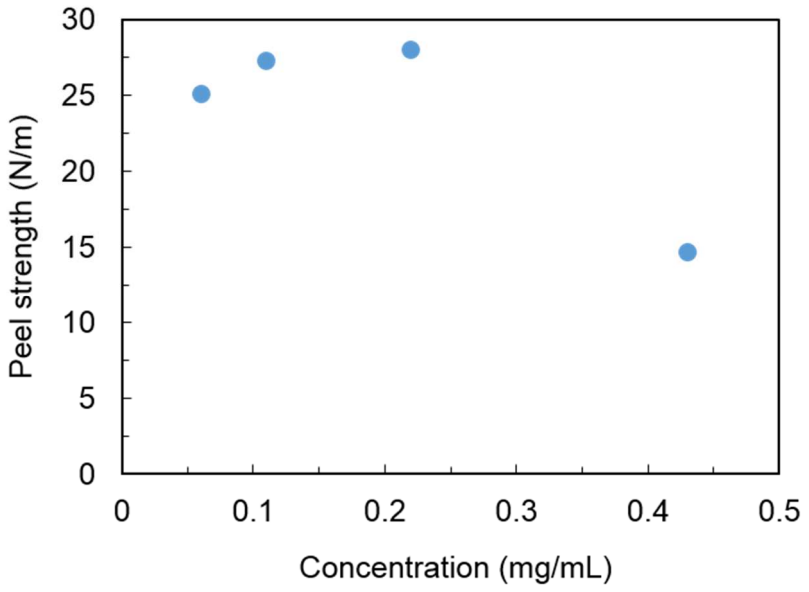

Figure 5.6. Effect of dip coat solution $P_{15}E_{20}$ concentration (in xylenes) on bilayer adhesion.

5.5 Blends

5.5.1 Melt processing of blends

Samples were melt mixed either in a HAAKE Rheomix or a DSM Xplore MC 5 batch mixer. The Xplore samples were mixed at 100 rpm and 180 °C for 5 min before extruding into liquid nitrogen. These samples were used for morphology, rheology, and tensile samples. The HAAKE blends were made at 100 rpm and 180 °C for 5 min, and were used for injection molding impact strength specimens (the larger scale mixer was necessary to make enough material for injection molding). The blend composition was held constant at 90/10/1 wt fraction iPP/HDPE/iPP-*b*-HDPE or iPP/LLDPE/iPP-*b*-LLDPE.

5.5.2 Morphology from TEM

Toughness is closely correlated to the morphology of blends, with smaller droplet size leading to improved toughness for a variety of systems.[7] Droplet sizes were obtained for select blends, using cryo-microtoming, RuO_4 staining, and TEM. Samples were microtomed at −80 to −160 °C using a diamond knife, a 250 μm × 250 μm cutting face, cutting speed 1 mm/s, and thickness 50–70 nm. These sections were transferred to Cu grids (Ted Pella, with handle), then vapor stained in the Charfac black box for 25 min, 2 cm away from the edge (0.5 wt% RuO_4 stain, 1.5 mL). The PE portions are preferentially stained (dark) in this study, although other studies have shown either PE or iPP preferentially stained in iPP/PE blends.[182,183] The contrast mechanism is still not completely understood. We hypothesize there are trace double bonds from the PE polymerization, allowing RuO_4 to form covalent bonds and localize more strongly in PE.[183] Finally, the stained sections were vented overnight, then imaged in TEM (Technai Spirit, 120 kV).

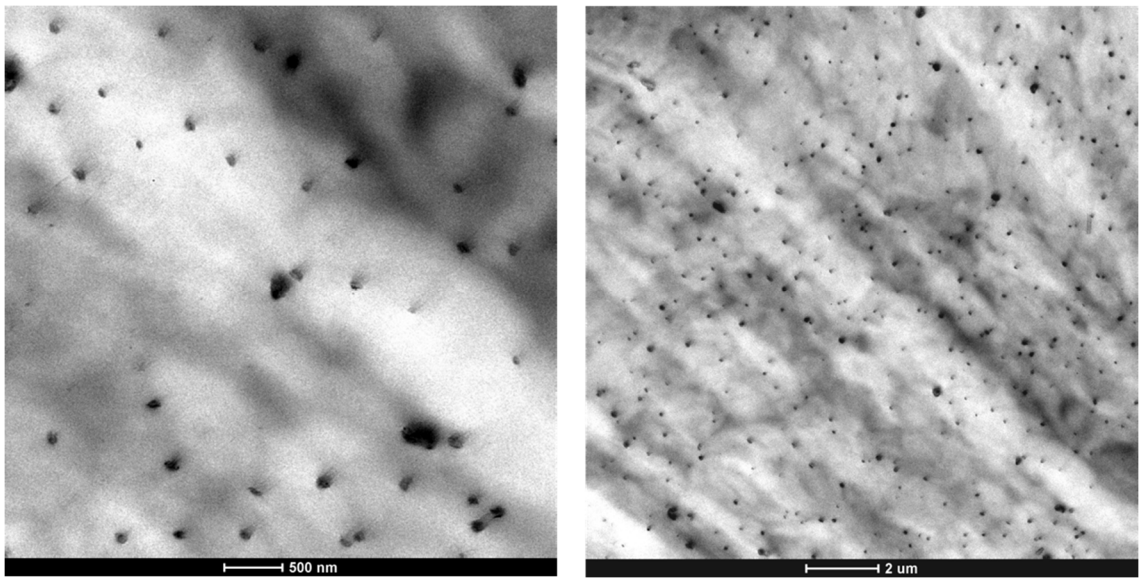

Figure 5.7. TEM images of iPP and 5 wt% $P_{81}E_{69}$ (120 kV, RuO_4 vapor stain, 50–70 nm thick sections). The dark spots are iPP-*b*-PE micelles, in a light iPP matrix. Matrix color variation may be due to crystallinity difference or thickness differences in the section. These images show the expected micelle size for the $P_{81}E_{69}$ blend shown later.

Figure 5.8 shows representative images of the binary HDPE blend at three separate magnifications. Droplet sizes range from ~ 1 μm to ~50 nm. The color variation in the matrix may be due to overstaining, crystalline/amorphous regions, or thickness variations.

Figure 5.9 shows images of the $P_{81}E_{69}$ blend. Droplets are similar in size to those observed in the HDPE binary blend. At high magnification, however, micelles and swollen micelles are clearly visible (right image). This suggests that at least some block copolymer is forming micelles instead of going to the interface. High molecular weight block copolymers are more likely to form micelles instead of going to the interface, so these images direct synthetic efforts towards lower molecular weight materials.[8]

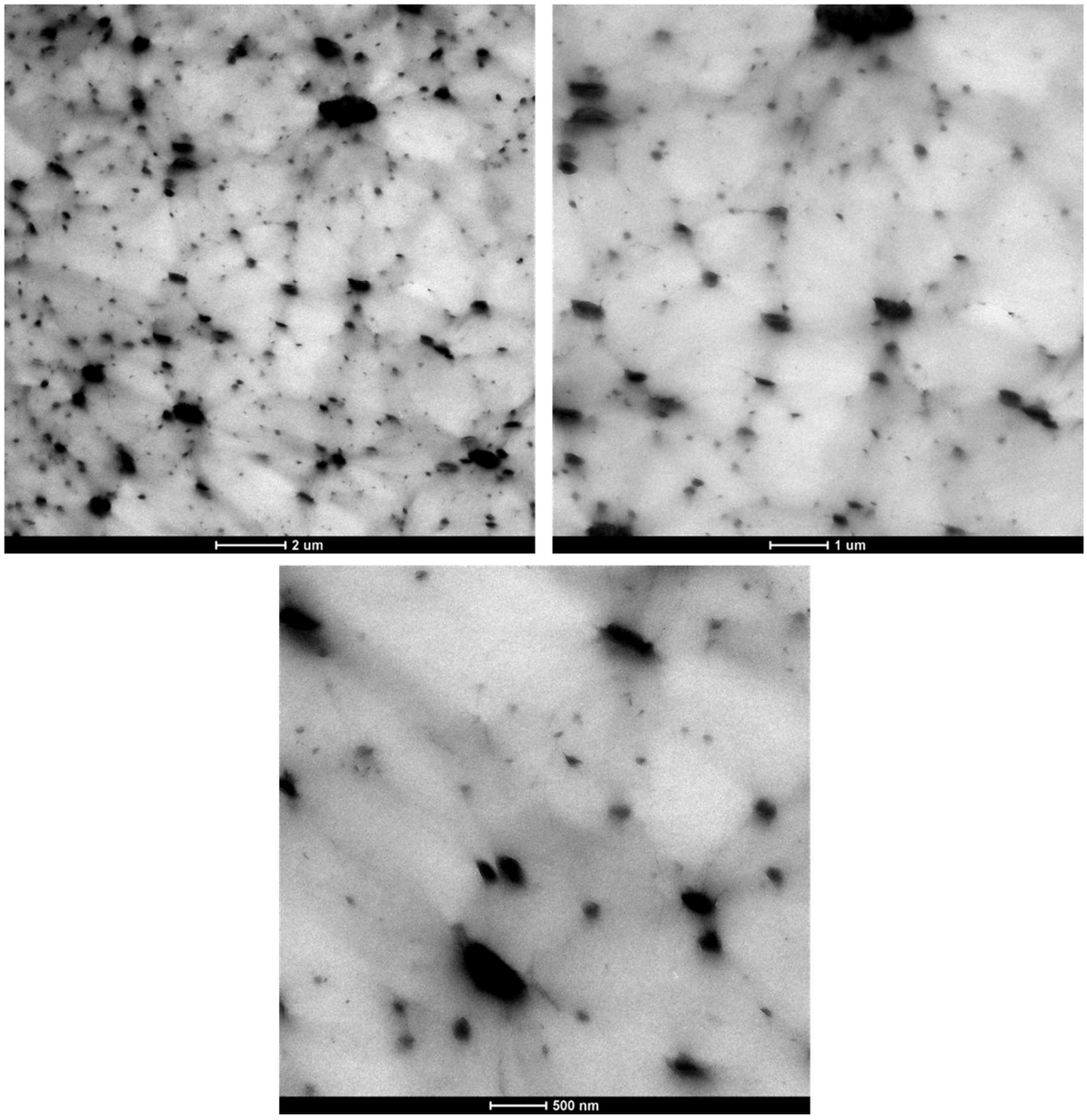

Figure 5.8. TEM images of binary iPP/HDPE blend (120 kV, RuO_4 vapor stain, dark PE droplets, 50–70 nm thick sections). Since the homopolymers are viscosity matched, droplets are small. The smallest droplets are close to the same size as the micelles shown in Figure 5.7, but are not numerous.

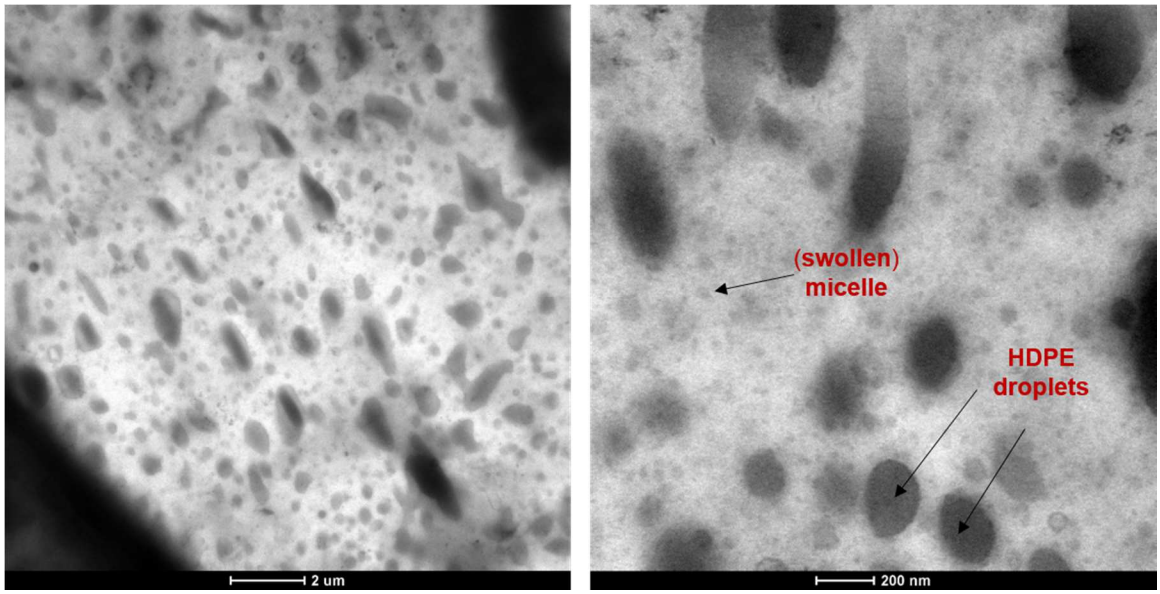

Figure 5.9. TEM images of iPP/HDPE/$P_{81}E_{69}$ blend (120 kV, RuO_4 vapor stain, 50–70 nm thick sections). Left image shows only HDPE droplets. Higher magnification (right) shows many light grey micelles, some of which may be swollen with HDPE due to their disperse size. These micelles are not visible in the binary blend and are of a size similar to that seen in the iPP/$P_{81}E_{69}$ images.

Figure 5.10 shows TEM images of the $P_{29}E_{14}$ blend. The droplets are lighter than the matrix in these images, presumably due to PE droplet pullout during microtoming or under-staining. There is not a visible difference in droplet size compared to the HDPE binary blend. Therefore, it is unlikely that the block copolymer is localized at the interface. Figure 5.11 shows images of the $P_{82}E_{38}$ blend, with similar results. Lower molecular weight iPP-*b*-HDPE will be needed in future studies to preclude micelle formation.

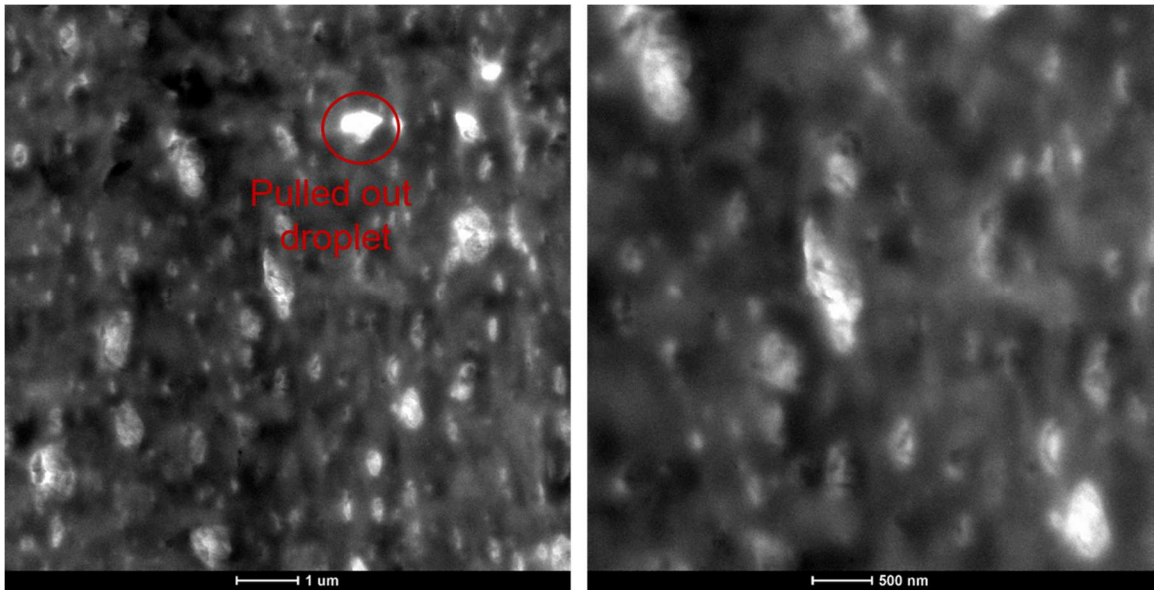

Figure 5.10. TEM images of iPP/HDPE/$P_{29}E_{14}$ blend (120 kV, RuO_4 vapor stain, 50–70 nm thick sections). PE drops are light due to pullout or understaining.

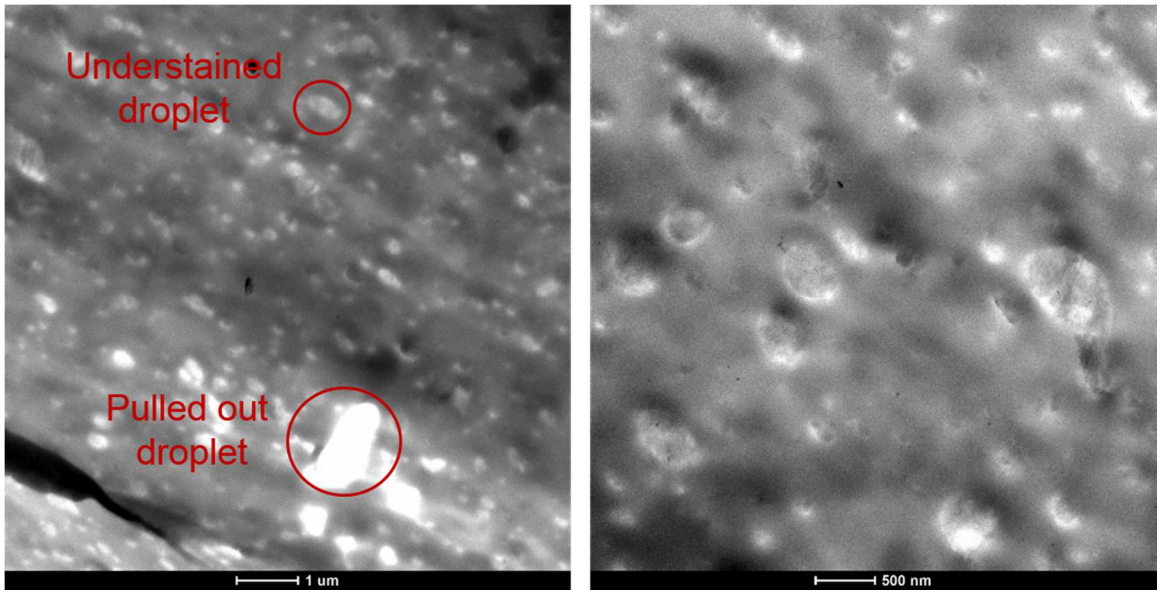

Figure 5.11. TEM images of iPP/HDPE/$P_{82}E_{38}$ blend (120 kV, RuO_4 vapor stain, 50–70 nm thick sections). PE droplets are light due to pullout or understaining.

$P_{55}LE_{31}$ blend images are shown in Figure 5.12. These materials are much easier to stain, due to the large differences in crystallinity between LLDPE and iPP, resulting in higher contrast images. We are unsure if the small dark spots are micelles or small droplets at this point.

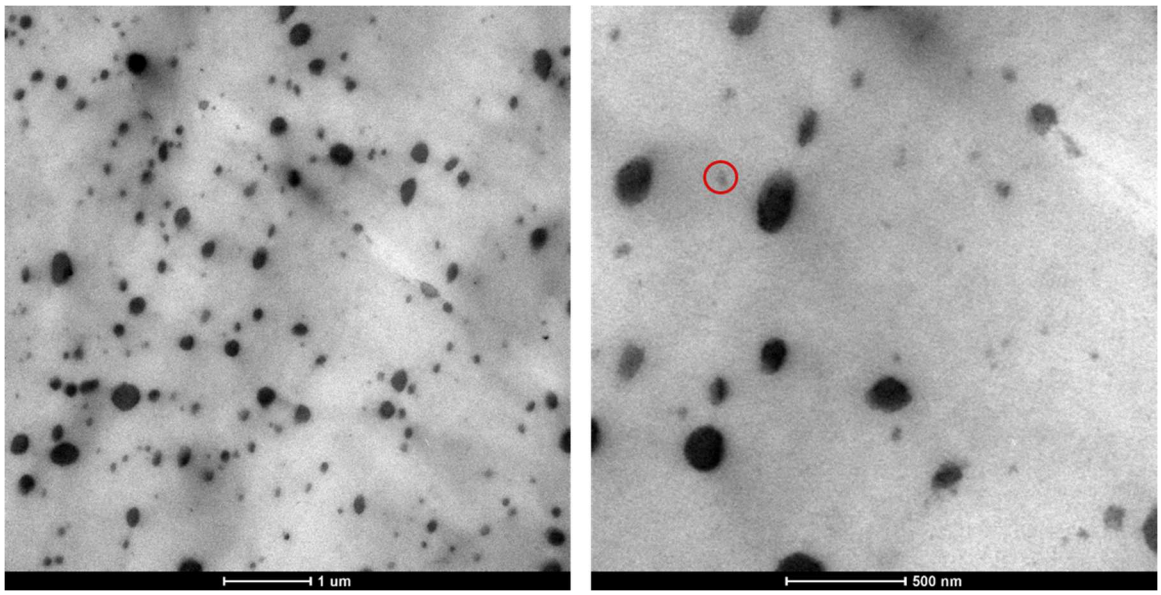

Figure 5.12. TEM images of iPP/LLDPE/$P_{55}LE_{31}$ blend (120 kV, RuO_4 vapor stain, 50–70 nm thick sections). The red circle highlights a dark spot that could be a micelle or a small droplet. Images of binary LLDPE blends have not been obtained, but would be necessary to determine if $P_{55}LE_{31}$ forms micelles.

Droplet sizes were measured using ImageJ software. The compiled droplet size results are shown below in Table 5.3. These results are skewed by the many micelles. However, it is clear that there is good dispersion of PE droplets, which is promising for mechanical properties studies.

Table 5.3. Average droplet sizes for iPP/HDPE blends

blend	$<d_n>$ ± S.D. (μm)	number of drops sized
binary HDPE	0.11 ± 0.09	120
$P_{81}E_{69}$	0.10 ± 0.08	136
$P_{55}LE_{31}$	0.07 ± 0.05	228

5.5.3 Morphology from SEM

Creating contrast in scanning electron microscopy (SEM) is typically more difficult than that for TEM, so several procedures were attempted to create enough contrast for droplet sizing. Binary HDPE blend microtomed samples showed insufficient contrast for focusing and droplet sizing (Figure 5.13). Freeze fracture sample preparation shows very small droplets, but is not reliable for droplet sizing due to the propensity of the blend to fracture by large particles (Figure 5.14). Li et al. used acid etching to remove iPP droplets from HDPE majority blends. Their 1 wt/vol% potassium permanganate with 10 part vol fraction sulfuric acid, 4 part vol phosphoric acid solution etch for 1 h was effective for removing iPP from HDPE in this work, but it also distorted the HDPE morphology (Figure 5.15). Additionally, this method is not useful for iPP matrix blends. Many solvents and temperatures were examined for selective dissolution of one material, but every solvent that dissolved droplets would also swell or dissolve the matrix as well.[79] RuO_4 vapor was used by Kontopoulou et al. to obtain contrast in SEM between iPP and LLDPE,[184] but staining had no discernable effect on contrast at short times and small concentrations in this work. At longer times and larger concentrations, a thick layer of stain is observed on the surface. Microtoming through this layer and re-imaging shows insufficient contrast (Figure 5.16, bottom right is Ru coating, top left is exposed interface with no contrast between drops and matrix). In summary TEM should be used for droplet sizing in future work.

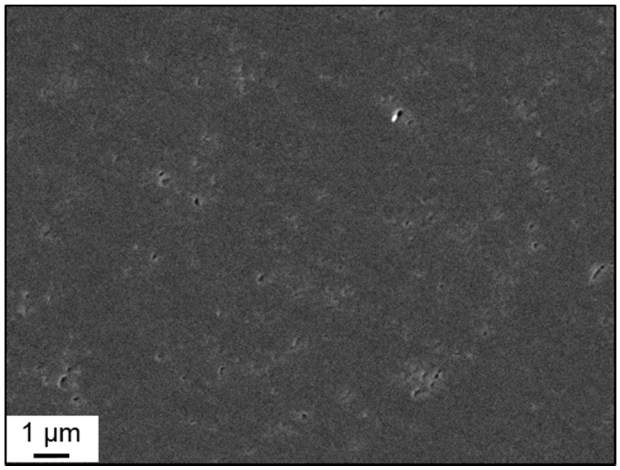

Figure 5.13. SEM image of microtomed binary iPP/HDPE blend. This method yields insufficient contrast for droplet sizing.

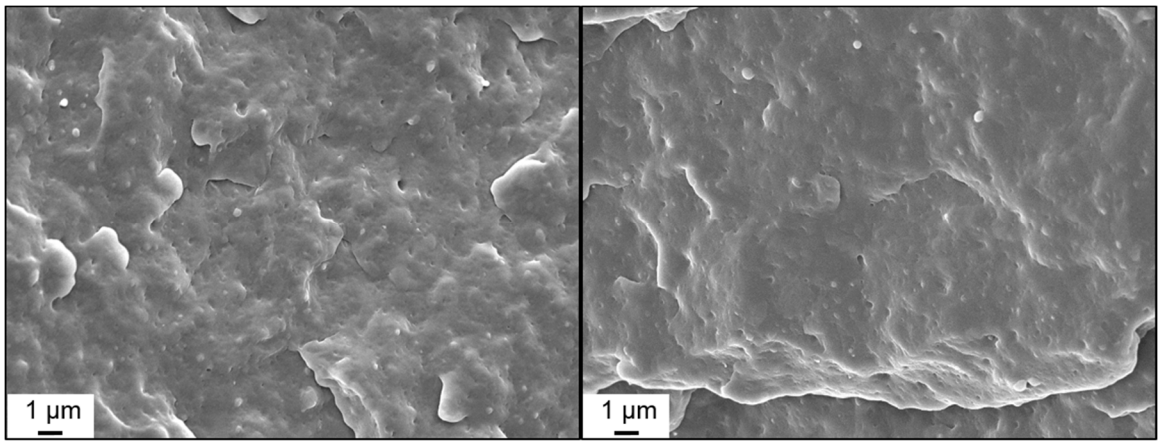

Figure 5.14. SEM images of iPP/HDPE/$P_{81}E_{69}$ blend (left) and iPP/HDPE/$P_{71}E_{139}$ blend (right) freeze fractured surfaces

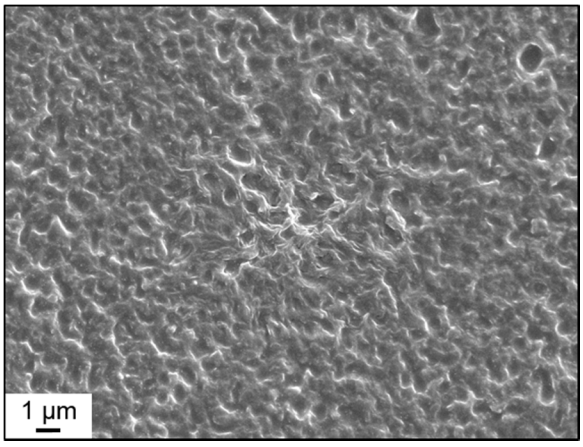

Figure 5.15. SEM image of microtomed and acid etched 20/80 iPP/HDPE blend

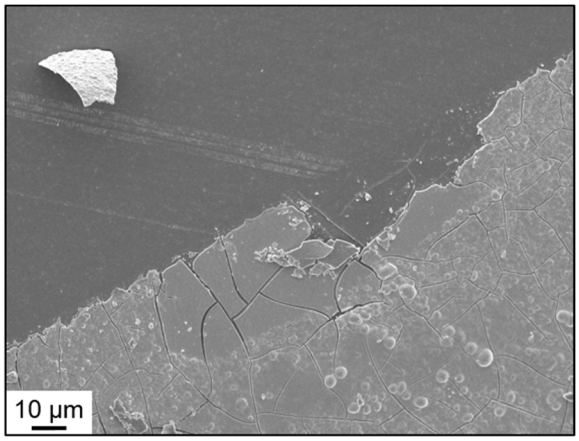

Figure 5.16. SEM image of microtomed, RuO_4 vapor stained, and microtomed iPP/HDPE/$P_{81}E_{69}$ blend. Bottom left shows coating from RuO_4 vapor stain. Top left is exposed surface from second microtoming.

5.5.4 Rheology

Rheology can be used to determine changes in surface tension and droplet size upon addition of compatibilizer. Gradients in surface copolymer concentration can be caused by shear flow. The resultant Marangoni stresses act as a restoring force on droplet shape, increasing the elastic modulus of the entire blend at low frequencies. This is quite sensitive, even at low loadings (< 1 wt%). Here, we use an upturn in G' at low frequency to signal that copolymer is localized at the interface, to corroborate TEM results.

Blends were compression molded at 190 °C for 5 min and ~3 MPa to form 25 mm discs. These were loaded on an ARES rheometer at 180 °C. Time sweeps verified the melt stability of the neat materials and blends for over 1 h. Strain sweeps defined the linear viscoelastic (LVE) regime limits. Finally, frequency sweeps were performed in the LVE regime.

The HDPE binary blend and $P_{82}E_{38}$ blend frequency sweep curves almost overlay (Figure 5.17). Therefore, there is not a large change in droplet elasticity with the addition of 1 wt% $P_{82}E_{38}$. Similar results were also obtained for $P_{29}E_{14}$, $P_{31}E_{33}$, $P_{71}E_{139}$, $P_{32}E_{57}$, and $P_{32}E_{20}$ blends (omitted below for clarity). The LLDPE binary blend and $P_{55}LE_{31}$ blend overlay as well (Figure 5.18). This corroborates the TEM evidence showing block copolymer away from the interface, in micelles. In the future, it is expected that higher G′ at low frequency upon addition of block copolymer will be a good method for elucidating block copolymer localization. Surface tension reduction will be estimated using Palierne model fittings.[47]

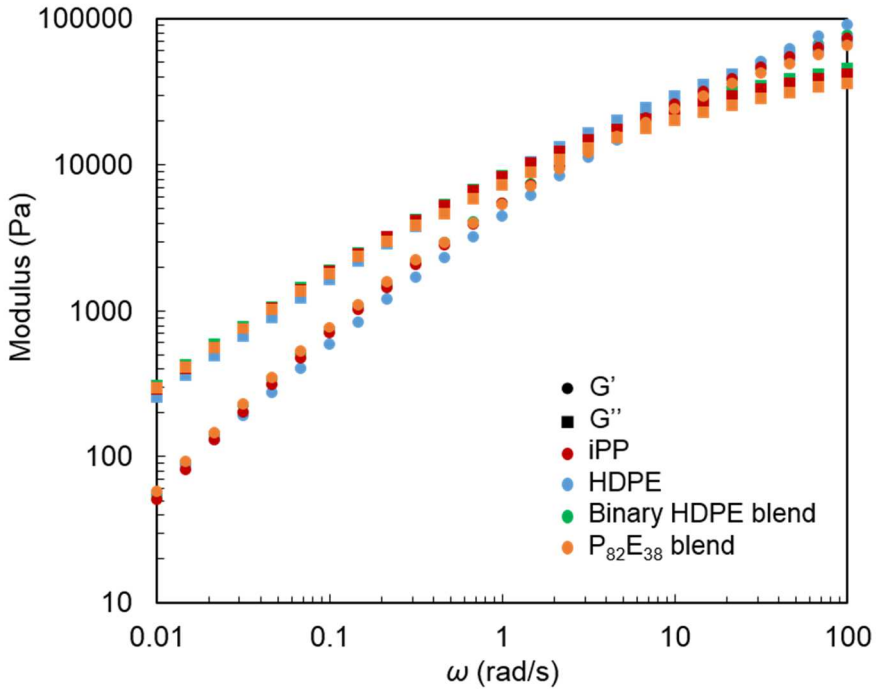

Figure 5.17. iPP and HDPE blend rheology from dynamic frequency sweeps at 180 °C.

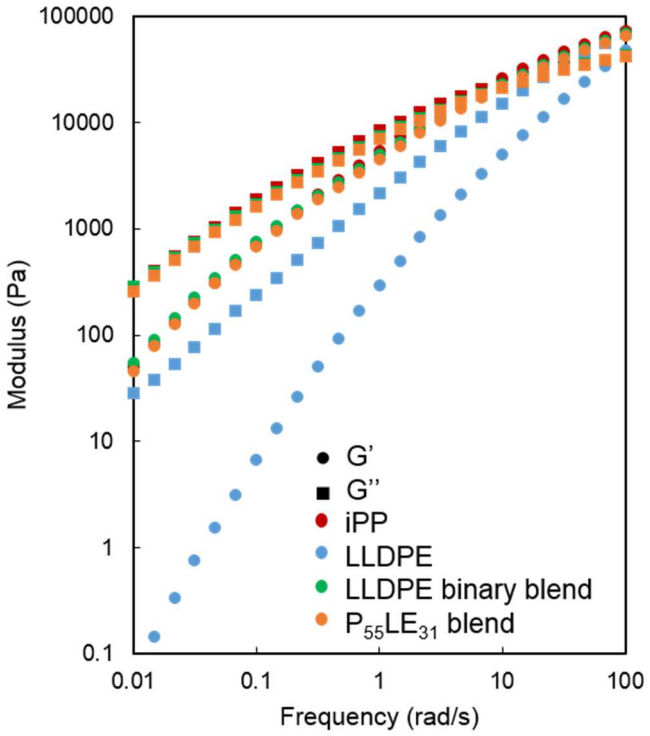

Figure 5.18. iPP and LLDPE blend rheology from dynamic frequency sweeps at 180 °C.

5.5.5 Tensile tests

Tensile specimens were compression molded at 190 °C for 5 min and ~3 MPa before cooling at a rate of −40 °C/min to room temperature and aged for at least 48 h prior to testing (ASTM D1708, 0.6 mm thick, 5 mm gage width, 22 mm gage length). Uniaxial extension tests were performed on a Shimadzu-AGX at a rate of 5 mm/min. Blends were evaluated based on toughness (area under stress-strain curve), modulus (initial slope of stress-strain curve), extension at break, and yield stress. Representative stress-strain curves are shown in Figure 5.19.

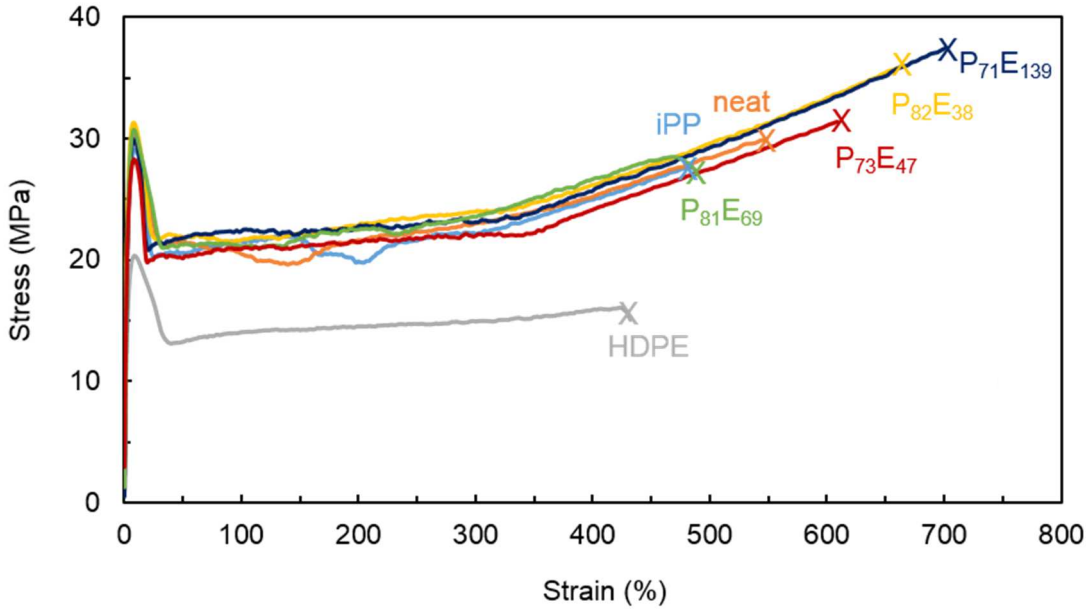

Figure 5.19. Stress-strain curves for iPP/HDPE/iPP-b-PE blends (compression molded samples, 5 mm/min, Shimadzu-AGX). The modulus and yield strength of all blends is similar to that of iPP, but extension at break and toughness are increased.

The toughness of iPP is surprisingly high, with an extension at break of over 500%. This is attributed to the fast cooling of the tensile specimens. Slow cooling at a rate of −4 °C/min leads to an extension at break of just 6%. Similar results were shown for two other grades of iPP (Exxon PP 6262 and PP 3155). This highlights the importance of processing history on physical properties, and the variability in literature values for tensile toughness of these materials. Despite using iPP that is already tough, the neat HDPE blend shows slight improvement in extension at break and toughness. This effect is stronger when iPP-*b*-HDPE is added (Table 5.4).

Table 5.4. Tensile toughness testing of 90/10/1 wt fraction iPP/HDPE/iPP-b-PE blends

material	E' (GPa)	ε_b (%)	toughness (MJ m^{-3})
HDPE (J-Rex)	0.8	530 ± 80	90 ± 14
iPP (H314-02Z)	1.1	510 ± 40	110 ± 14
binary HDPE blend	1.1	600 ± 50	130 ± 12
$P_{82}E_{38}$ blend	1.1	650 ± 20	160 ± 14
$P_{81}E_{69}$ blend	1.1	530 ± 30	140 ± 6
$P_{73}E_{47}$ blend	1.1	590 ± 40	150 ± 20
$P_{71}E_{139}$ blend	1.1	610 ± 130	160 ± 62

It is promising to note that the yield strength and modulus of the blends is nearly identical to that of the pure iPP. For rubber toughening, there is usually a tradeoff between yield strength and extension at break. However, for semi-crystalline / semicrystalline blends, the elastic modulus and extension at break can be independently adjusted.[146] This is one major advantage of blending iPP with HDPE rather than LLDPE.

Also, the tensile properties of polyolefin blends are often comparable or worse than their substituent materials (Figure 5.1).[160] This data shows the tensile performance has not deteriorated significantly with addition of block copolymer. The main advantage of blending is often improved impact strength.[146]

5.5.6 Impact strength

Izod impact strength specimens were created using a Morgan Press injection molder (barrel temperature = 185 °C, nozzle temperature = 220 °C, mold temperature = 60 °C, ram pressure = 3 – 5 kpsi, pilot valve pressure = 100 psi, clamp force = 13 tons, cycle time = 30 s, sample 3.35 mm wide, 12.7 mm thick, 120 mm long ASTM D256).[185,186] Samples were aged for at least 48 h in a room temperature vacuum oven before notching and testing. A band saw was used to trim the samples to 63.5 mm long, then notches were created using a Tinus Olsen 899 Impact Specimen Notcher.

A CEAST instrumented impact instrument (model 6545) was used for testing (0.372 m arm, 150° drop angle, 3.45 m/s impact speed, 2.75 J hammer). Results are shown in Table 5.5. The pure iPP and HDPE values are close to those shown in Figure 1.1, but the binary blend does not show a similar increase in impact strength noted by Rabe et al.[6] Note that most samples showed incomplete break, which may explain deviation from literature values. Also, cross sections of the broken samples showed a core/shell morphology on millimeter length scales, presumably from injection molding cooling the outside of the sample more quickly. The neat iPP value does not agree with the published datasheet (5.3 kJ/m^2 versus 17 kJ/m^2).

The main conclusions from this data are that instrumentation and various injection molding conditions will be necessary to obtain more accurate data, and that blending with HDPE did not significantly increase impact strength over neat materials. It may be that micellization of the block copolymers is preventing interfacial reinforcement, leading to no improvement in impact strength.

Table 5.5. Notched Izod impact strength of iPP, HDPE, and blends

material	notched impact strength (kJ/m^2)	type of break
HDPE	28 ± 5	incomplete break
iPP	5.3 ± 0.2	complete break
binary HDPE blend	5.0 ± 0.4	complete break
$P_{71}E_{139}$ blend	5.5 ± 0.4	complete break
$P_{55}LE_{31}$ blend	5.0 ± 0.4	incomplete break

5.6 Flory-Huggins parameter estimation

It is not currently understood why iPP and PE phase separate, since their unfavorable enthalpic interactions are not large. A first step in understanding their phase separation is to accurately measure the effective Flory-Huggins interaction parameter between the two homopolymers (χ). Lo et al. estimated χ between LLDPE and iPP to be

$-0.0367 + 16.01/T$ with small angle X-ray scattering (SAXS), or −0.0013 at 180 °C.[187] Negative χ should indicate miscibility, but these materials are often phase separated in the melt state. There is variability in reported χ values for iPP and HDPE, between 0.003 and 0.09 by various methods (between 170 and 230 °C).[188] The precise architecture of the iPP-*b*-PE copolymers in this study give the opportunity to improve estimations of χ for LLDPE/iPP and HDPE/iPP.

χ can be estimated by the order disorder transition (ODT) of symmetric block copolymers, measured in rheology, which occurs at $\chi N = 10.5$ (where N is the degree of polymerization). Frequency sweeps were performed on iPP-*b*-HDPE copolymer on an ARES rheometer with 25 mm parallel plates, every 10 °C from 150 °C to 220 °C (Figure 5.20 – 5.22). No deviation in G' was observed at low frequencies for $P_{81}E_{69}$, $P_{73}E_{47}$, and $P_{31}E_{33}$ indicating that the ODT is not accessible for these materials, confirmed by continuous G' in temperature ramps.[189,190] $P_{15}E_{20}$ displayed different behavior, with $G'' > G'$, a Newtonian viscosity, and a higher slope for G'' compared to the other ordered samples. We hypothesize that the ODT is slightly over 220 °C for this sample, but scattering and TEM should be performed to confirm this sample is ordered.

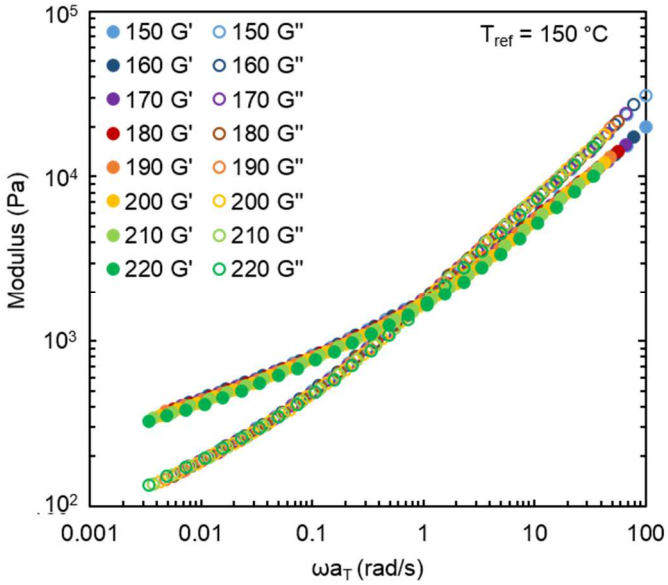

Figure 5.20. $P_{81}E_{69}$ rheology master curve, from frequency sweeps. The data was only shifted horizontally, with a reference temperature of 150 °C. No deviation is seen in *G′*, so we expect this sample is ordered at all temperatures tested.

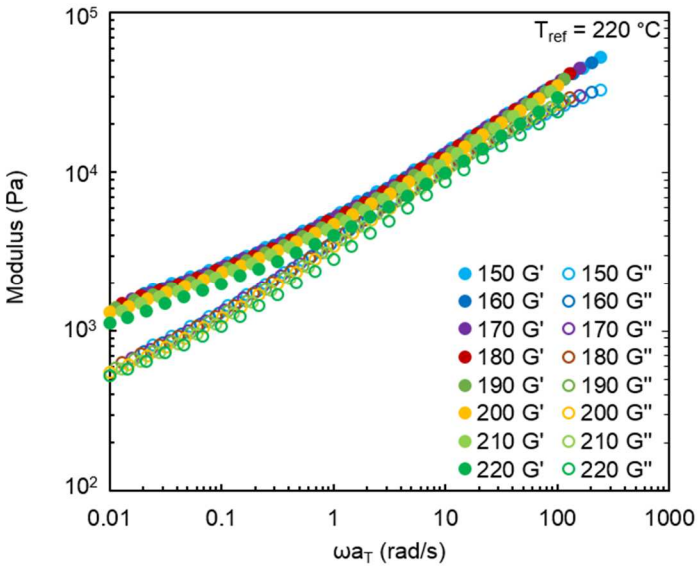

Figure 5.21. $P_{73}E_{47}$ rheology master curve. The data was only shifted horizontally, with a reference temperature of 220 °C. No deviation is seen in *G′*, so we expect this sample is ordered at all temperatures tested. Moduli are higher for this sample, possibly due to different ordered morphology or high normal force after loading.

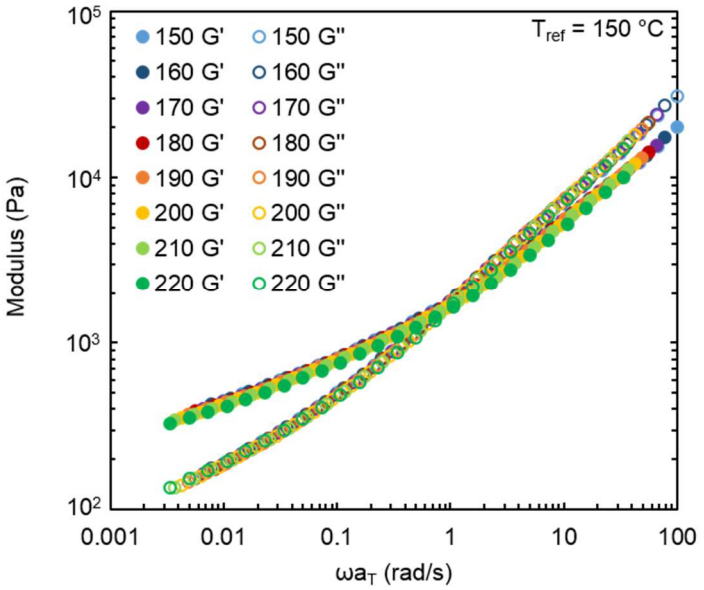

Figure 5.22. $P_{31}E_{33}$ rheology master curve. The data was only shifted horizontally, with a reference temperature of 150 °C. No deviation is seen in G', so we expect this sample is ordered at all temperatures tested.

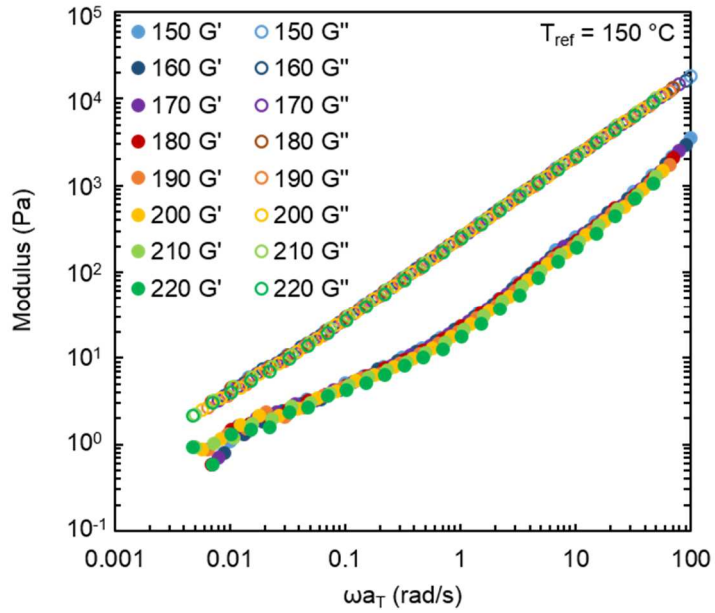

Figure 5.23. $P_{15}E_{20}$ rheology master curve. The data was only shifted horizontally, with a reference temperature of 150 °C. The slope of G'' is slightly higher than the other ordered samples, and $G'' > G'$.

Frequency sweeps were performed on P_8E_3 using 50 mm parallel plates and the same conditions as above. The torque was very low for this sample, so G′ data was not obtainable. G'' and η^* are plotted against ω at 180 °C for several iPP-*b*-PEs in Figure 5.24. This data is representative of all the temperatures examined (150 – 220 °C). The sharp decrease in viscosity from $P_{15}E_{20}$ to P_8E_3 cannot be explained by molecular weight changes alone. We also expect a substantial viscosity drop when block copolymers become disordered. Therefore, P_8E_3 is probably disordered. This sets bounds on future experiments, which should test materials between 11 kg/mol and 35 kg/mol to determine χ. Also, based on these experiments, χ is between 0.010 and 0.038 for all temperatures between 150 °C and 220 °C.

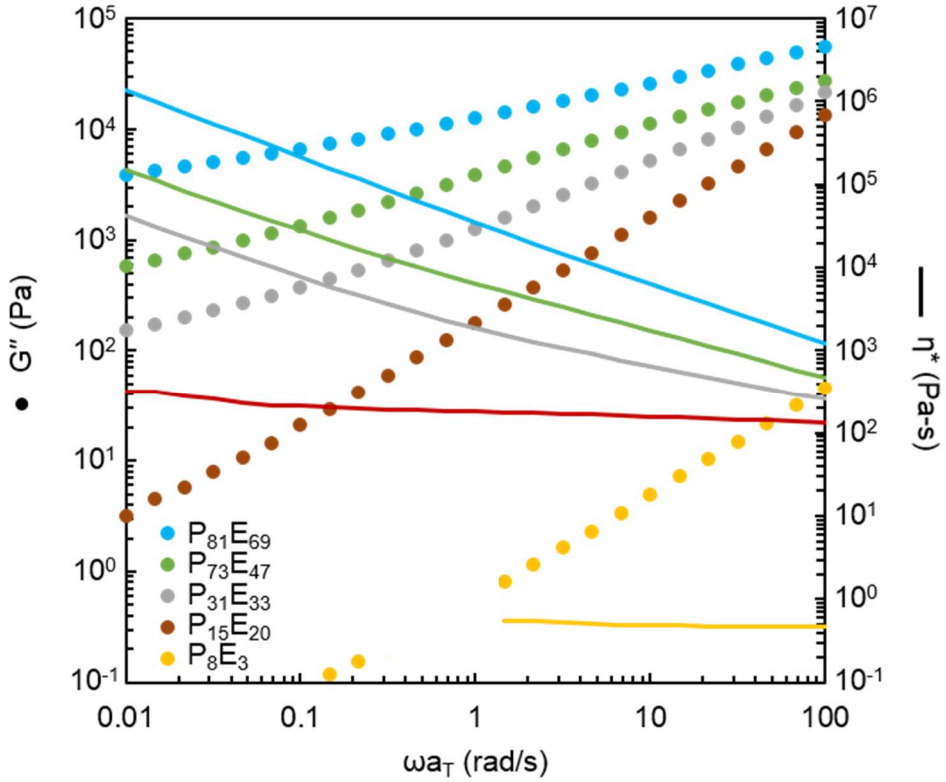

Figure 5.24. Loss modulus and complex viscosity for iPP-*b*-PEs as a function of frequency at 180 °C.

5.7 Conclusions and future work

This work attempts to develop a tough iPP by blending with small amounts of PE and premade block copolymer compatibilizers. Adhesion in bilayer samples was substantially increased by the addition of iPP-*b*-PE to the interface. However, in melt blending the iPP-*b*-PE tends to form micelles instead of going to the interface. This leads to incremental toughness improvements in tensile and impact strength for iPP/HDPE blends

Future synthetic efforts will aim for iPP-*b*-PE between 11 kg/mol and 35 kg/mol, to determine χ between PE and iPP by rheology and scattering. These lower molecular weight materials will also be useful for localizing block copolymer at the interface of blends, with the goal of further enhancing toughness of iPP/PE blends.

Chapter 6. Capillary coextrusion

6.1 Summary

This chapter describes the design and use of a small scale coextrusion unit, developed in collaboration with Prof. Patrick Lee at the University of Vermont. The coextruder consists of a heated die that can be attached to a commercial Malvern RH 7 dual-bore capillary rheometer. Design of the new equipment addressed two issues associated with currently available coextrusion lines: (1) even "small scale" coextrusion lines use several kilograms of sample, which is too much to synthesize at bench scale, and (2) the existing coextrusion equipment at the University of Minnesota can only accept pellet feeds, necessitating pressing and cutting powdered samples before use. This new capillary coextrusion die requires as little as 20 g of material per run, accepts powder feeds, and produces 1 cm wide × 1 mm thick bilayers. Development of this tool facilitates coextrusion with synthesized polymers and allows for faster turnaround on experiments. Future design options will include adding layer multipliers and examining the effect of compressive flow on a variety of reactive systems.

6.2 Introduction

Coextrusion is a widely used method for manufacturing multilayer products with useful barrier, mechanical, and optical properties at large scale.[191,192] In the packaging industry, improved barrier properties can be achieved by decreasing layer thicknesses (e.g., via layer multipliers).[193] For example, Wang et al. decreased oxygen permeability by about two orders of magnitude by changing the thickness of poly(ethylene oxide) and poly(ethylene-*co*-acrylic acid) layers from ~3 μm to ~30 nm.[194] This effect results from confined crystals in nanolayered films.[194,195] The well-defined, flat interface also makes the resultant films useful for fundamental interdiffusion, slip, adhesion, and interfacial reaction studies.[23,26,65,196,197]

One obstacle to forming robust multilayer structures is low adhesion between homopolymers, which can lead to delamination and mechanical failure.[196] Interfacial

reactions to form block copolymer at the interface is a prevalent method of increasing adhesion.[72] Previous work elucidates the correlation between interfacial copolymer concentration and adhesion (also see Chapter 1).[20] For practical purposes, it is desirable to test interfacial adhesion on a small scale before industrial scale coextrusion lines are used, leading many researchers to perform interfacial reactions by lamination. In doing so, predictions of copolymer concentration and adhesion can be made at low equipment costs (heated compression molder) and small sample sizes (grams).

Recent work, however, shows that reaction rates with compressive flow are quite different from lamination, strongly affecting adhesion. Jeon et al. reported a ~1,000-fold increase in the reaction rate between static interfaces and heterogeneous melt-mixed blends, based on estimated interfacial volume in the blends.[38] Zhang et al. expanded this work to coextrusion with a similar PS-NH_2/PMMA-anh system, which also exhibited ~1,000-fold faster kinetics than those by static interfaces. Finally, Song et al.[26] isolated the effects of compressional flow and shear flow on reaction kinetics by comparing a compressive and non-compressive coextrusion die. Adhesion and X-ray photoelectron spectroscopy both showed that the compressive die resulted in a reaction rate constant that was two orders of magnitude higher than the non-compressive die (which showed similar kinetics to lamination). From these results, it is clear that compressive flow has a significant effect interfacial reaction kinetics. Therefore, adhesion tests of laminated samples are not appropriate for predicting adhesion for coextruded films.

Only a few reactive compatibilization systems are accessible to study this phenomena, since current coextrusion equipment requires large amounts of materials. Batch synthesis of functional polymers at the lab scale offers no efficient route to quickly screen reactions on continuous equipment. Commercial pellets offer limited functionality for reactive compatibilization studies. The only end-functional polymers are step growth (e.g., Nylon), with large dispersity. Graft-functional polyolefins are available (maleic anhydride, glycidyl methacrylate copolymers, acetic acid copolymers), but their use for fundamental studies is limited by non-randomly distributed functional groups, the

possibility of crosslinking, and the tendency of these materials to be heterogeneous. For example, the commercial EGMA described in Chapter 3 has reported dispersities ranging from 5-10, unknown branching content, and undetermined reactive group distribution among chains. Preferably, model materials featuring low dispersity, end-functionalization, and many possible combinations of reactive groups would be used. In this sense, a small scale coextrusion process is necessary to process lab-scale synthesized polymers, in order to better understand interfacial reaction kinetics in layered systems.

The design of a capillary coextrusion die was attempted to facilitate reactive studies on a small scale, for processing of synthesized model materials (shown in Figure 1.1). The capillary bores are 15 mm in diameter and can contain about 40 cm^3 material each (although less can be used), which accomodates one batch of lab-scale synthesized material. Additionally, the bores allow for powder feeds because tamping compresses and densifies powders. The capillary rheometer provides precise, variable flow rate control (0.01 to 600 mm/min), and a measure of pressure drop.

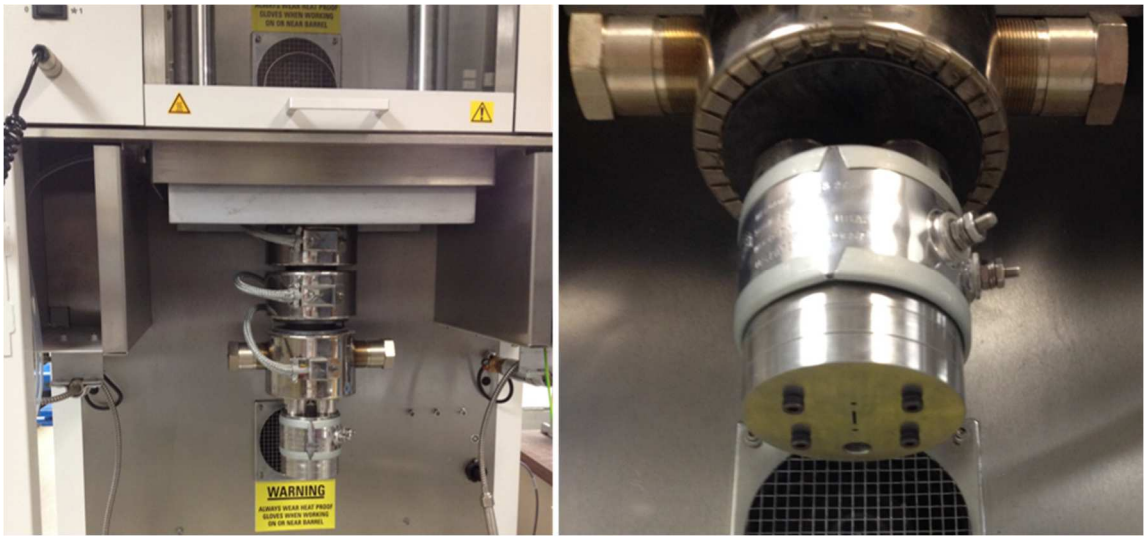

Figure 6.1. Picture of capillary coextrusion die installed

6.3 Die design

Die design was completed in Fluent (Ansys Workbench) and Autodesk 15 CAD software at the Minnesota Supercomputing Institute (MSI). Design criteria included:

1. Small volume (< 5 cm^3), since small amounts of polymer are being used
2. Machinable (no interior curves or slopes > 27°, straight cuts only)
3. Easy to assemble/disassemble
4. Modular, to accommodate different dies in the future, to study compression ratio and multilayer materials
5. Uniform die exit velocity, to prevent instabilities
6. Attachment to capillary rheometer via existing threaded connections
7. Able to withstand 300 °C and 10,000 psi pressure

The die geometry was created in Designmodeler software within Ansys Workbench. Symmetry was employed to reduce computation time, modeling only half the die (from one capillary rheometer bore). Finer mesh was employed near the die exit, to resolve exit velocity as a function of cross sectional position. The final die is geometry is 10 cm long, and is shown in Figure 6.2. The two streams are in contact for 4 cm, during which the x-direction compression ratio is 10, the y-direction expansion ratio is 2, and the expansion in the z-direction (due to flow and volume conservation) is 5.

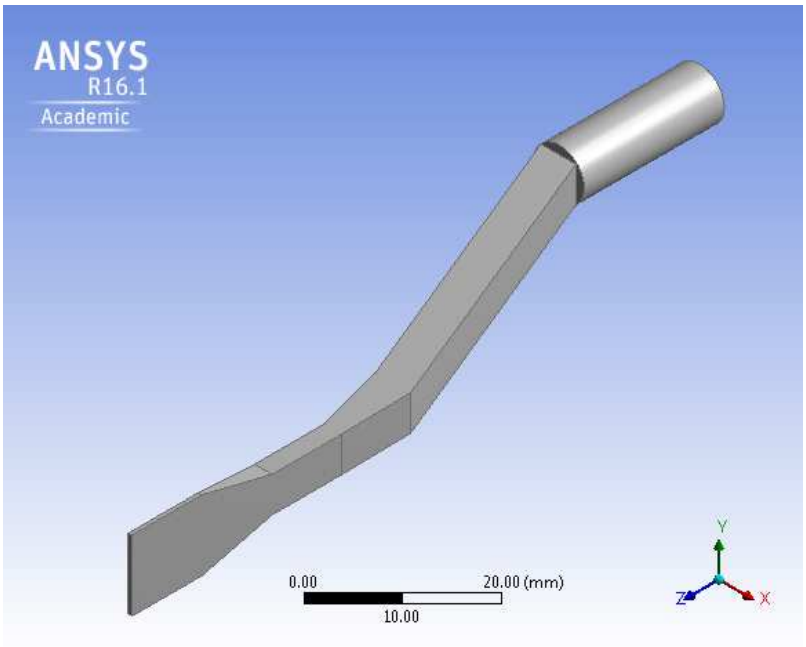

Figure 6.2. Designmodeler geometry for fluent simulations. Fluid enters at top right and exits lower left. The other half of the die is modeled by a symmetric boundary condition in the blue-green axis plane.

The fluid modeled was based on Engage 8200 LLDPE with Cross model parameters $\eta_0 = 2500$ Pa-s, $\lambda = 0.035$ s, $n = 0.45$, and density 0.7 g/cm^3. Boundary conditions were no-slip walls, except for the inlet, outlet, and midline (after the streams come into contact). The inlet boundary condition was specified as constant velocity, and varied from 1 – 100 mm/min in various simulations. The outlet boundary condition was constant pressure at atmospheric conditions. A symmetry condition was imposed on the midline.

Exit velocity contour plots were generated for several die designs and inlet velocities. Die design was evaluated based on how far velocity gradients propagated from the walls. More than 1 mm was unacceptable, because the die exit is 10 mm wide, and 8 mm of uniform sample is necessary for parallel plate rheology. Results for the final design with 10 mm/min inlet velocity are shown in Figure 6.3, and these are representative of the range of velocities studied. The edge velocity gradients stay within 1 mm of the die walls, meeting the requirements for rheology studies.

Several phenomena are not captured by these simulations. A Cross model fluid is used, which ignores fluid elasticity. Two separate fluids are usually used in coextrusion, which may have different rheological properties (although they should be chosen to be close in viscosity). Slip may also be an issue, along with a variety of other common coextrusion challenges (e.g., sharkskin).

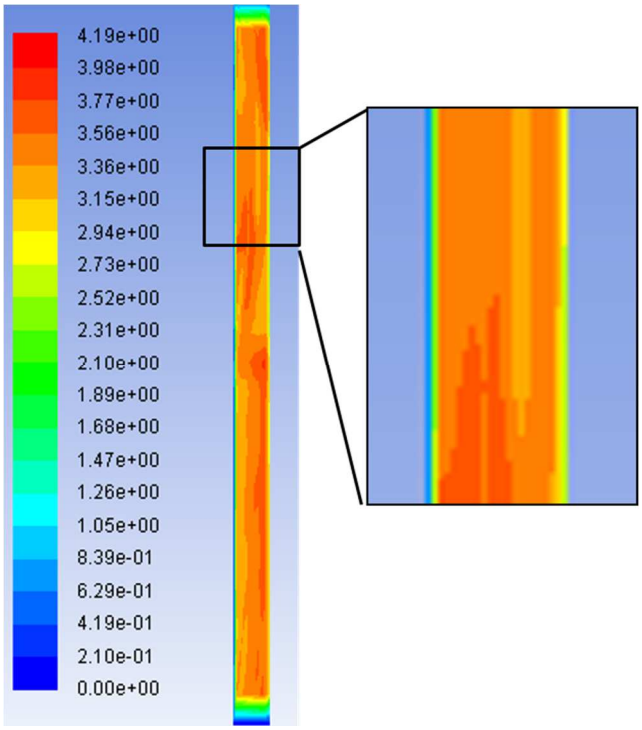

Figure 6.3. Simulated die exit velocity for Engage 8200 LLDPE at 10 mm/min inlet velocity. Colormap indicates exit speed contours in mm/s. Left side is the wall (no slip) and right side is midline (symmetry). Zoomed out contour map is 10 mm x 0.5 mm (size of die exit for one of the fluids).

Autodesk 15 was used to create designs for machining. The die body was chosen to be cylindrical with 75 mm diameter, so commercial heating bands could be used to heat the part uniformly. A threaded receptacle was introduced for a thermocouple, between the heating band and flow channel, running vertically through the die. The cylinder is sliced horizontally, like a stack of hockey pucks, to make machining feasible. Parts are aligned using commercial 2 x 6 mm dowel rods and compressed together using standard M4 hex bolts (held by threading in the top flange piece). The final design is

shown in Figure 6.4. Individual piece machine drawings and an installation procedure can be found in Appendix 3.

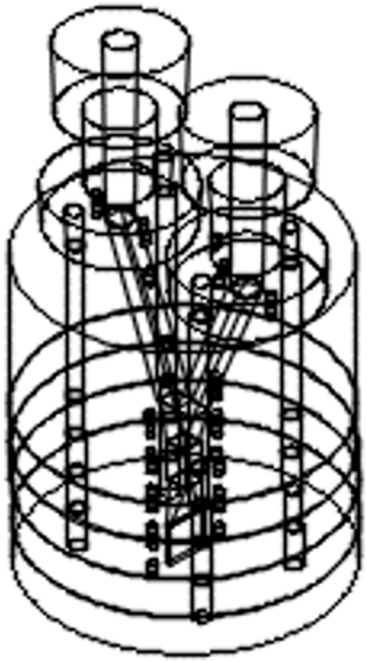

Figure 6.4. Assembly drawing of capillary coextrusion die (isometric view, from top–right). See appendices for individual part machine drawings.

The maximum operating pressure was compared to the shear strength of the M4 bolts to ensure overpressure would not occur. The shear strength of M4 bolts with 15 mm engagement length and 375 MPa material shear strength is approximately 30 kN. Since there are two bolts per flange, 60 kN is the maximum allowable force on the die. The capillary rheometer maximum pressure is 10,000 psi acting on a 15 mm diameter face, which is equivalent to about 12 kN. Therefore, bolt shearing from overpressure has a safety factor ≈ 5.

The heating control system was made from commercial parts. Omega, Inc. heating band MBH-00199 (3” ID, 2” length, 500 W, 240 V), J-type thermocouple CF-

090-J-4-60-2 (3/16” dia, 1/8” NPT screw fitting), controller CN742, and solid state relay SSR3300010 were purchased and wired according to manufacturer specifications.

6.4 Preliminary results

Bilayer samples of linear low density polyethylene (LLDPE)/ polylactide (PLA) and poly(ethylene-*co*-glycidyl methacrylate) (EGMA)/PLA were created at 180 °C and constant piston speed (Figure 6.5, materials are described in Chapter 4). Bilayers displayed a small amount of LLDPE wrap-around, but uniform dimensions (about 9 mm wide and 1.3 mm thick) and flat interfaces are observed. Adhesion was tested by peel tests on a Shimadzu-AGX tensile tester at 5 mm/min (described in Chapters 3, 4, and 5), after trimming the samples to 6 mm wide (to match the typical sample width of laminated bilayers). LLDPE/PLA bilayers and EGMA/PLA bilayers had peel strengths of 3.8 ± 0.8 N/m and 4.6 ± 0.8 N/m, respectively (n = 5), at 20 mm/min piston speed. The adhesion between LLDPE and PLA is low, as expected for homopolymer interfaces. The reactive EGMA/PLA bilayer peel strength was lower than expected, probably due to the short contact time in the extruder (< 10 s). This value is more than two orders of magnitude below that reported in literature for EMA-GMA/PLA interfaces laminated at 180 °C for 1 min (750 N/m).[34] This result highlights how adhesion results depend on processing parameters, and emphasizes the potential utility of this small scale extrusion experiment for scale-up.

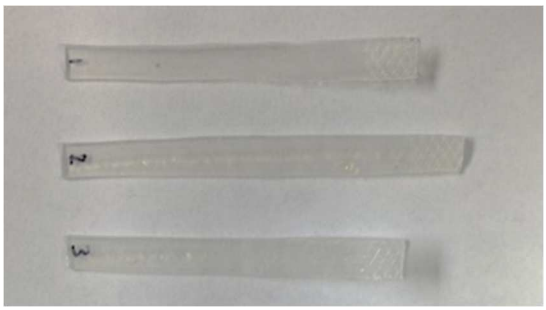

Figure 6.5. Capillary coextrusion LLDPE/PLA bilayers after adhesion testing. Samples are about 6 mm wide and 1 mm thick.

The adhesion of EGMA/PLA bilayers was examined as a function of piston speed of the capillary rheometer (Figure 6.6). The contact times were calculated as 281 s, 140 s, 70 s, 28 s, 14 s, and 7.0 s, in order of increasing piston speed. At high piston speeds (high flow rate, short contact time) there is not enough time for significant copolymer formation to occur, resulting in low adhesion. We hypothesize that low piston speeds (low flow rate, long contact time) correspond to negligible compressional flow rates normal to the interface. This subsequently results in lower reaction rates than demonstrated by the high flow rate cases, and therefore lower copolymer conversions. A maximum peel strength of about 280 N/m was observed at a piston speed of 5 mm/min. We hypothesize this flow rate is fast enough to cause functional polymers to deform near the interface, increasing reaction rate, but slow enough that the reaction has time to proceed.

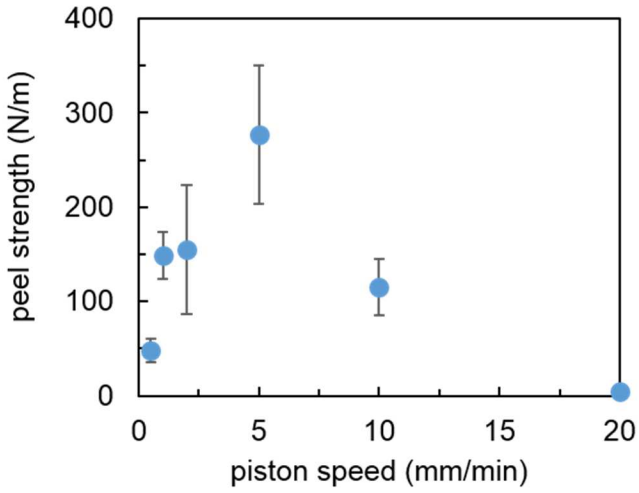

Figure 6.6. EGMA/PLA bilayer adhesion as a function of piston speed.

6.5 Conclusions and future work

A small scale coextrusion die was created to test interfacial properties of bilayer polymer films. Fluent simulations revealed a relatively uniform exit velocity at a variety of flow rates, which was confirmed experimentally by the production of high-quality

bilayers of LLDPE/PLA and EGMA/PLA. The reactive interface (EGMA/PLA) showed the strong dependence of adhesion on flow rate.

One potential capability of the new small scale extrusion die is extending previous work on the effect of compression ratio on reaction rate, similar to Song et al.[26] This would merely require replacement of the die exit and first expansion piece with flow channels of appropriate widths. Future work could then extend the relationship between compressional flow towards the interface and reaction rate to other reactions and homopolymers, as well as separate the effects of compression ratio and compression rate.

Due to the modular design of the die, layer multipliers can easily be introduced upstream of the die exit and first expansion pieces. Multilayer samples would increase the interfacial area available per unit volume, facilitating detection of copolymer formation by simpler rheology or SEC techniques (instead of XPS or adhesion). These multilayer products are also interesting for barrier tests and the packaging industry.

Another study could test entanglement theory by extruding the same homopolymer through both bores at different rates. The adhesion could be measured versus contact time, to test how quickly entanglements occur at the interface.

Finally, capillary coextrusion offers a new method to detect how additives migrate to the interface in polymer blends and multilayer structures. By first blending catalysts or copolymers with one of the homopolymers prior to extrusion the localization or interfacial effects of the bilayer film can be examined for various residences times.

The capillary coextruder developed in this chapter is a useful tool for testing the interfacial properties of polymer bilayers made in a continuous process. Its small scale, flow rate control, and modular nature will afford many future research opportunities.

Bibliography

(1) Utracki, L. A. Introduction to Polymer Blends Technology. In *Encyclopedic Dictionary of Commercial Polymer Blends*; ChemTec Publishing: Toronto, 1994; p 12.

(2) Koning, C.; Van Duin, M.; Pagnoulle, C.; Jerome, R. Strategies for compatibilization of polymer blends. *Prog. Polym. Sci.* **1998**, *23*, 707–757.

(3) Akkapeddi, M. K. Commercial Polymer Blends. In *Polymer Blends Handbook*; Utracki, L. A., Wilkie, C. A., Eds.; Springer, 2014; pp 1733–1833.

(4) Utracki, L. A.; Mukhopadhyay, P.; Gupta, R. K. Polymer Blends: Introduction. In *Polymer Blends Handbook*; 2014; pp 3–170.

(5) Utracki, L. A. Introduction to Polymer Blends. In *Polymer Blends Handbook*; Kluwer, 2003; pp 1–122.

(6) Schurmann, B. L.; Niebergall, U.; Severin, N.; Burger, C.; Stocker, W.; Rabe, J. P. Polyethylene (PEHD)/ polypropylene (iPP) blends : mechanical properties, structure, and morphology. *Polymer* **1998**, *39* (22), 5283–5291.

(7) Wu, S. Phase structure and adhesion in polymer blends : A criterion for rubber toughening. *Polymer* **1985**, *26*.

(8) Macosko, C. W.; Jeon, H. K.; Hoye, T. R. Reactions at polymer-polymer interfaces for blend compatibilization. *Prog. Polym. Sci.* **2005**, *30* (8-9), 939–947.

(9) Sundararaj, U.; Macosko, C. W.; Rolando, R. J.; Chan, H. T. Morphology development in polymer blends. *Polym. Eng. Sci.* **1992**, *32* (24), 1814–1823.

(10) Macosko, C. W.; Gue, P.; Khandpur, A. K.; Nakayama, A.; Marechal, P.; Inoue, T. Compatibilizers for melt blending : premade block copolymers. *Macromolecules* **1996**, *29*, 5590–5598.

(11) Xu, Y.; Thurber, C. M.; Lodge, T. P.; Hillmyer, M. A. Synthesis and remarkable efficacy of model polyethylene-graft- poly(methyl methacrylate) copolymers as compatibilizers in polyethylene/poly(methyl methacrylate) blends. *Macromolecules* **2012**.

(12) Xu, Y.; Thurber, C. M.; Macosko, C. W.; Lodge, T. P.; Hillmyer, M. A. Poly(methyl methacrylate)- block-polyethylene-block-poly(methyl methacrylate) triblock copolymers as compatibilizers for polyethylene/poly(methyl methacrylate) blends. *Ind. Eng. Chem. Res.* **2014**, *53*, 4718–4725.

(13) Helfand, E. Block copolymers, polymer-polymer interfaces, and the theory of inhomogeneous polymers. *Rubber Chem. Technol.* **1976**, *49* (2), 237–246.

(14) Shull, K. R. Theory of end-adsorbed polymer brushes in polymeric matrices. *J. Chem. Phys.* **1991**, *94* (8), 5723.

(15) Jiang, G.; Wu, H.; Guo, S. Reinforcement of adhesion and development of morphology at polymer-polymer interface via reactive compatibilization. *Polym. Eng. Sci.* **2010**, *50* (12), 2273–2286.

(16) Anderson, K. S.; Lim, S. H.; Hillmyer, M. A. Toughening of polylactide by melt blending with linear low-density polyethylene. *J. Appl. Polym. Sci.* **2003**, *89* (14), 3757–3768.

(17) Takeda, Y.; Keskkula, H.; Paul, D. . Effect of polyamide functionality on the morphology and toughness of blends with a functionalized block copolymer. *Polymer* **1992**, *33* (15), 3173–3181.

(18) Ho, C.-H.; Wang, C.-H.; Lin, C.-I.; Lee, Y.-D. Synthesis and characterization of TPO–PLA copolymer and its behavior as compatibilizer for PLA/TPO blends. *Polymer* **2008**, *49* (18), 3902–3910.

(19) Brown, H. R. The adhesion between polymers. *Annu. Rev. Mater. Sci.* **1991**, *21*, 463–489.

(20) Creton, C.; Kramer, E. J.; Hui, C.-Y.; Brown, H. R. Failure mechanisms of polymer interfaces reinforced with block copolymers. *Macromolecules* **1992**, *25*, 3075–3088.

(21) Boucher, E.; Folkers, J. P.; Hervet, H.; Le, L. Effects of the formation of copolymer on the interfacial adhesion between semicrystalline polymers. *Macromolecules* **1996**, *29*, 774–782.

(22) Boucher, E.; Folkers, J. P.; Creton, C.; Hervet, H.; Le, L. Enhanced adhesion between polypropylene and polyamide-6 : role of interfacial nucleation of the B-crystalline form of polypropylene. *Macromolecules* **1997**, *30*, 2102–2109.
(23) Song, J.; Bringuier, A.; Kobayashi, S.; Baker, A. Adhesion between polyethylene with different types of polypropylenes. *Polym. J.* **2012**.
(24) Seo, Y.; Ninh, T. H. Enhanced interfacial adhesion between polypropylene and nylon 6 by in situ reactive compatibilization. *Polymer* **2004**, *45* (25), 8573–8581.
(25) Kramer, E. J.; Berger, L. L. Fundamental Processes of Craze Growth and Fracture. *Adv. Polym. Sci.* **1990**, *91/92*, 1–68.
(26) Song, J.; Baker, A. M.; Ewoldt, R. H.; Macosko, C. W. Reactive coupling between immiscible polymer chains : acceleration by compressive flow. *AIChE J.* **2013**, *59* (9), 3391–3402.
(27) Jeon, H. K.; Zhang, J.; Macosko, C. W. Premade vs. reactively formed compatibilizers for PMMA/PS melt blends. *Polymer* **2005**, *46* (26), 12422–12429.
(28) Lyu, S.; Jones, T. D.; Bates, F. S.; Macosko, C. W. Role of block copolymers on suppression of droplet coalescence. *Macromolecules* **2002**, *35* (20), 7845–7855.
(29) Liu, N. C.; Baker, W. E. Reactive polymers for blend compatibilization. *Adv. Polym. Tech.* **1992**, *11* (4), 249–262.
(30) Yu, Z.; Ou, Y.; Hu, G. Influence of Interfacial Adhesion on Toughening of Polyethylene – Octene Elastomer / Nylon 6 Blends. *J. Appl. Polym. Sci.* **1998**, *69*, 1711–1718.
(31) Pracella, M.; Chionna, D. Reactive compatibilization of blends of PET and PP modified by GMA grafting. *Macromol. Symp.* **2003**, *198*, 161–171.
(32) Su, Z.; Li, Q.; Liu, Y.; Hu, G. H.; Wu, C. Compatibility and phase structure of binary blends of poly(lactic acid) and glycidyl methacrylate grafted poly(ethylene octane). *Eur. Polym. J.* **2009**, *45* (8), 2428–2433.
(33) Liu, H.; Chen, F.; Liu, B.; Estep, G.; Zhang, J. Super toughened poly(lactic acid) ternary blends by simultaneous dynamic vulcanization and interfacial compatibilization. *Macromolecules* **2010**, *43* (14), 6058–6066.
(34) Xu, Y.; Loi, J.; Delgado, P.; Topolkaraev, V.; McEneany, R. J.; Macosko, C. W.; Hillmyer, M. a. Reactive compatibilization of polylactide/polypropylene blends. *Ind. Eng. Chem. Res.* **2015**, 150603105722001.
(35) Guegan, P.; Macosko, C. W.; Ishizone, T.; Hirao, A.; Nakahaha, S. Kinetics of chain coupling at melt interfaces. *Macromolecules* **1994**, *27*, 4993–4997.
(36) Orr, C. A.; Cernohous, J. J.; Guegan, P.; Hirao, A.; Jeon, H. K.; Macosko, C. W. Homogeneous reactive coupling of terminally functional polymers. *Polymer* **2001**, *42*, 8171–8178.
(37) Jeon, H. K.; Feist, B. J.; Koh, S. B.; Chang, K.; Macosko, C. W.; Dion, R. P. Reactively formed block and graft copolymers as compatibilizers for polyamide 66/PS blends. *Polymer* **2004**, *45* (1), 197–206.
(38) Jeon, H. K.; Macosko, C. W.; Moon, B.; Hoye, T. R.; Yin, Z. Coupling reactions of end- vs mid-functional polymers. *Macromolecules* **2004**, *37*, 2563–2571.
(39) Moon, B.; Hoye, T. R.; Macosko, C. W. Anionic synthesis and detection of fluorescence-labeled polymers with a terminal anhydride group. *J. Polym. Sci., Part A Polym. Chem.* **2000**, *38* (12), 2177–2185.
(40) Schulze, J. S.; Moon, B.; Lodge, T. P.; Macosko, C. W. Measuring copolymer formation from end-functionalized chains at a PS / PMMA interface using FRES and SEC. *Macromolecules* **2001**, *34*, 200–205.
(41) Nofar, M.; Maani, A.; Sojoudi, H.; Heuzey, M. C.; Carreau, P. J. Interfacial and rheological properties of PLA / PBAT and PLA / PBSA blends and their morphological stability under shear flow. *J. Rheol.* **2015**, *59* (2), 317–333.
(42) Trifkovic, M.; Hedegaard, A.; Huston, K.; Sheikhzadeh, M.; Macosko, C. W. Porous films via PE/PEO cocontinuous blends. *Macromolecules* **2012**, *45* (15), 6036–6044.

(43) Dil, E. J.; Carreau, P. J.; Favis, B. D. Morphology, miscibility and continuity development in poly(lactic acid)/poly(butylene adipate-co-terephthalate) blends. *Polymer* **2015**, *68*, 202–212.
(44) Van Hemelrijck, E.; Van Puyvelde, P.; Velankar, S.; Macosko, C. W.; Moldenaers, P. Interfacial elasticity and coalescence suppression in compatibilized polymer blends. *J. Rheol.* **2004**, *48* (1), 143.
(45) Velankar, S.; Van Puyvelde, P.; Mewis, J.; Moldenaers, P. Effect of compatibilization on the breakup of polymeric drops in shear flow. *J. Rheol.* **2001**, *45* (4), 1007.
(46) Van Puyvelde, P.; Velankar, S.; Moldenaers, P. Rheology and morphology of compatibilized polymer blends. *Curr. Opin. Colloid Interface Sci.* **2001**, *6* (5-6), 457–463.
(47) Palierne, J. E. Linear rheology of viscoelastic emulsions with interfacial tension. *Rheol. Acta* **1990**, *29*, 204–214.
(48) Ojijo, V.; Sinha Ray, S.; Sadiku, R. Toughening of biodegradable polylactide/poly(butylene succinate-co-adipate) blends via in situ reactive compatibilization. *ACS Appl. Mater. Interfaces* **2013**, *5* (10), 4266–4276.
(49) Nazábal, J.; Aróstegui, A. Supertoughness and critical interparticle distance dependence in poly (butylene terephthalate) and poly (ethylene-co-glycidyl methacrylate) blends. *J. Polym. Sci. Part B Polym. Phys.* **2003**, *41*, 2236–2247.
(50) Saleem, M.; Baker, W. E. In situ reactive compatibilization in polymer blends: Effects of functional group concentrations. *J. Appl. Polym. Sci.* **1990**, *39* (3), 655–678.
(51) Coltelli, M.-B.; Bianchi, S.; Aglietto, M. Poly(ethylene terephthalate) (PET) degradation during the Zn catalysed transesterification with dibutyl maleate functionalized polyolefins. *Polymer* **2007**, *48* (5), 1276–1286.
(52) Pagnoulle, C.; Koning, C.; Leemans, L.; Je, R. Reactive Compatibilization of SAN / EPR Blends . 1 . Dependence of the phase morphology development on the reaction kinetics. **2000**, 6275–6283.
(53) Sundararaj, U.; Macosko, C. W. Drop breakup and coalescence in polymer blends: the effects of concentration and compatibilization. *Macromolecules* **1995**, *28*, 2647–2657.
(54) Thurber, C. M.; Xu, Y.; Myers, J. C.; Lodge, T. P.; Macosko, C. W. Accelerating reactive compatibilization of PE/PLA blends by an interfacially localized catalyst. *ACS Macro Lett.* **2015**, *4*, 30–33.
(55) Song, J.; Thurber, C. M.; Kobayashi, S.; Baker, A. M.; Macosko, C. W.; Silvis, H. C. Blends of polyolefin/PMMA for improved scratch resistance, adhesion and compatibility. *Polymer* **2012**, *53* (16), 3636–3641.
(56) Milner, S. T.; Xi, H. How copolymers promote mixing of immiscible homopolymers. *J. Rheol.* **1996**, *40* (4), 663–687.
(57) Zhang, J.; Lodge, T. P.; Macosko, C. W. Interfacial morphology development during PS/PMMA reactive coupling. *Macromolecules* **2005**, *38* (15), 6586–6591.
(58) Kim, H. Y.; Ryu, D. Y.; Jeong, U.; Kho, D. H.; Kim, J. K. The effect of chain architecture of in situ formed copolymers on interfacial morphology of reactive polymer blends. *Macromol. Rapid Commun.* **2005**, *26* (17), 1428–1433.
(59) Kim, H. Y.; Jeong, U.; Kim, J. K. Reaction kinetics and morphological changes of reactive polymer−polymer interface. *Macromolecules* **2003**, *36* (5), 1594–1602.
(60) Yin, Z.; Koulic, C.; Pagnoulle, C.; Jérôme, R. Reactive blending of functional PS and PMMA: interfacial behavior of in situ formed graft copolymers. *Macromolecules* **2001**, *34* (15), 5132–5139.
(61) Yin, Z.; Koulic, C.; Jeon, H. K.; Pagnoulle, C.; Macosko, C. W.; Jerome, R. Effect of molecular weight of the reactive precursors in melt reactive blending. *Macromolecules* **2002**, *35* (24), 25–27.
(62) Chaturvedi, U. K.; Steiner, U.; Zak, O.; Krausch, G.; Klein, J. Interfacial structure in polymer mixtures below the critical point. *Phys. Rev. Lett.* **1989**, *63* (6), 616–619.
(63) Song, J.; Bringuier, A.; Kobayashi, S.; Baker, A. M.; Macosko, C. W. Adhesion between polyethylenes and different types of polypropylenes. *Polym. J.* **2012**, *44* (9), 939–945.

(64) Jones, T.; Schulze, J. S.; Macosko, C. W.; Lodge, T. P. Effect of thermodynamic interactions on reactions at polymer / polymer interfaces. *Macromolecules* **2003**, *36*, 7212–7219.
(65) Zhang, J.; Ji, S.; Song, J.; Lodge, T. P.; Macosko, C. W. Flow accelerates interfacial coupling reactions. *Macromolecules* **2010**, *43* (18), 7617–7624.
(66) Pillon, L. Z.; Utracki, L. A. Compatibilization of polyester/polyamide blends via catalytic ester-amide interchange reaction. *Polym. Eng. Sci.* **1984**, *24* (17), 1300–1305.
(67) Pillon, L. Z.; Utracki, L. A.; Pilon, D. W. Spectroscopic study of poly(ethylene terephthalate) / poly(amide-6,6) blends. *Polym. Eng. Sci.* **1987**, *27* (8), 562–567.
(68) Feng, Y.; Zhao, G.; Yin, J.; Jiang, W. Reactive compatibilization of high-impact poly(lactic acid)/ethylene copolymer blends catalyzed by N , N -dimethylstearylamine. *Polym. Int.* **2014**, No. 63, 1263–1269.
(69) Legros, A.; Carreau, P. J.; Favis, B. D.; Michel, A. Morphology modification by interfacial chemical reaction in a polyester/ethylene vinyl acetate/polyethylene blend. *Polymer* **1997**, *38* (20), 5085–5089.
(70) Fredrickson, G. H.; Milner, S. T. Time-dependent reactive coupling at polymer-polymer interfaces. *Macromolecules* **1996**, *29* (23), 7386–7390.
(71) Mueller, M. Reactions at polymer interfaces: a Monte Carlo simulation. *Macromolecules* **1997**, *9297* (96), 6353–6357.
(72) Song, J.; Ewoldt, R. H.; Silvis, H. C.; Macosko, C. W. Flow accelerates adhesion between functional polyethylene and polyurethane. *AIChE J.* **2011**, *57* (12), 3496–3506.
(73) Schulze, J. S.; Cernohous, J. J.; Hirao, A.; Lodge, T. P.; Macosko, C. W. Reaction kinetics of end-functionalized chains at a polystyrene/ poly(methyl methacrylate) interface. *Macromolecules* **2000**, *33*, 1191–1198.
(74) Jeon, H. K.; Kim, J. K. Effect of reaction rate on morphological change of reactive blends. *Macromolecules* **2000**, *33* (22), 8200–8210.
(75) Hu, G. H.; Lindt, J. T.; Lambla, M. Transesterification reaction of poly(ethylene-co-vinyl acetate) with alcohols: A kinetic study in solution and in the bulk. *J. Appl. Polym. Sci.* **1992**, *46* (6), 1039–1044.
(76) Oyama, H. T.; Inoue, T. Kinetics and mechanism of coupling of functionalized chains at the immiscible polymer−polymer interface. *Macromolecules* **2001**, *34* (10), 3331–3338.
(77) Scott, C.; Macosko, C. Model experiments for the interfacial reaction between polymers during reactive polymer blending. *J. Polym. Sci. Part B Polym. Phys.* **1994**, *32* (2), 205–213.
(78) Kramer, E. J. Grafting Kinetics of End-Functional Polymers at Melt Interfaces. *Isr. J. Chem.* **1995**, *35* (1), 49–54.
(79) Brandup, J.; Immergut, E. H.; Grulke, E. A.; Abe, A.; Bloch, D. R. *Polymer Handbook*, 4th Editio.; Sons, J. W. &, Ed.; 1999.
(80) Sagel, E. Polyethylene global overview http://www.ptq.pemex.com/productosyservicios/eventosdescargas/Documents/Foro PEMEX Petroquímica/2012/PEMEX PE.pdf (accessed Jan 23, 2012).
(81) China chemical & fiber economic information network www.ccfei.net/ (accessed Mar 5, 2012).
(82) Utracki, L. A. *Polymer Alloys and Blends*; Hanser Gardner Publ., 1990.
(83) Market report plastics http://plasticker.de/.
(84) Hong'en, J.; Xiujuan, L. 50,000t/year PMMA http://plasticker.de/ (accessed Dec 2, 2012).
(85) Feng, J.; Chan, C.; Li, J. A method to control the dispersion of carbon black in an immiscible polymer blend. *Polym. Eng. Sci.* **2003**, *43* (5), 1058–1063.
(86) Chand, N.; Vashishtha, S. R. Development, structure and strength properties of PP/ PMMA/ FA blends. *Bull. Mater. Sci.* **2000**, *23* (2), 103–107.
(87) Chung, T. C.; Rhubright, D.; Jiang, G. J. Synthesis of polypropylene graft poly(methyl methacrylate) copolymers by the borane approach. *Macromolecules* **1993**, *26* (14), 24–28.

(88) Chung, T. C. Synthesis of functional polyolefin copolymers with graft and block structures. *Prog. Polym. Sci.* **2002**, *27*, 39–85.
(89) Thirtha, V.; Lehman, R.; Nosker, T. Glass transition effects in immiscible polymer blends. *ANTEC* **2005**, 2380–2384.
(90) Souza, A. M. C. de; Calvão, P. S.; Demarquette, N. R. Linear viscoelastic behavior of compatibilized PMMA/PP blends. *J. Appl. Polym. Sci.* **2013**, *129* (3), 1280–1289.
(91) Badel, T.; Beyou, E.; Bounor-Legaré, V.; Chaumont, P.; Cassagnau, P.; Flat, J. J.; Michel, A. Synthesis of poly(methyl methacrylate)-grafted poly(ethylene-co-octene) copolymers by a "grafting from" melt process. *Macromol. Mater. Eng.* **2012**, *297* (7), 702–710.
(92) Einhorn, J.; Einhorn, C.; Luche, J.-L. A mild and efficient sonochemical tert-butoxycarbonylation of amines from their salts. *SYNLETT* **1991**, No. January, 37–38.
(93) Boyer, C.; Otazaghine, B.; Boutevin, B.; Joly-Duhamel, C.; Robin, J.-J. Synthesis of maleimide terminated N-butyl acrylate oligomers by atom transfer radical polymerization: Study of their copolymerization with vinyl ethers. *J. Polym. Sci., Part A Polym. Chem.* **2005**, *43* (18), 4303–4322.
(94) Robin, J.-J.; Boyer, C.; Boutevin, B.; Loubat, C. Synthesis and properties of polyolefin graft copolymers by a grafting "onto" reactive process. *Polymer* **2008**, *49* (21), 4519–4528.
(95) Still, C. W.; Kahn, M.; Mitra, A. Rapid chromatographic technique for preparative separations with moderate resolution. *J. Org. Chem.* **1978**, *43* (14), 2923–2925.
(96) Weitman, M.; Lerman, K.; Nudelman, A.; Major, D. T.; Hizi, A.; Herschhorn, A. Structure-activity relationship studies of 1-(4-chloro-2,5-dimethoxyphenyl)-3-(3-propoxypropyl) thiourea, a non-nucleoside reverse transcriptase inhibitor of human immunodeficiency virus type-1. *Eur. J. Med. Chem.* **2011**, *46* (2), 447–467.
(97) Ahn, K. D.; Chung, C.-M.; Koo, D.-I. Photochemical acid generation in solid-state and application as resist materials. *Chem. Mater.* **1994**, No. 10, 1452–1456.
(98) Ahn, K. D.; Willson, C. G. Synthesis of polymers having N-hydroxymaleimide units by thermolysis of N-(isopropyloxycarbonyloxy)-maleimide polymers. *Bull. Korean Chem. Soc.* **1995**, *16*, 443–443.
(99) Robertson, J. *Protecting Group Chemistry*; Oxford University Press, 2000.
(100) Wang, J.-S.; Matyjaszewski, K. Controlled/"living" radical polymerization. Halogen atom transfer radical polymerization promoted by a Cu(I)/Cu(II) redox process. *Macromolecules* **1995**, *28* (23), 7901–7910.
(101) Jakubowski, W.; Matyjaszewski, K. Activator generated by electron transfer for atom transfer radical polymerization. *Macromolecules* **2005**, *38*, 4139–4146.
(102) Matyjaszewski, K.; Wei, M.; Xia, J.; Mcdermott, N. E. Controlled/"living" radical polymerization of styrene and methyl methacrylate catalyzed by iron complexes. *Macromolecules* **1997**, *30*, 8161–8164.
(103) Tang, W.; Matyjaszewski, K. Effects of initiator structure on activation rate constants in ATRP. *Macromolecules* **2007**, *40*, 1858–1863.
(104) Passingham, C.; Hendra, P. J.; Cudby, M. E. A.; Zichy, V.; Weller, M. The re-evaluation of multiple peaks in the DSC melting endotherm of isotactic polypropylene. *Eur. Polym. J.* **1990**, *26* (6), 631–638.
(105) Pitet, L. M.; Amendt, M. A.; Hillmyer, M. A. Nanoporous linear polyethylene from a block polymer precursor. *J. Am. Chem. Soc. Commun.* **2010**, *132* (24), 8230–8231.
(106) Pangborn, A. B.; Giardello, M. A.; Grubbs, R. H.; Rosen, R. K.; Timmers, F. J. Safe and convenient procedure for solvent purification. *Organometallics* **1996**, No. 15, 1518–1520.
(107) Mbarek, S.; Jaziri, M. Recycling poly(ethylene terephtalate) wastes: Properties of poly(ethylene terephtalate)/polycarbonate blends and the effect of a transesterification catalyst. *Polym. Eng. Sci.* **2006**.
(108) Fedors, R. F. A method for estimating both the solubility parameters and molar volumes of liquids. *Polym. Eng. Sci.* **1974**, *14*, 147–154.

(109) Marechal, P.; Chiba, T.; Inoue, T. Melt blending of dissimilar polymers by a small scale mixer: Mixing with steel balls. *Polym. Networks Blends* **1997**, *7*, 61.
(110) Maric, M.; Macosko, C. W. Improving polymer blend dispersions in mini-mixers. *Polym. Eng. Sci.* **2001**, *41* (1), 118–130.
(111) Mark, J. E. *Physical properties of polymers handbook*; AIP: New York, NY, 1996.
(112) Anderson, K.; Schreck, K.; Hillmyer, M. Toughening polylactide. *Polym. Rev.* **2008**, *48* (1), 85–108.
(113) Tselios, C.; Bikiaris, D.; Maslis, V.; Panayiotou, C. In situ compatibilization of polypropylene–polyethylene blends: a thermomechanical and spectroscopic study. *Polymer* **1998**, *39* (26), 6807–6817.
(114) Xanthos, M.; Warth, H. Effects of Transreactions on the Compatibility and Miscibility of Blends of Condensation Polymers. In *Transreactions in Condensation Polymers*; Fakirov, S., Ed.; Wiley-VCH, 1999; pp 411–424.
(115) Lee, P.-C.; Kuo, W.-F.; Chang, F.-C. In situ compatibilization of PBT/ABS blends through reactive copolymers. *Polymer* **1994**, *35* (26), 5641–5650.
(116) Singh, A. K.; Prakash, R.; Pandey, D. Reactive compatibilization of polycarbonate and poly(methyl methacrylate) in the presence of a novel transesterification catalyst SnCl2·2H2O. *J. Phys. Chem. B* **2011**, *115*, 1601–1607.
(117) Coltelli, M.-B.; Aglietto, M.; Ciardelli, F. Influence of the transesterification catalyst structure on the reactive compatibilization and properties of poly(ethylene terephthalate) (PET)/dibutyl succinate functionalized poly(ethylene) blends. *Eur. Polym. J.* **2008**, *44* (5), 1512–1524.
(118) Sadik, T.; Becquart, F.; Majeste, J. C.; Taha, M. In-melt transesterification of poly(lactic acid) and poly(ethylene-co-vinylalcohol). *Mater. Chem. Phys.* **2013**, *140*, 559–569.
(119) Manabe, K.; Kobayashi, S. Mannich-type reactions of aldehydes, amines, and ketones in a colloidal dispersion system created by a Brønsted acid − surfactant − combined catalyst in water. *Org. Lett.* **1999**, *1* (12), 1965–1967.
(120) Manabe, K.; Iimura, S.; Sun, X.; Kobayashi, S. Dehydration reactions in water. Brønsted acid - surfactant -combined catalyst for ester , ether, thioether, and dithioacetal formation in water. *J. Am. Chem. Soc.* **2002**, *124* (6), 11971–11978.
(121) Manabe, K.; Mori, Y.; Wakabayashi, T.; Nagayama, S.; Kobayashi, S. Organic synthesis inside particles in water: Lewis acid - surfactant - combined catalysts for organic reactions in water using colloidal dispersions as reaction media. *J. Am. Chem. Soc.* **2000**, *122* (5), 7202–7207.
(122) Stridsberg, K. M.; Ryner, M.; Albertsson, A. Controlled ring-opening polymerization: Polymers with designed macromolecular architecture. *Adv. Polym. Sci.* **2002**, *157*, 41–65.
(123) López-Barrón, C. R.; Macosko, C. W. Rheology of compatibilized immiscible blends with droplet-matrix and cocontinuous morphologies during coarsening. *J. Rheol.* **2014**, *58* (6), 1935–1953.
(124) Cerclé, C.; Sarazin, P.; Favis, B. D. High performance polyethylene/thermoplastic starch blends through controlled emulsification phenomena. *Carbohydr. Polym.* **2013**, *92* (1), 138–148.
(125) Cho, C. S.; Kim, D. T.; Choi, H.; Kim, T.; Shim, S. C. Catalytic activity of tin (II) chloride in esterification of carboxylic acids with alcohols. *Bull. Korean Chem. Soc.* **2002**, *23* (4), 539–540.
(126) Moon, S. I. L.; Lee, C. W. O. O.; Miyamoto, M.; Kimura, Y. Melt polycondensation of L-lactic acid with Sn (II) catalysts activated by various proton acids : A direct manufacturing route to high molecular weight poly(L-lactic acid). *J. Polym. Sci., Part A Polym. Chem.* **2000**, *38*, 1673–1679.
(127) Chen, C.-T.; Kuo, J.-H.; Ku, C.-H.; Weng, S.-S.; Liu, C.-Y. Nucleophilic acyl substitutions of esters with protic nucleophiles mediated by amphoteric, oxotitanium, and vanadyl species. *J. Org. Chem.* **2005**, *70* (4), 1328–1339.
(128) Zhang, J.; Cole, P. J.; Nagpal, U.; Macosko, C. W.; Lodge, T. P. Direct correlation between adhesion promotion and coupling reaction at immiscible polymer-polymer interfaces. *J. Adhes.* **2006**, *82* (9), 887–902.

(129) Cole, P. J.; Cook, R. F.; Macosko, C. W. Adhesion between immiscible polymers correlated with interfacial entanglements. *Macromolecules* **2003**, *36* (8), 2808–2815.
(130) Zhang, J.; Lodge, T. P.; Macosko, C. W. Interfacial slip reduces polymer-polymer adhesion during coextrusion. *J. Rheol.* **2006**, *50* (1), 41.
(131) Rath, T.; Edler, M.; Haas, W.; Fischereder, A.; Moscher, S.; Schenk, A.; Trattnig, R.; Sezen, M.; Mauthner, G.; Pein, A.; et al. A direct route towards polymer/copper indium sulfide nanocomposite solar cells. *Adv. Energy Mater.* **2011**, *1*, 1046–1050.
(132) Brundle, C. R.; Evans, C.; Wilson, S. Electron Beam Instruments. In *Encyclopedia of Materials Characterization: Surfaces, Interfaces, Thin Films*; Gulf Professional Publishing, 1992; pp 120–134.
(133) Weast, R. C. *CRC Handbook of Chemistry and Physics*, 60th ed.; CRC Press: Boca Raton, FL, 1979.
(134) Stokes, R. J.; Evans, D. F. *Fundamentals of Interface Engineering*; Wiley-VCH: New York, NY, 1996.
(135) Liu, H.; Zhang, J. Research progress in toughening modification of poly(lactic acid). *J. Polym. Sci. Part B Polym. Phys.* **2011**, *49* (15), 1051–1083.
(136) Kim, N.-Y.; Yun, Y. S.; Lee, J.-Y.; Choochottiros, C.; Pyo, H.; Chin, I.-J.; Jin, H.-J. Enhanced impact properties of polylactide by poly(lactide-b-butadiene-b-lactide) triblock copolymer. *Macromol. Res.* **2011**, *19* (9), 943–947.
(137) Jin, H.; Chin, I.; Kim, M.; Kim, S.; Yoon, J. Blending of poly(L-lactic acid) with poly(cis-1,4-isoprene). *Eur. Polym. J.* **2000**, *36*, 165–169.
(138) Anderson, K. S.; Hillmyer, M. A. The influence of block copolymer microstructure on the toughness of compatibilized polylactide/polyethylene blends. *Polymer* **2004**, *45* (26), 8809–8823.
(139) Baker, W. E.; Scott, C.; Hu, G. H. *Reactive Polymer Blending*; Hanser.: Cincinnati, 2001.
(140) Ajji, A.; Utracki, L. A. lnterphase and compatibilization of polymer blends. *Polym. Eng. Sci.* **1996**, *3* (12), 1574–1585.
(141) Magalhles, A. M. L.; Borggreve, R. J. M. Contribution of the crazing process to the toughness of rubber-modified polystyrene. *Macromolecules* **1995**, *28*, 5841–5851.
(142) Lee, I.; Panthani, T. R.; Bates, F. S. Sustainable poly(lactide-b-butadiene) multiblock copolymers with enhanced mechanical properties. *Macromolecules* **2013**, *46* (18), 7387–7398.
(143) Mbarek, S.; Jaziri, M.; Chalamet, Y.; Carrot, C. Effect of the viscosity ratio on the morphology and properties of PET / HDPE blends with and without compatibilization. *J. Appl. Polym. Sci.* **2010**.
(144) Bartczak, Z.; Galeski, A. *Polymer Blends Handbook, Volume 2*; 2014.
(145) Kowalczyk, M.; Piorkowska, E. Mechanisms of plastic deformation in biodegradable polylactide/poly(1,4-cis-isoprene) blends. *J. Appl. Polym. Sci.* **2012**, *124*, 4579–4589.
(146) Bartczak, Z.; Galeski, A. Mechanical properties of polymer blends. In *Polymer Blends Handbook*; Utracki, L. A., Wilkie, C. A., Eds.; Springer, 2014; pp 1203–1297.
(147) Oyama, H. T. Super-tough poly(lactic acid) materials: Reactive blending with ethylene copolymer. *Polymer* **2009**, *50* (3), 747–751.
(148) Li, D.; Shentu, B.; Weng, Z. Morphology, rheology, and mechanical properties of polylactide/poly(ethylene-co-octene) blends. *J. Macromol. Sci. Part B* **2011**, *50* (10), 2050–2059.
(149) Bai, H.; Bai, D.; Xiu, H.; Liu, H.; Zhang, Q.; Wang, K.; Deng, H.; Chen, F.; Fu, Q.; Chiu, F.-C. Towards high-performance poly(l-lactide)/elastomer blends with tunable interfacial adhesion and matrix crystallization via constructing stereocomplex crystallites at the interface. *RSC Adv.* **2014**, *4* (90), 49374–49385.
(150) Lee, J. S.; Park, K. Y.; Yoo, D. J.; Suh, K. D. In situ compatibilization of PET/PS blends through carbamate-functionalized reactive copolymers. *J. Polym. Sci. Part B Polym. Phys.* **2000**, *38* (10), 1396–1404.
(151) Stewart, M. E.; George, S. E.; Miller, R. L. Effect of catalyst on the reactive processing of polyesters With epoxy-functional polymers. *Polym. Eng. Sci.* **1993**, *33* (11), 675–685.

(152) Merfeld, G.; Molaison, C.; Koeniger, R.; Acar, A. E.; Mordhorst, S.; Suriano, J.; Irwin, P.; Warner, R. S.; Gray, K.; Smith, M.; et al. Acid/epoxy reaction catalyst screening for low temperature (120°C) powder coatings. *Prog. Org. Coatings* **2005**, *52* (2), 98–109.
(153) Blank, W. J.; He, Z. A.; Picci, M. Catalysis of the epoxy-carboxyl reaction. *J. Coatings Technol.* **2002**, *74* (926), 33–41.
(154) Tadmor, Z.; Gogos, C. G. *Principles of Polymer Processing*, 2nd ed.; Wiley-Interscience: Hoboken, NJ, 2006.
(155) Badel, T.; Beyou, E.; Bounor-Legaré, V.; Chaumont, P.; Flat, J. J.; Michel, A.; Lyon, D. Melt grafting of poly(methyl methacrylate) onto poly (ethylene-co-octene) by reactive extrusion: Model compound approach. *J. Polym. Sci., Part A Polym. Chem.* **2007**, *45*, 5215–5226.
(156) Kwak, J.; Lacroix-Desmazes, P.; Robin, J. J.; Boutevin, B.; Torres, N. Synthesis of mono functional carboxylic acid poly(methyl methacrylate) in aqueous medium using sur-iniferter. Application to the synthesis of graft copolymers polyethylene-g-poly(methyl methacrylate) and the compatibilization of LDPE/PVDF blends. *Polymer* **2003**, *44* (18), 5119–5130.
(157) Xanthos, M. Recycling of the #5 polymer. *Science* **2012**, *337* (6095), 700–702.
(158) Bertin, S.; Robin, J. J. Study and characterization of virgin and recycled LDPE/PP blends. *Eur. Polym. J.* **2002**, *38* (11), 2255–2264.
(159) Teh, J. W. Structure and properties of polyethylene-polypropylene blend. *J. Appl. Polym. Sci.* **1983**, *28* (2), 605–618.
(160) Teh, J. W.; Rudin, A.; Keung, J. C. A review of polyethylene-polypropylene blends and their compatibilization. *Adv. Polym. Technol.* **1994**.
(161) D'Orazio, L.; Greco, R.; Mancarella, C.; Martuscelli, E.; Ragosta, G.; Silvestre, C. Effect of the addition of ethylene-propylene random copolymers on the properties of high-density polyethylene/isotactic polypropylene blends: Part 1 - morphology and impact behavior of molded samples. *Polym. Eng. Sci.* **1982**, *22* (9), 536–544.
(162) D'Orazio, L.; Greco, R.; Martuscelli, E.; Ragosta, G. Effect of the addition of EPM copolymers on the properties of high density polyethylene/isotactic polypropylene blends: II. Morphology and mechanical properties of extruded samples. *Polym. Eng. Sci.* **1983**, *23* (9), 489–497.
(163) Nakamura, S.; Tokumitsu, K.; Kitamura, M.; Miyagawa, E.; Kanzawa, T.; Tanaka, A. Morphology and mechanical properties of PE/PP blends with compatibilizer. *Resour. Process.* **2008**, *55* (2), 56–65.
(164) Nakamura, S.; Tokumitsu, K.; Kitamura, M.; Miyagawa, E.; Tanaka, A. A study for improvement of mechanical properties of recycle PE/PP Blends. *Resour. Process.* **2007**, *54* (4), 167–174.
(165) D'Orazio, L.; Greco, R.; Mancarella, C.; Martuscelli, E.; Ragosta, G.; Silvestre, C. . In *Polymer Blends Processing, Morphology, and Properties*; Kryszewski, M., Gateski, A., Martuscelli, E., Eds.; Plenum: New York, NY, 1984; pp 111–125.
(166) Ha, C. S.; Kim, S. C. Rheological properties and crystalline structure of the dynamically cured EPDM and PP/HDPE ternary blends. *J. Appl. Polym. Sci.* **1988**, *35*, 2211–2221.
(167) Martuscelli, E. Influence of composition, crystallization conditions and melt phase structure on solid morphology, kinetics of crystallization and thermal behavior of binary polymer/polymer blends. *Polym. Eng. Sci.* **1984**, *24* (8), 563–586.
(168) Bartlett, D. W.; Barlow, J. W.; Paul, D. R. Mechanical properties of blends containing HDPE and PP. *J. Appl. Polym. Sci.* **1982**, *27*, 2351–2360.
(169) Nolley, E.; Barlow, J. W.; Paul, D. R. Mechanical properties of polypropylene-low density polyethylene blends. *Polym. Eng. Sci.* **1980**, *20* (5), 364–369.
(170) Choudhary, V.; Varma, H. S.; Varma, I. K. Effect of EPDM rubber on melt rheology , morphology and mechanical properties of polypropylene/HDPE (90/10) blend. 2. *Polymer* **1991**, *32* (14), 2541–2545.
(171) Chen, H. Y.; Poon, B.; Chum, S. P.; Dias, P.; Hiltner, A.; Baer, E. Olefin block copolymers as polyolefin blend compatibilizer. In *SPE Annual Technical Conference Proceedings*; 2007; pp 1–5.

(172) Marchand, G.; Walton, K.; Hu, Y.; Shan, L. P. S.; Barry, R.; Carnahan, E.; Garcia-Meitin, E. Polypropylene based olefin block copolymers as compatibilizers for polyethylene and polypropylene. In *SPE International Polyolefins Conference*; 2014; pp 1–3.
(173) Lin, Y.; Yakovleva, V.; Chen, H.; Hiltner, A.; Baer, E. Comparison of olefin copolymers as compatibilizers for propylene and high-density polyethylene. *J. Appl. Polym. Sci.* **2009**, *113*, 1945–1952.
(174) Chaffin, K. A.; Bates, F. S.; Brant, P.; Brown, G. M. Semicrystalline blends of polyethylene and isotactic polypropylene: Improving mechanical performance by enhancing the interfacial structure. *J. Polym. Sci. Part B Polym. Phys.* **2000**, *38* (1), 108–121.
(175) Chaffin, K. A.; Knutsen, J. S.; Brant, P.; Bates, F. S. High-strength welds in metallocene polypropylene/polyethylene laminates. *Science* **2000**, *288* (5474), 2187–2190.
(176) Fredrickson, G. H.; Liu, A. J.; Bates, F. S. Entropic corrections to the Flory-Huggins theory of polymer blends: Architectural and conformational effects. *Macromolecules* **1994**, *24*, 2503–2511.
(177) Krishnamoorti, R.; Graessley, W. W.; Dee, G. T.; Walsh, D. J.; Fetters, L. J.; Lohse, D. J. Pure component properties and mixing behavior in polyolefin blends. *Macromolecules* **1996**, *29*, 367–376.
(178) Graessley, W. W.; Krishnamoorti, R.; Reichart, G. C.; Balsara, N. P.; Fetters, L. J.; Lohse, D. J. Regular and irregular mixing in blends of saturated hydrocarbon polymers. *Macromolecules* **1995**, *28*, 1260–1270.
(179) Schweizer, K. S.; Yethiraj, A. Polymer reference interaction site model theory: New molecular closures for phase separating fluids and alloys. *J. Chem. Phys.* **1993**, *98* (11), 9053–9079.
(180) Schweizer, K. S.; Singh, C. Microscopic solubility-parameter theory of polymer blends: general predictions. *Macromolecules* **1995**, *28*, 2063–2080.
(181) Park, H. E. Effect of pressure on the rheological properties of three polyethylenes, McGill University, 2005.
(182) Trent, J. S.; Scheinbeim, J. I.; Couchman, P. R. Ruthenium tetraoxide staining of polymers for electron microscopy. *Macromolecules* **1983**, *16*, 589–598.
(183) Khandpur, A. K.; Macosko, C. W.; Bates, F. S. Transmission electron microscopy of saturated hydrocarbon block copolymers. *J. Polym. Sci. Part B* **1995**, *33* (2), 247–252.
(184) Kontopoulou, M.; Wang, W.; Gopakumar, T. G.; Cheung, C. Effect of composition and comonomer type on the rheology, morphology and properties of ethylene-α-olefin copolymer/polypropylene blends. *Polymer* **2003**, *44* (24), 7495–7504.
(185) Chaffin, K. A. Semi-crystalline polymer blends: thermodynamics, morphology, and toughness enhancement, University of Minnesota, 1999.
(186) *Standard Test Methods for Determining the Izod Pendulum Impact Resistance of Plastics (D256-10)*; 2014.
(187) Lo, C. T.; Seifert, S.; Thiyagarajan, P.; Narasimhan, B. Phase behavior of semicrystalline polymer blends. *Polymer* **2004**, *45* (11), 3671–3679.
(188) Zhao, L.; Choi, P. Measurement of solvent-independent polymer-polymer Flory-Huggins interaction parameters with the use of non-random partitioning solvents in inverse gas chromatography. *Polymer* **2002**, *43* (25), 6677–6681.
(189) Ruokolainen, J.; Mezzenga, R.; Fredrickson, G. H.; Kramer, E. J.; Hustad, P. D.; Coates, G. W. Morphology and thermodynamic behavior of syndiotactic polypropylene-poly(ethylene-co-propylene) block polymers prepared by living olefin polymerization. *Macromolecules* **2005**, *38*, 851–860.
(190) Colby, R. H. Melt Rheology of Block Copolymers. *Encyclopedia of Materials: Science and Technology*; 2001; pp 727–730.
(191) Ponting, M.; Burt, T. M.; Korley, L. T. J.; Andrews, J.; Hiltner, A.; Baer, E. Gradient multilayer films by forced assembly coextrusion. *Ind. Eng. Chem. Res.* **2010**, *49* (23), 12111–12118.

(192) Ponting, M.; Hiltner, A.; Baer, E. Polymer nanostructures by forced assembly: Process, structure, and properties. *Macromol. Symp.* **2010**, *294* (1), 19–32.
(193) Lee, P. C.; Dooley, J.; Robacki, J.; Jenkins, S.; Wrisley, R. Improvements in flex oxygen barrier properties of polymeric films by microlayer coextrusion. *J. Plast. Film Sheeting* **2013**, *30* (3), 234–247.
(194) Wang, H.; Keum, J. K.; Hiltner, A.; Baer, E.; Freeman, B.; Rozanski, A.; Galeski, A. Confined crystallization of polyethylene oxide in nanolayer assemblies. *Science* **2009**, *323* (5915), 757–760.
(195) Carr, J. M.; Langhe, D. S.; Ponting, M. T.; Hiltner, A.; Baer, E. Confined crystallization in polymer nanolayered films: A review. *J. Mater. Res.* **2012**, *27* (10), 1326–1350.
(196) Zhao, R.; Macosko, C. W. Slip at polymer-polymer interfaces: Rheological measurements on coextruded multilayers. *J. Rheol.* **2002**, *46* (1), 145.
(197) Lee, P. C.; Park, H. E.; Morse, D. C.; Macosko, C. W. Polymer-polymer interfacial slip in multilayered films. *J. Rheol.* **2009**, *53* (4), 893.

Appendix 1: Supplementary information for Chapter 3

A1.1 Reaction of PLA and poly(ethylene-*co*-vinyl alcohol) (EVOH)

This section explores the use of the acid/hydroxyl group reaction between PLA and PE for commercial polymers. EVOH was purchased from Polysciences, Inc. with 15 wt% vinyl alcohol content, and was pressed into a sheet at 150 °C and ~0.3 MPa for 4 min before use. PLA Ingeo Biopolymer 2003D was dried for 2 d in a vacuum oven at room temperature prior to use in this study. 90/10 PLA/EVOH blends were made on the Xplore MC5 microcompounder at 100 rpm and 180 °C for 5 min, with and without 0.01 M $SnOct_2$. Mixer force curves for the two blends are shown in Figure A1.1.

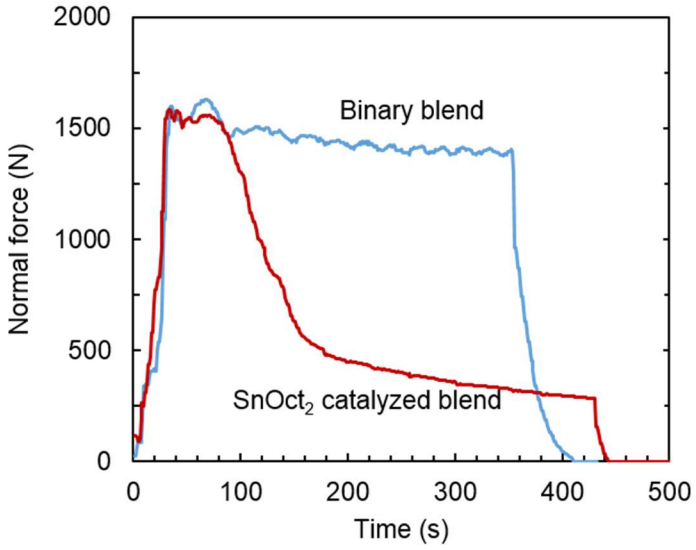

Figure A1.1 Mixer normal force for 90/10 PLA/EVOH blends. The binary blend contains no catalyst and $SnOct_2$ blend contains 0.01 M $SnOct_2$.

The mixer force decreases over time, probably because of transesterification reactions occurring between the numerous hydroxyl groups on EVOH and the ester groups of PLA. Since PLA has a much higher viscosity than EVOH, transesterification has the potential to lower the overall viscosity of the mixture. This agrees with the SEC results in Section 3.4.7 .

Addition of $SnOct_2$ catalyst leads to a much sharper decline in mixer force compared to the neat blend. This is more evidence that $SnOct_2$ facilitates faster interfacial reactions in PE/PLA blends.

A1.2 Dilute HO-PE-OH blends

Chapter 3 discusses 60/30/10 wt% HDPE/HO-PE-OH/PLA reactive blends. Most applications require small amounts of functional polymer. Therefore, an 85/5/10 wt% HDPE/HO-PE-OH/PLA blend was created at the same conditions for comparison, to see if compatibilization occurs with less HO-PE-OH. The average droplet size was measured to be 0.48 ± 0.21 μm, close to the value for the 60/30/10 wt% blend (0.44 ± 0.07 μm). We expect that there is excess HO-PE-OH in the 60/30/10 blends, and that lower concentrations of HO-PE-OH would work similarly well for compatibilization.

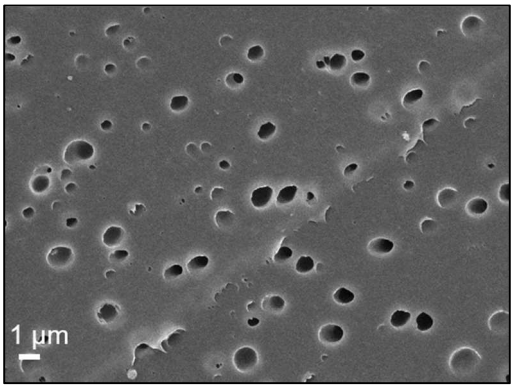

Figure A1.2 SEM image of 85/5/10 wt% HDPE/HO-PE-OH/PLA blend.

Appendix 2: Supplementary information for Chapter 4

A2.1 Tensile samples extruded with a backflow element

Processing parameters in twin screw extrusion and injection molding play a large role in final material toughness. The same blends from Chapter 4 were extruded with a backflow element added to the screws, and otherwise identical conditions. Mass flow rates were roughly the same as before, but residence times were increased to 12 – 25 min, die exit pressures varied from 300 – 700 psi, and torque values ranged from 6 – 16 N-m. The melt strength of the $CoOct_2$, 5 EGMA blend was noticeably higher, forming a self-supporting but flexible rod from the strand die. In contrast, the $CoOct_2$, 1 EGMA blend showed low melt strength and die drool. Injection molding was performed at lower ram pressure (3 kpsi) and higher barrel temperature (200 °C).

Tensile properties are shown in Table A2.1. The $CoOct_2$ blends show surprisingly low extensions at break. This is attributed to PLA degradation, as verified by SEC (in Table A2.2, reported molecular weights are PS equivalent molecular weights). There is competition between degradation and molecular weight increase from the acid-epoxy interfacial reaction, leading to extremely broad dispersities. At shorter residence times (section 4.4.7) the interfacial reaction dominates, leading to improved toughness, but long processing times and higher temperatures allow for degradation and deteriorated mechanical properties. DDA shows little improvement over uncatalyzed, reactive blends, presumably because the reaction can go to near completion with long residence times. The non-catalyzed blends are generally stronger than the short residence time extrusion samples, but 12 – 25 min is too long for large scale extrusion.

Table A2.1 Tensile properties with long extruder residence times

blend	σ_y (MPa)	ε_b (%)	toughness (MJ/m^3)	tensile modulus (MPa)
0 EGMA	48 ± 2	47 ± 6	7 ± 1.3	1800 ± 210
1 EGMA	57 ± 1	140 ± 13	31 ± 2.6	2100 ± 70
DDA, 1 EGMA	47 ± 2	154 ± 19	29 ± 3.9	1700 ± 100
$CoOct_2$, 1 EGMA	41 ± 1	14 ± 4	2 ± 0.7	1700 ± 110
5 EGMA	58 ± 1	194 ± 10	45 ± 2.9	2000 ± 180
DDA, 5 EGMA	44 ± 2	198 ± 24	35 ± 4.3	1600 ± 120
$CoOct_2$, 5 EGMA	43 ± 0	165 ± 38	29 ± 4.3	1700 ± 160

Table A2.2 High temperature SEC of processed materials

sample		M_n (kg/mol)	M_w (kg/mol)	Đ
PLA	pellet	43	130	3.1
	extruded	43	130	3.1
	injection molded	34	110	3.2
$CoOct_2$, 1 EGMA	extruded	26	100	4.0
	injection molded	7	59	8.4
$CoOct_2$, 5 EGMA	extruded	30	140	4.6
	injection molded	26	90	3.3

A2.2 Effect of catalyst concentration on mixer force

Since $CoOct_2$ is not interfacially localized, it is expected that there is a dependence of catalyst concentration on reaction rate. This was probed by mixer force in the Xplore microcompounder (Figure A2.3). 0, 0.001, and 0.01 M catalyst was added to the 5 EGMA blend. As expected, the slope with 0.001 M catalyst concentration is between the two other curves. It has over double the slope of the uncatalyzed curve (slopes of 1.9 and 4.5 for the 0 and 0.001 M, respectively), showing that even at mmol levels $CoOct_2$ is effective. This also highlights the sensitivity of the Xplore microcompounder towards detecting interfacial reaction.

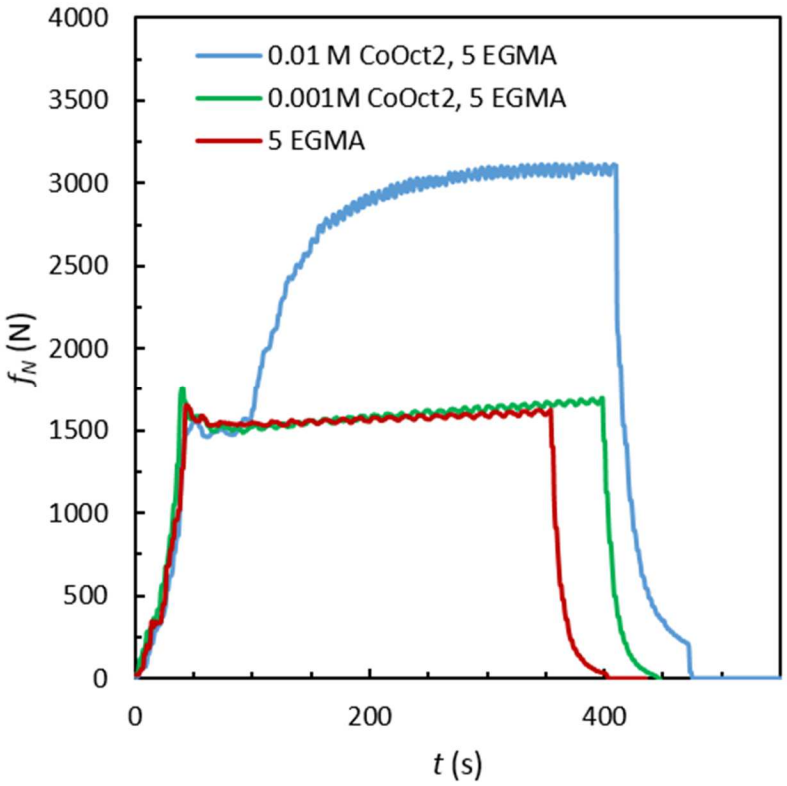

Figure A2.3 Mixer force as a function of catalyst concentration for 5 EGMA blends

A2.3 SEM images of 0 EGMA and 20 EGMA blends

SEM images of 0 EGMA and 20 EGMA blends in Chapter 4 for brevity. They are shown in Figure A2.4.

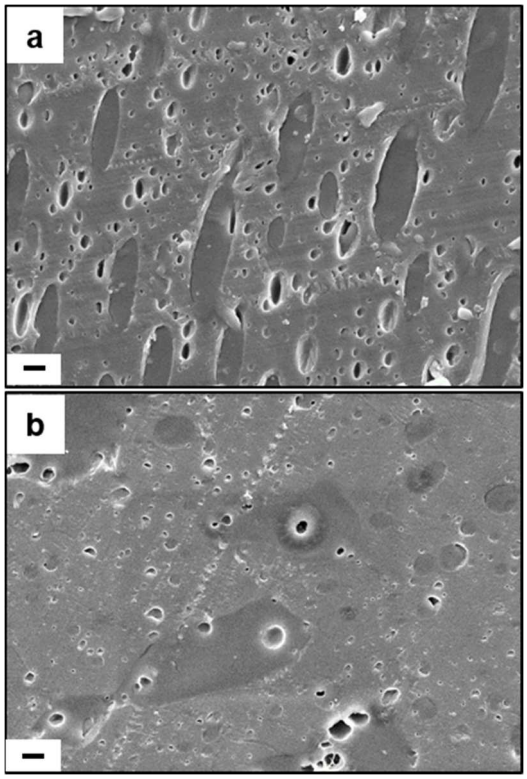

Figure A2.4 SEM images of (a) 0 EGMA and (b) 20 EGMA blends

A2.4 Mixer loading versus normal force

The normal force on the Xplore MC 5 mixer was studied as a function of volume polymer loaded (Figure A2.5, courtesy Liangliang Gu). Polystyrene PS 666D (Dow Chemical) was loaded at four different volumes and mixed at 180 °C for 10 min and 200 rpm. Mixer normal force was recorded after achieving steady state. There is a linear dependence between mixer normal force and loading for PS at the mixer conditions used in this study.

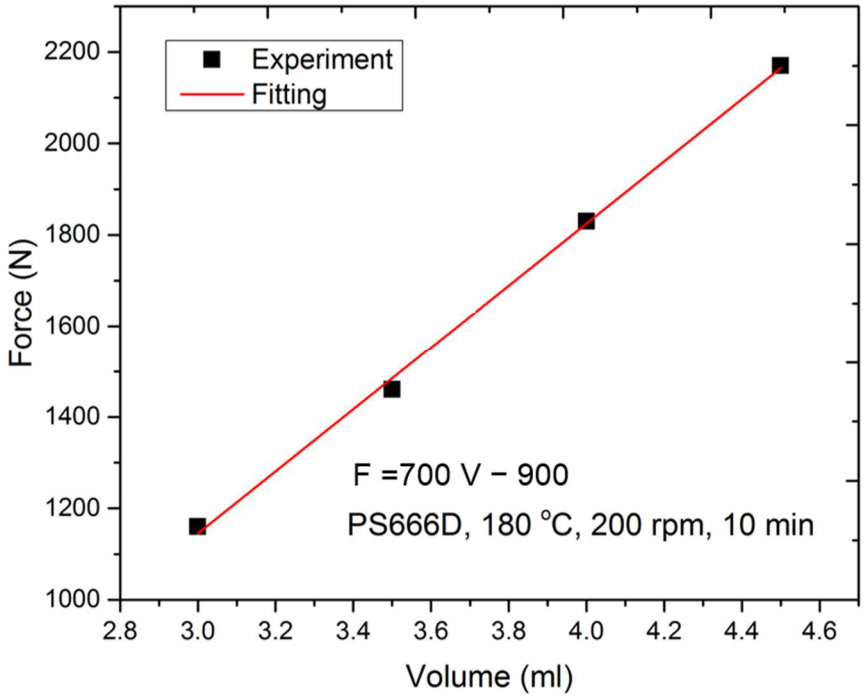

Figure A2.5 Mixer normal force as a function of loading (courtesy Liangliang Gu).

A2.5 Impact strength tests

ASTM D256 impact strength specimens (3.35 mm wide, 12.7 mm thick, 63.5 mm long) were created using a Morgan Press injection molder (barrel temperature = 185 °C, nozzle temperature = 220 °C, mold temperature = 60 °C, ram pressure = 3 – 5 kpsi, pilot valve pressure = 100 psi, clamp force = 13 tons, cycle time = 30 s). Samples were aged for at least 48 h in a room temperature vacuum oven.

A CEAST instrumented impact tester (model 6545) measured notched impact resistances in accordance with ASTM D256 (0.372 m arm, 150° drop angle, 3.45 m/s impact speed, 2.75 J hammer). Samples were notched using CEAST model 6186 sample notcher. Reported values are notched Izod impact strengths (J/m^2), based on test method A.

Notched Izod impact tests were performed on injection molded samples, with results shown in Table A2.3. Most samples failed with incomplete break, so these values

must be interpreted cautiously. Addition of LLDPE or EGMA increases impact energy of PLA by about a factor of two, but in general interfacial reaction did not correlate with impact strength. DDA increases impact resistance substantially, whereas $CoOct_2$ decreases impact strength.

These values agree well with those obtained by Oyama et al.[147] for pure PLA and 20 EGMA. They also noted a 50-fold increase in notched impact strength with annealing the 20 EGMA blend. Feng et al. studied a similar system for notched impact strength.[68] However, their results showed a much more dramatic increase with compatibilizer loading and amine catalyst addition. This could be due to the difference in specimen preparation, since they used long compression molding cycles instead of quick injection molding cycles, effectively annealing the samples. The $CoOct_2$ blend decreasing impact strength is probably due to the drop in molecular weight, noted above. $CoOct_2$, 1 EGMA did not yield enough injection molded specimens for tensile testing, due to low melt strength and viscosity.

Table A2.3 Notched Izod impact strength of PLA and blends

material	notched impact strength (kJ/m^2)	type of break
PLA	3.7 ± 0.2	complete break
0 EGMA	7.9 ± 0.8	incomplete break
1 EGMA	7.1 ± 0.5	incomplete break
5 EGMA	7.5 ± 0.5	incomplete break
20 EGMA	5.9 ± 0.7	incomplete break
DDA, 1 EGMA	7.6 ± 0.6	incomplete break
DDA, 5 EGMA	9.8 ± 0.8	incomplete break
$CoOct_2$, 5 EGMA	4.9 ± 0.5	incomplete break

Appendix 3: Supplementary information for Chapter 6

A3.1 Procedure for installing capillary coextrusion die

1. Screw the flanges (A3.6) into the capillary rheometer.
2. Align the rest of the die separately with the dowel rods, and slide bolts in from bottom to top to hold it together.
3. Attach die to flanges and lightly tighten bolts to hold it on.
4. Install the heating band. Use the hex nuts on the terminals to tighten the wire connections, then use the plug to connect the heating band to the temperature controller. Place the ceramic caps on the terminals to prevent electrical shocks. Be sure to tighten the band so there is no air gap between the heating band and die. Use insulation to wrap the ceramic plugs against the die (so they don't fall off).
5. Install the thermocouple by screwing into the pipe-fitted threads in the bottom of the die. Connect this to the temperature controller.
6. Wrap with insulation. Heat to desired temperature using control box.
7. After waiting 30 minutes to reach the set temperature, tighten the hex bolts
8. Load and use the capillary rheometer, as described in the SOP for that instrument. Use manual control mode for constant speed experiments.

A3.2 Procedure for capillary coextrusion

1. Load the samples a few grams at a time, tamping with a Teflon plunger to eliminate air bubbles. If the materials are very low viscosity, plug the die exit first.
2. Insert the pistons
3. Use the handheld console to move the pistons down until they contact the samples. This can be observed by an increase in pressure.
4. Select a speed in the manual control console and press the down arrow.

5. As sample is extruded, cut into ~6 inch strips and lay on a flat metal plate. When 5 samples have been collected, lay another flat metal plate on top to prevent curl.
6. When all the sample is extruded, move the piston head to the top position. Clean the pistons with kimwipes or flannel rags.
7. Load additional samples

A3.3 Machine drawings for capillary coextrusion die

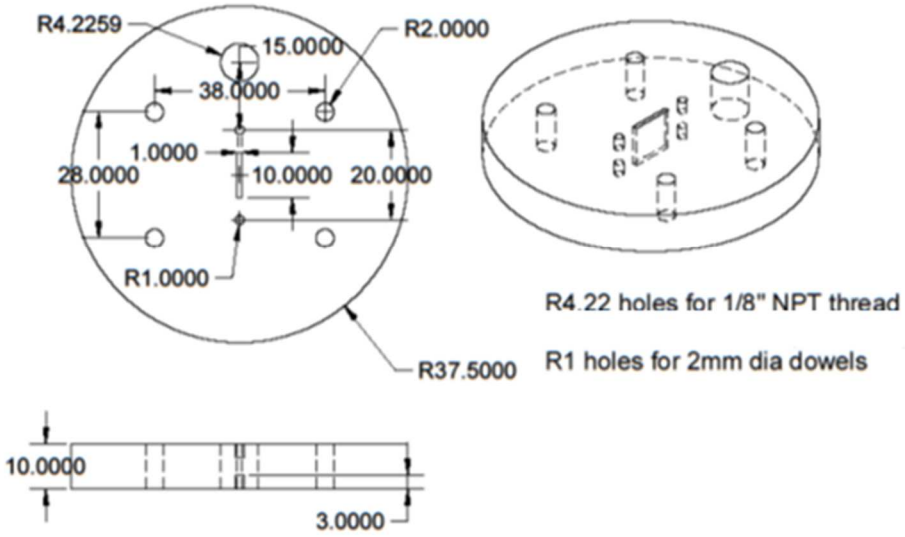

Figure A3.1 Die exit. Thermocouple hole (R4.226 mm) is NPT 1/8” pipe threaded. All units are mm.

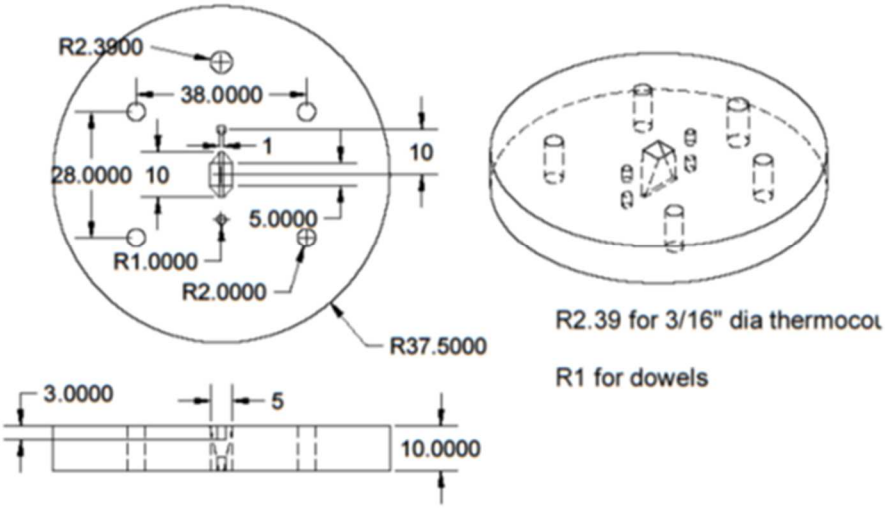

Figure A3.2 Expansion piece. This has the main compressional flow for the die.

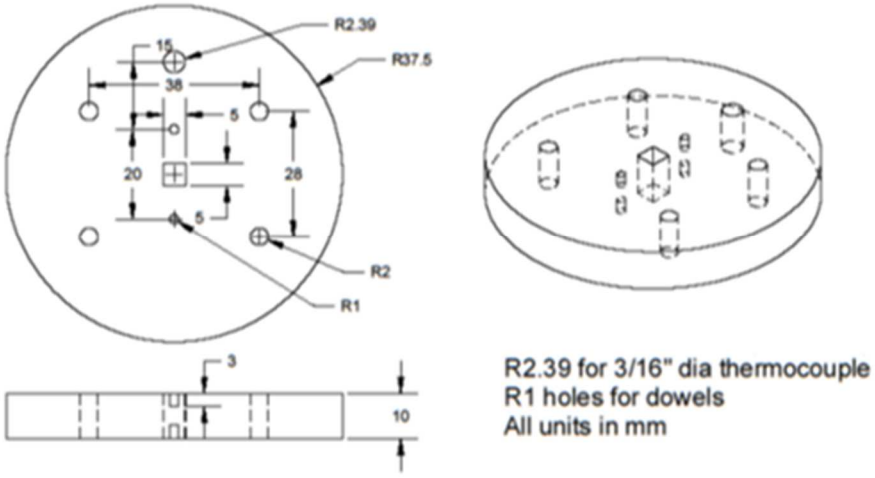

Figure A3.3 Straight connector

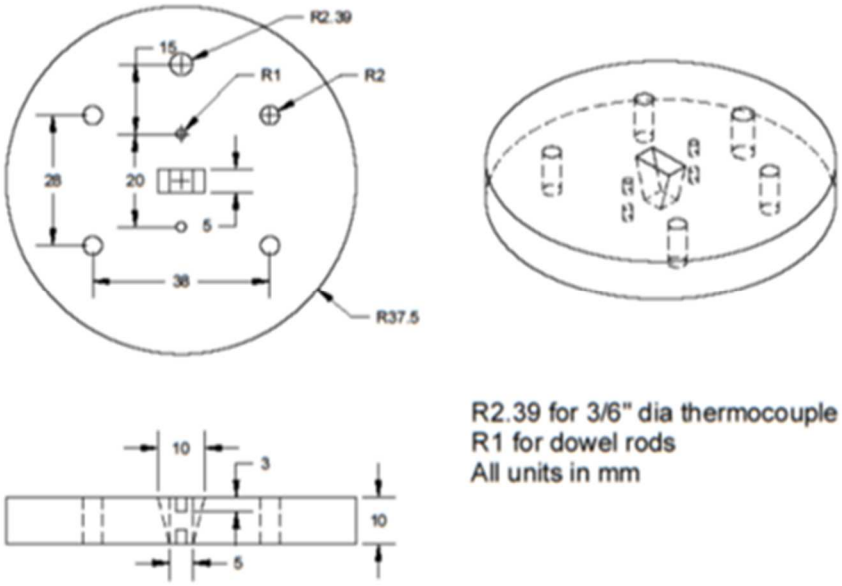

Figure A3.4 Expansion piece, just after the streams converge

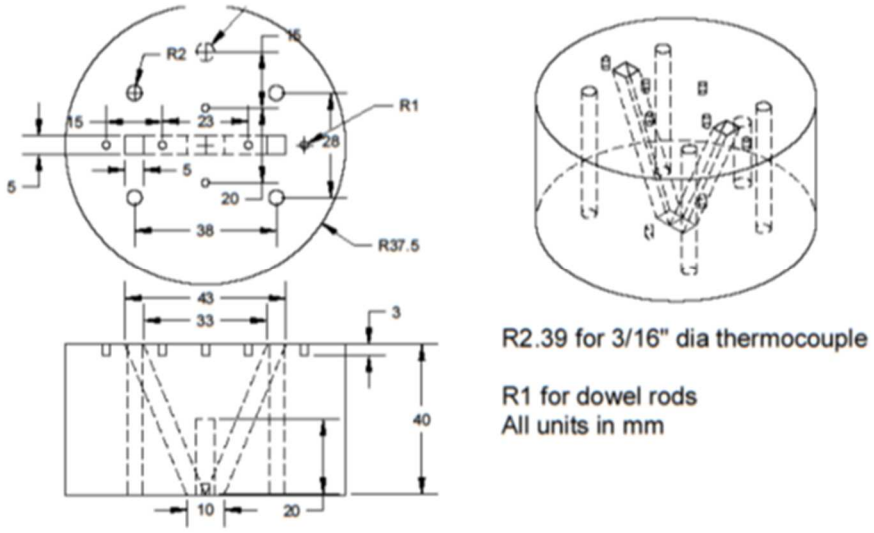

Figure A3.5 Convergence piece

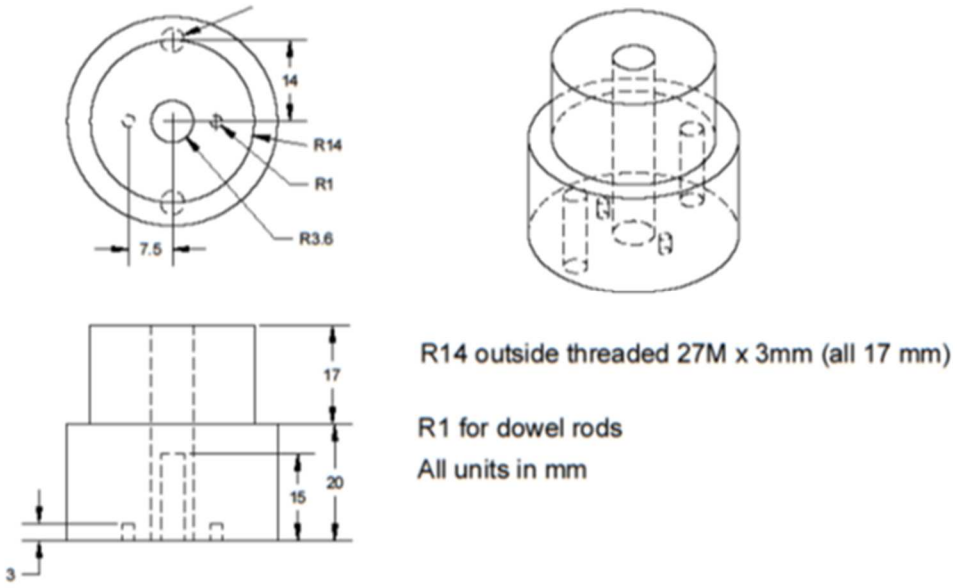

Figure A3.6 Flange connector to capillary rheometer. Blind holes (15 mm deep) are threaded for hex bolts.